CHAPTER 10

NITROGEN SPECIES

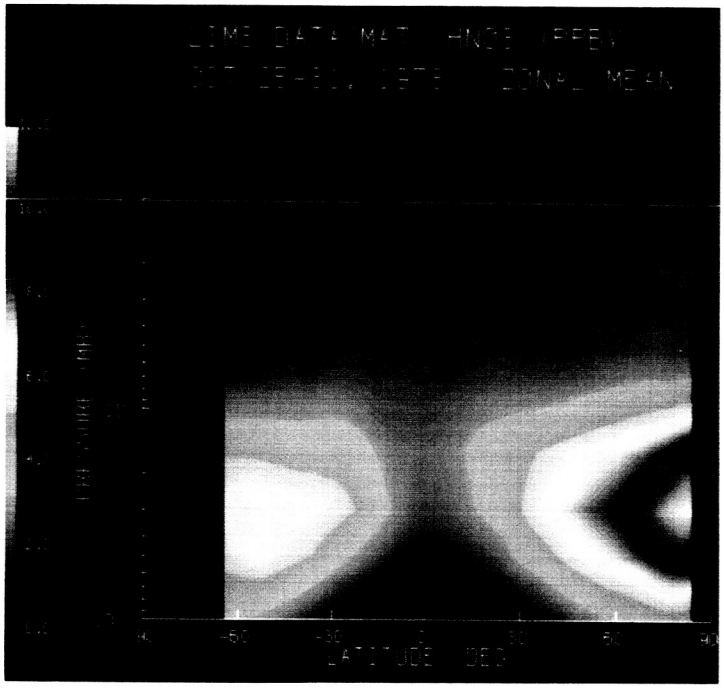

Panel Members

J.E. Harries, Chairman

G. Brasseur
M.T. Coffey
H. Fischer
J. Gille
R. Jones
N. Louisnard
M.P. McCormick
J. Noxon
A.J. Owens
J. Pyle
B.A. Ridley
H. Roscoe
A.L. Schmeltekopf
S. Solomon
N.D. Sze

CHAPTER 10
NITROGEN SPECIES: OBSERVATIONS AND INTERPRETATION

TABLE OF CONTENTS

10.0 INTRODUCTION 497

10.1 NON-SATELLITE DATA 499

10.1.1 Nitric Oxide (NO) 499
10.1.2 Nitrogen Dioxide (NO_2) 508
10.1.3 Nitric Acid (HNO_3) 516
10.1.4 Nitrous Oxide (N_2O) 521
10.1.5 Nitrogen Trioxide (NO_3) 522
10.1.6 Dinitrogen Pentoxide (N_2O_5) 523
10.1.7 Chlorine Nitrate ($ClONO_2$) 524
10.1.8 Peroxynitric Acid (HNO_4) 525
10.1.9 Hydrogen Cyanide (HCN) 525
10.1.10 Methyl Cyanide (CH_3CN) 525
10.1.11 Latitudinal, Diurnal and Seasonal Variations 525

10.2 SATELLITE DATA 529

10.2.1 Nitrogen Dioxide (NO_2) 532
10.2.2 Nitric Acid (HNO_3) 553
10.2.3 Nitrous Oxide (N_2O) 563
10.2.4 Nitric Oxide (NO) 570
10.2.5 Intercomparisons of NO_2 Satellite Data 570
10.2.6 Representativeness of Palestine and Aire sur l'Adour Launch Sites Compatibility between Satellite and Balloon Observations 574

10.3 ODD NITROGEN MODELLING 576

10.3.1 Sources of Odd Nitrogen 576
10.3.2 Distribution and Comparisons to Data 583
10.3.3 Photochemical Considerations 597

10.4 CONCLUSIONS 601

10.5 FUTURE RESEARCH 603

10.0 INTRODUCTION

Total odd nitrogen (NO_y) may be defined as the sum of all active nitrogen species that interchange photochemically with one another on a time scale of the order of weeks or less, i.e. $NO + NO_2 + NO_3 + 2N_2O_5 + ClONO_2 + HNO_4 + HNO_3$. The interchange of the NO and NO_2 free radicals occurs on a time scale of minutes in the sunlit atmosphere, and can result in a catalytic loss process for stratospheric ozone. As noted in the Introduction to this and the other species chapters in this report, $NO + NO_2$ reactions dominate the processes controlling the ozone balance in the contemporary stratosphere; further increased chlorine abundances may change this situation, but presently this dominance is evident. As a result, accurate direct measurements of the NO_2/NO ratio in the stratosphere must be considered central to any verification of ozone chemistry. Significant progress regarding this question is now available from balloon observations, as discussed in Section 10.1 and 10.3. It is also important to understand spatial and temporal variations in NO and NO_2, both on scales ranging from a few hundred meters or a few seconds, to global and seasonal levels, in order to evaluate the role played by variations in NO_y insofar as the diverse behaviour of stratospheric ozone is concerned. Both *in situ* and satellite techniques have revealed important insights into these questions, as will be shown below.

Study of the odd nitrogen family must also include the longer-lived reservoir species, such as N_2O_5, $ClONO_2$, HNO_3, and HNO_4, N_2O_5 plays a particularly important role in the diurnal and seasonal variability of NO and NO_2, because of its unique chemical properties. N_2O_5 is produced during the night via the reactions:

$$NO_2 + O_3 \rightarrow NO_3 + O_2$$

$$NO_3 + NO_2 + M \rightarrow N_2O_5 + M \qquad (2)$$

This process occurs almost exclusively at night because NO_3 is destroyed rapidly by photolysis in the sunlit atmosphere, and is therefore present in quantity only at night. The N_2O_5 produced at night then photolyzes in the sunlit atmosphere on a time scale of hours to days, depending on altitude and temperature:

$$\begin{aligned} N_2O_5 + h\upsilon &\rightarrow NO_2 + NO_3 \\ &\rightarrow 2NO_2 + O \end{aligned} \qquad (3)$$

In a twelve hour night at midlatitude in summer, perhaps 50% of the NO_2 present at sunset is converted to N_2O_5 near 10 mbar, and subsequently slowly released in the following day. Therefore, this species plays a critical role in the diurnal variations of NO and NO_2. Similar, but substantially less important roles are played by $ClONO_2$, and HNO_4 in the contemporary atmosphere. HNO_3 is produced via

$$OH + NO_2 + M \rightarrow HNO_3 + M \qquad (4)$$

and destroyed by photolysis and reaction with OH:

$$HNO_3 + h\upsilon \rightarrow NO_2 + OH \qquad (5)$$

$$HNO_3 + OH \rightarrow H_2O + NO_3 \qquad (6)$$

Because the time scale for loss of HNO_3 is generally longer than a few days to weeks at the altitudes where it is present in large quantities, HNO_3 is of importance to our understanding of NO_y on somewhat larger temporal and spatial scales.

We have briefly reviewed how the principal members of the NO_y family are related chemically to one another, but we must also consider the production and loss of the family as a whole, as well as its relationship to atmospheric transport processes. The various sources of NO_y will be discussed in detail in Section 10.3, but here we briefly mention that the primary source of stratospheric NO_y is provided by N_2O via the reaction:

$$N_2O + O(^1D) \rightarrow 2NO. \quad (7)$$

N_2O, in turn, is strongly controlled by atmospheric transport. Balloon observations before 1981 revealed large latitudinal gradients in N_2O vertical distributions; further balloon and particularly satellite observations of this constituent have not only quantified our knowledge of NO_y sources, but have also led to a greatly improved understanding of atmospheric transport.

Another manifestation of the importance of transport in NO_y distributions is provided by the Noxon "cliff" phenomenon, first observed in ground based studies in 1977 (Noxon 1979). A cliff is an abrupt decrease in NO_2 column abundance as a function of latitude, in winter by as much as a factor of 4 in only 5-10° of latitude. Other ground based and aircraft studies, however, obtained much less dramatic changes in NO_2. Noxon (1979) showed that particular meteorological conditions characterize the NO_2 "cliff" phenomenon; i.e. large scale wave activity seemed to be a prerequisite for cliff formation. Recent theoretical work has shown that this phenomenon is likely to be related to N_2O_5 chemistry and transport. The broad spatial and temporal coverage of satellite NO_2 observations, under varied meteorological conditions, has led to a much more complete understanding of the cliff than previously possible. Balloon data have also revealed the precise altitudes where the NO_2 variations occur during cliff conditions, with very high vertical resolution: yet another example of the role of transport processes in variations in NO_y column abundance, both from aircraft and satellite data.

These and other aspects of stratospheric nitrogen species are discussed in this chapter, with the aim of reviewing the status of observational data and theory. Particular emphasis is placed on advances in our interpretation of observations with regard to developments since the last major NASA/WMO assessment report. This chapter is organised as follows:

Section 10.1 reviews observational data from non-satellite platforms;
Section 10.2 considers the somewhat explosive growth in available satellite data in the past four years;
Section 10.3 then presents a discussion of some of the most important scientific issues which have been addressed, taking into account new results from atmospheric models (mainly 2-D), and the comparison of these model results with observational data.
Section 10.4 presents a summary and conclusions; and
Section 10.5 recommends future research needs.

The chapter shows that remarkable progress in our knowledge of odd nitrogen chemical and physical balances has occurred in recent years, but that many processes are still far from perfectly understood.

10.1 NON-SATELLITE DATA

Balloon, ground-based and aircraft measurements have always played a central role in our understanding of stratospheric chemistry and in confirming photochemical theory. Recently, the emphasis of balloon-borne measurements has shifted to a more detailed testing of photochemistry and dynamics. Diurnal cycle measurements within a moving air parcel can be conveniently made by balloons. *In situ* measurements made from balloons and rockets retrieve data at vertical scales far beyond the capabilities of remote sensing methods, leading to improved understanding of small scale variability. Ground based observations can provide continuous time series data at particular points, revealing important temporal information.

In this section, *in situ* and remote data on odd nitrogen species will be presented and intercompared. Results from several measurement techniques will be compared, and photochemical variations associated with their interpretation (i.e. as a function of local time) will be considered. As described in the Introduction (10.0), it is also of interest to examine the total NO_y abundance obtained from the sum of available observations of the constituent family members. This provides a test of our understanding of the chemical and transport budget of the family as a whole (see Section 10.3). To this end, best estimate profiles for NO, NO_2 and HNO_3 are evaluated from their composite database.

10.1.1 Nitric Oxide (NO)

In contrast to the large amount of data available for nitrogen dioxide and nitric acid from satellite retrievals (LIMS, SAGE, SME), no such direct temporal and spatial information exists for nitric oxide. Instead, most of our knowledge of the distribution of nitric oxide in the stratosphere results from discrete measurements made from the ground, from high-altitude balloons, aircraft, rockets, and, more recently, the Space Shuttle platforms. Additional information can be inferred from measurements of nitrogen dioxide; daytime to nighttime differences from satellite observations can provide at a minimum a lower limit to the nitric oxide abundance. Nitric oxide can also be estimated from satellite measurements of nitrogen dioxide, temperature and ozone if the photodissociation rate of nitrogen dioxide is known, since the two free radicals, NO and NO_2, are in photochemical equilibrium in the sunlit atmosphere.

Since the last detailed assessments of 1981 and 1982, further measurements have been made using new techniques and by different groups. These include *in situ* optical and chemiluminescence measurements, daytime observations using the pressure modulator radiometer (PMR) and sunset occultation measurements. Simultaneous *in situ* and long-path measurements of nitric oxide and nitrogen dioxide have been obtained (Louisnard *et al.*, 1983, and McFarland *et al.*, 1985). Most importantly, some instrument intercomparison studies were undertaken during the MAP-GLOBUS and BIC-2 balloon campaigns. Seasonal changes in the altitude distribution of NO have been observed at high latitudes in North America.

Table 10-1 summarizes most of the *in situ* balloon and aircraft experiments that have been undertaken. Excluded from consideration are the experiments listed in the footnote. Further, only those experiments for the summer and fall seasons at latitudes from 32 to 44 °N are considered explicitly; this restriction allows the inclusion of most of the studies, by the largest number of techniques, and eliminates possible biases due to seasonal or latitudinal variation. Observations at other latitudes are consistent with the lack of marked variations in the total column measurements in summer and fall discussed in Section 10.1.11.

The observations of nitric oxide can be conveniently separated into measurements made below and above about 32 km. There are two reasons for this separation: (1) many of the techniques were designed

to operate optimally in one of these two altitude regions; (2) the variance of the observations by different techniques are quite different for the two regions. The data sets obtained within a few hours of local noon are considered first.

Table 10-1a. *In situ* Observations of Stratospheric Nitric Oxide.

	Group	Location	Date	Alt (km)	± Error (%)
A	Webster and Menzies	32 °N	Oct 16/83	36	30
*B	Kondo *et al.*	44 °N	Sept 20/83	7-32	5-10
*BB	Fabian *et al.*	44 °N	Sept 20/83		
C	McFarland *et al.*	32 °N	Nov 04/81	22-32	20
D		32 °N	Jul 08/82	21-30	20
E		51 °N	Aug 10/82	22-32	20
F	Horvath *et al.*	38 °N	Aug 29/78	32-51	20-30
G		38 °N	Oct 01/79	31-47	20-25
H		38 °N	Oct 10/80	29-46	20
J		38 °N	Jul 23/81+	29-54	10-20
K	Weiler *et al.*	44 °N	Jun 26/77	31-33	20
L		44 °N	Jun 6/78	14-31	7-20
M	Drummond *et al.*	43 °N	Jun 27/76	12-45	25
N	Maier *et al.*	32 °N	Apr 26/77	27-38	25-34
O	Patel *et al.*	32 °N	Oct 19/73	28	8
P	Patel *et al.*	33 °N	May 22/74	25,28	30
Q	Loewenstein *et al.*	32-44 °N	Summer/75/Fall/76	18.3,21.3	25
R	Loewenstein *et al.*	50 °N	Summer/75/Fall/76	18.3,21.3	25
S	Roy *et al.*	34 °S	Dec 11/77	12-33	30
T		34 °S	Dec 13/77	15-33	30
U	Galbally *et al.*	34 °S	May 15/79	18-33	30
V		34 °S	Oct 10/79	14-33	30
W	Ridley and Schiff	32 °N	Oct 25/77	15-33	—
X		32 °N	Oct 30/78	14-40	—
Y		32 °N	Nov 08/78	14-40	—
Z	Ridley and Hastie	51 °N	Aug 28/76	17-34	—
ZZ		51 °N	Aug 12/78	14-33	—

*MAP-GLOBUS Intercomparison
+Two flights.

Other observations have been reported but are not included in this review. Most of the early measurements by the York University group were rejected because sampling problems likely existed (Ridley and Schiff, 1981). The results of McGhan *et al.* (1979) were not considered because the instrument was damaged during the launch process and it did not operate completely according to design. (Data reported from this flight above 27 km are in good agreement with the majority of the balloon measurements for 32 °N.) The June 26/78 flight results reported by Weiler *et al.* (1980) were also not considered because of a mechanical malfunction that increased the error estimate to ± 50%. The results from the resonance fluorescence technique of Anderson and co-workers (1979) were not considered. As well, the early rocket flights of Mason and Horvath (1976) are not included in the analysis. Instead, only the data obtained during parachute descent from the rocket apogee are discussed (Horvath *et al.*, 1983).

Table 10-1b. Oxford University Pressure Modulated Radiometer Measurements of NO

June/75	44 °N	Drummond and Jarnot, 1978
Sept/78	32 °N	Roscoe *et al.*, 1981
Oct/80	32 °N	Roscoe *et al.*, 1985
Oct/82	32 °N	Roscoe *et al.*, 1985
*June/83	32 °N	Roscoe *et al.*, 1985

Table 10-1c. Sunset Solar Occultation Measurements of NO

May/73	44 °N	Ackerman *et al.*, 1975
May/74	44 °N	Ackerman *et al.*, 1975
Sept/80	44 °N	Louisnard *et al.*, 1983
*June/83	32 °N	Louisnard *et al.*, 1985
Oct/79	33 °N	Rinsland *et al.*, 1984c

*BIC 2 Intercomparison

10.1.1.1 Balloon and Aircraft Observations below 32 km

Figure 10-1 gives the data obtained below about 32 km for the 32-44 °N latitude band from the balloon and aircraft measurements of Table 10-1. For clarity, and where appropriate, only hand-drawn curves through the reported data are given. Data reported since the 1981 WMO assessment are emphasized by heavier printing. Two of these profiles (B and BB of Table 10-1) were obtained simultaneously; these two observations are in substantial disagreement below 24 km but above this altitude the agreement is very good and consistent with the majority of other measurements.

Considering the ± 20-30% error of individual experiments, several profiles appear disproportionately low. The first is the data below 34 km of Maier *et al.* (1978). This flight was made near local noon on April 26, 1977 but the shape resembles several winter profiles obtained near 50 °N that are discussed in a subsequent section. Upper atmospheric meteorological charts have not been examined to determine if unusual dynamics could explain the low values. Since there are no other winter/spring measurements for this latitude band to corroborate this unusual profile, the values reported below 34 km are not included in the ensuing analysis. Second, although the instrument flown by Weiler *et al.* (1980) employed an on-board calibration system, these observations also appear anomalously low below about 30 km. A third flight also gave mixing ratios of only 0.2 to 0.3 ppbv between 15 and 26 km. Fabian (private communication) has indicated that the earlier flights of Weiler *et al.* (1980) suffered from uncertainties in the determination of the zero level signal of the instrument. Consequently these flights are not considered further. The profile of Drummond *et al.* (1977) is also about a factor of two smaller than the bulk of the data shown in Figure 10-1. There is a reasonable explanation of this result. The payload was launched shortly after visible sunrise on the ground. Morning solar zenith angles at 10, 20, 30 and 40 km were approximately 84, 79, 73, and 67 degrees. Burkhardt *et al.* (1975), Ridley *et al.* (1977) and McFarland *et al.* (1985) have measured the growth of nitric oxide and/or nitrogen dioxide during the morning at constant altitudes. These studies observed a growth of almost a factor of two during the morning which is attributed to the slow photolysis of N_2O_5 that was formed overnight. Consequently, the profile of Drummond *et al.* (1977) is expected to be significantly lower than the bulk of the other measurements that were made near local noon or in the afternoon.

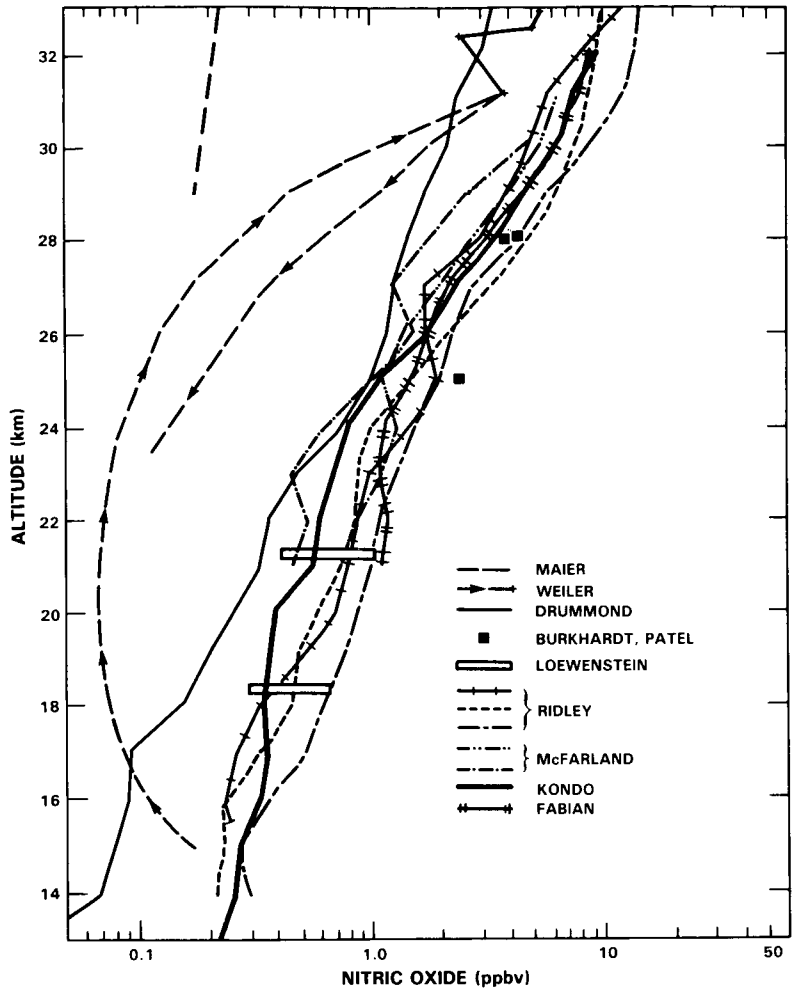

Figure 10-1. Balloon and aircraft observations of NO below 32 km in the latitude range 32–44°N.

The remaining profiles form a reasonably consistent data set and allow a best estimate of the altitude distribution for the 30-40 °N latitude region, the summer through fall season, daytime conditions and below 32 km by calculating a simple weighted average.

From the hand-drawn altitude profile curves, mixing ratios were noted at 1 km intervals. The mean and standard deviation of the mean were calculated. All of the measurements made since 1980 with instrumentation designed to operate optimally below about 32 km were assigned a weighting factor of two simply because of technological improvements and the experience gained with calibration standards and sampling methods. The aircraft measurements near 18 and 21 km were assigned a weighting factor of four simply due to the volume of data obtained by that group. The result is given in Figure 10-2. This mean profile does not include flights K, L, M, N of Table 10-1.

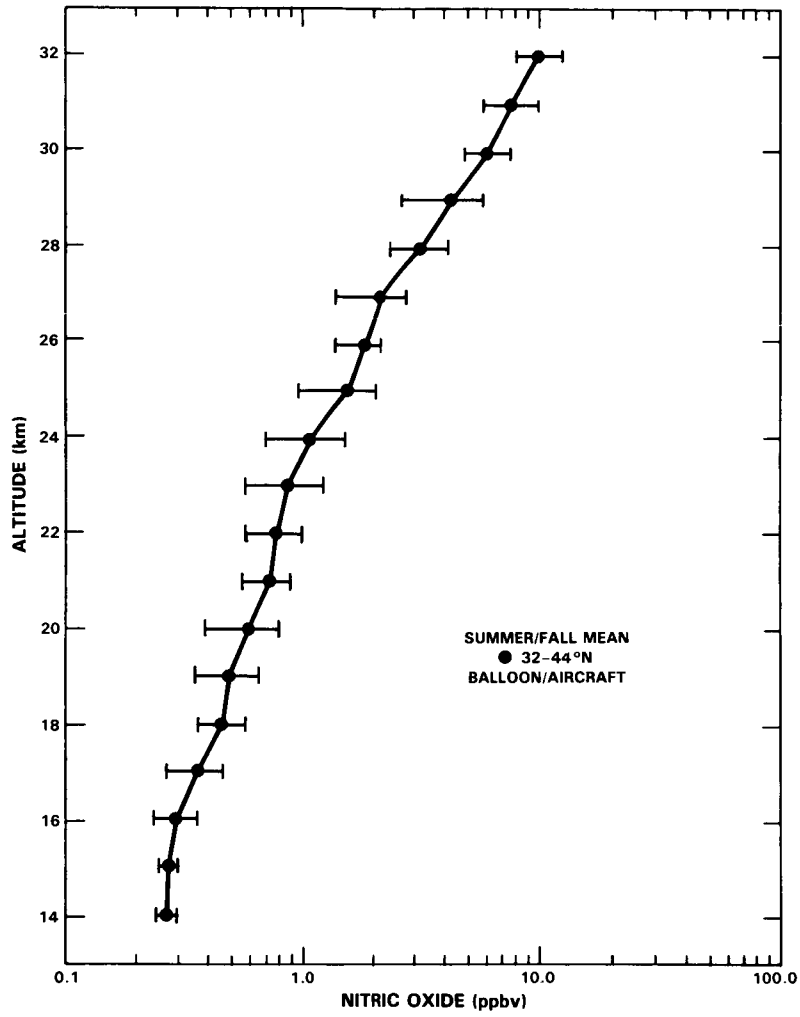

Figure 10-2. Best estimate of NO profile 32–44 °N latitude, up to 32 km.

10.1.1.2 Observations at Higher Altitudes

There are also a large number of observations for the summer/fall season at 32-44 °N both from instruments designed to operate only above about 30 km and from some of the previously discussed balloon experiments. There are also a number of recent observations from the Oxford PMR instrument. Although this is not an *in situ* technique, it does allow measurements during high sun conditions. All of these data were obtained in the afternoon and are included in the analysis of the observations for this altitude regime.

Above about 35 km, nitric oxide begins to dominate total odd-nitrogen. Near 40 km, nitric oxide is almost equivalent to total odd-nitrogen in current atmospheric models. Unfortunately, NO profiles measured by different techniques differ by as much as a factor of 4 to 6 in the 30-45 km region.

Figure 10-3 contains all of the non-occultation data from Table 10-1 for 32-44 °N above 29 km and for the summer/fall seasons. Flights K and L and N below 34 km are not included for the reasons given previously. Clearly, the range is large; at 36 km the mixing ratio ranges from a low of 2.8 ppbv from the PMR flight to a high of 17 ppbv from the diode laser instrument of Webster and Menzies (1984).

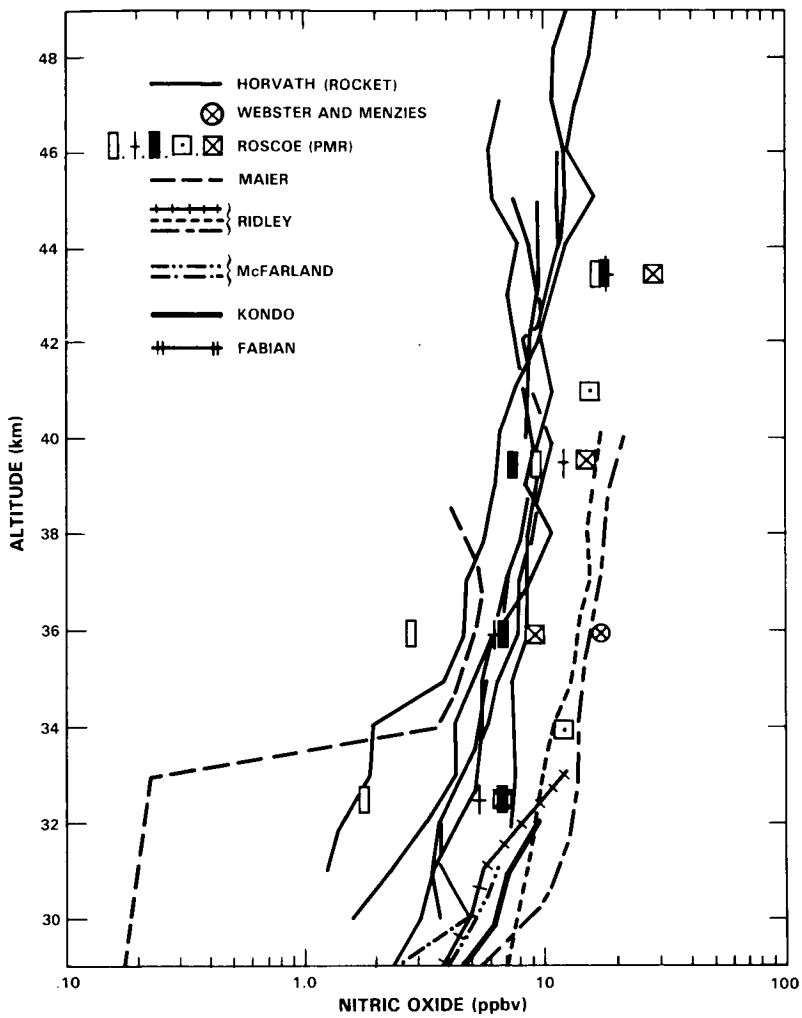

Figure 10-3. Non-occultation measurements of NO above 29 km for latitudes between 32 and 44°N.

The bulk of the higher altitude measurements have been obtained by Horvath *et al.* (1983), using a rocket-borne chemiluminescence instrument. A close examination of the rocket profiles of Figure 10-3 reveals that the variance between profiles increases markedly at altitudes below about 35 km; at 32 km there is over a factor of 5 difference in the mixing ratio. This is in contrast to the majority of the *in situ* balloon results in the 30-32 km of Figure 10-1. The average of the rocket data at 32 km is a factor of 2.8 lower than the mean derived from the balloon measurements shown in Figure 10-2; a discrepancy noted in the WMO assessment of 1981 and one that still needs to be resolved. Part of the difference and the increased variance of lower altitudes may be due to a loss in cryopump efficiency in the rocket instrument below 32-33 km (Horvath, private communication). None of the rocket measurements shown in Figure 10-3 employed an in-flight calibration procedure. More recently, in-flight calibration was employed on a flight in winter (January 1983). The results at 30 km agreed very well with a value near 2.8 ppbv, and the in-flight calibration confirmed the preflight laboratory calibration. Since substantial seasonal differences have been observed at more northern latitudes, these observations do not necessarily substantiate the summer/fall values near 30 km.

However, the variance in the measurements from the other instruments in Figure 10-3 is also large. Consequently, in an attempt to estimate the high altitude distribution of NO, the rocket data below 34 km is not considered. Even so, a broad range remains in the data.

Figure 10-4 shows the best estimate of the NO profile from the data in Figures 10-1 and 10-3. The profile above 30 km was determined by averaging the data by technique (rocket, balloon chemiluminescence, PMR and diode laser) rather than by averaging individual profiles. Flight M was included since diurnal trends are not expected to substantially perturb the data. This average profile above 32 km must be considered to have substantially larger uncertainty than that at altitudes below 32 km. Certainly, the confidence in the profile at altitudes where nitric oxide is expected to dominate the abundance of NO_y is not high.

10.1.1.3 Other Information

Further information about stratospheric nitric oxide can be derived from satellite measurements of nitrogen dioxide. These observations are discussed in detail in Sections 10.2 and 10.3. There are also

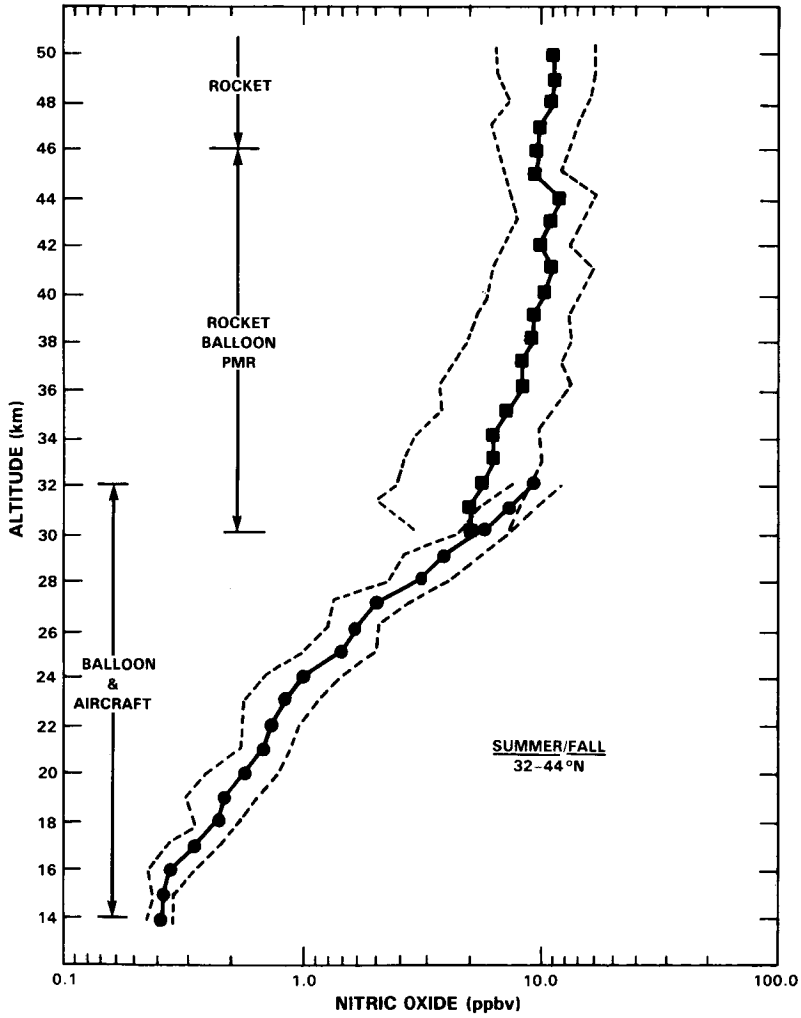

Figure 10-4. Best estimate of NO profile from all techniques, 14 to 50 km, 32–44°N latitude.

a few recent long-path solar occultation retrievals of nitric oxide. Together, these data bases can be examined to determine whether the range of mixing ratios at high altitudes can be further refined.

Zonal mean profiles for nitrogen dioxide at 32 °N in the summer/fall season during the afternoon (about 1300 local time) and at night (about 2300 local time) are available from the LIMS retrievals (see Section 10.2.1). Near 40 km, the daytime abundance is 2-3 ppbv while the nighttime abundance is 15-16 ppbv. The difference of 12-14 ppbv provides at least a lower limit to the afternoon abundance of nitric oxide. The difference should be larger and depends on the amount of nitrogen dioxide converted to NO_3 and N_2O_5 between sunset and 2330 (see Section 10.3). In any event, the lower limit difference is only about 25% larger than the mean at 40 km in Figure 10-4. At 34 km a similar analysis yields a lower limit of 10-11 ppbv, about 50% larger than the mean in Figure 10-4. Of course these differences depend upon the uncertainties in the satellite retrievals.

10.1.1.4 Solar Occultation Retrievals

Solar occultation measurements of nitric oxide during sunset have been reported since as early as 1973 (Ackerman *et al.*, 1973, 1975). The method has the advantage that absorption features of many different stratospheric species are recorded simultaneously. Mixing ratio profiles from this technique have not been discussed so far because they are not directly comparable to the daytime *in situ* and PMR data of Figures 10-1 and 10-3. Although the measurement technique is straightforward, the deconvolution of the infrared absorption as a function of zenith angle to obtain an altitude profile is particularly complicated for nitric oxide, for two reasons. First, as the solar zenith angle increases beyond 90° during sunset, nitric oxide is converted to nitrogen dioxide as both the photodissociation rate of nitrogen dioxide and, at appropriate altitudes, the atomic oxygen concentration decrease. Second, deconvolution techniques usually employ an "onion peeling" procedure in which NO is assumed constant in layers of about 2 km. Altitude gradients of nitric oxide within the layer further complicate the analysis. To obtain the best estimate of the profile of nitric oxide equivalent to sunset (a zenith angle of 90°) a diurnal model should be applied (Boughner *et al.*, 1980). Rinsland *et al.* (1984a) have developed this reduction technique to show that a sunset profile of NO with a model input yields a mixing ratio near 18 km about a factor of 1.7 larger than a retrieval with no model input. The difference was a strong function of altitude; above about 20 km the difference decreases from about 10% to zero near 33 km.

Once a 90° sunset profile is derived, a comparison with high sun *in situ* or PMR data requires a knowledge of the afternoon to sunset variation of nitric oxide. This variation should depend upon altitude for three reasons. First the vertical distribution of N_2O_5 and its photodissociation coefficient depend strongly on altitude. Photolysis of N_2O_5 during the morning and afternoon would tend to increase nitric oxide. Second, due to multiple scattering and the decreasing contribution of surface albedo, the photodissociation coefficient of NO_2 is expected to decrease in the afternoon towards sunset. Partitioning of the sum of NO and NO_2 should shift to lower NO. Third, the decrease in the atomic oxygen concentration with increasing afternoon zenith angle would tend to decrease nitric oxide. The detailed diurnal variation varies from model to model. However, the decay of nitric oxide near sunset has been observed in detail by Ridley and Schiff (1981), Knight *et al.* (1982) and Kondo *et al.* (1985). At 32 km, Kondo *et al.* (1985) have observed a slow decay of about 25% as the zenith angle increased from 80-90° and a rapid decay to zero nitric oxide by 94°. Near 40 km, the decay was not observed until near 90° (Ridley and Schiff, 1981). Consequently, it is reasonable to assume that the solar occultation measurements for 90° and at altitudes above 34 km are about 15% below afternoon *in situ* measurements. At lower altitudes, 90° occultation profiles are expected to be even lower than daytime *in situ* and PMR profiles.

Figure 10-5 shows the results of three recent interpretations of sunset spectra. The first, by Rinsland *et al.* (1984a), is obtained by a model modified deconvolution to 90° of spectra obtained by Blatherwick *et al.* (1980) from a balloon flight on October 10, 1979. The other two profiles (Louisnard *et al.*, 1983) do not include this type of correction. The errors estimated for these profiles are near ± 20% above about 30 km. Included in this figure is the result from the PMR instrument which was obtained simultaneously with the Louisnard *et al.* occultation profile of June 1983 (BIC 2). The PMR data were the result of signal integration over a three hour period ending one-half hour before a 90° zenith angle. There is good agreement between the BIC 2 instruments below 38 km, with the PMR results being larger on average as would be expected.

At high altitudes (above 30 km) the occultation data tend to nitric oxide values that fall between the extremes of the data of Figures 10-1 and 10-3. Consequently, these data do not help to decrease the range of the uncertainty in the high altitude measurements.

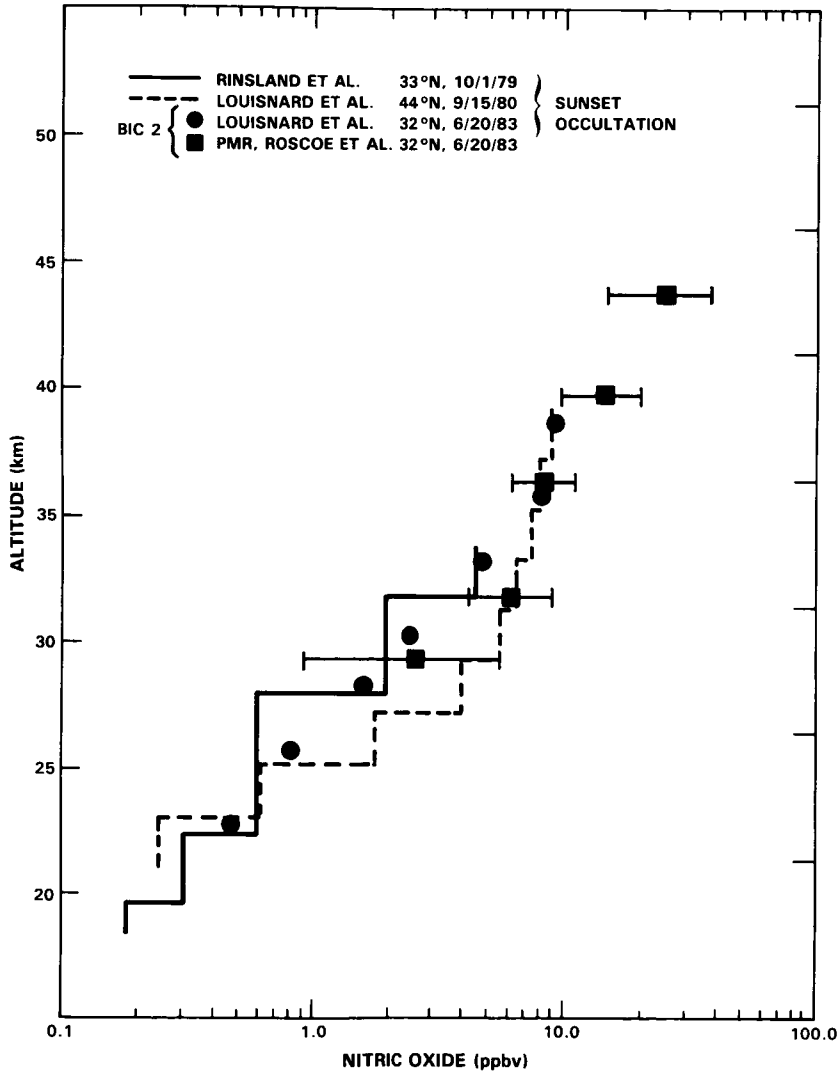

Figure 10-5. Sunset observations of stratospheric NO.

10.1.1.5 Seasonal Variations

The variation of nitric oxide with season observed near 18 and 21 km by Loewenstein *et al.* (1978a, b) was summarized in the 1981 WMO report. Total stratospheric column densities have also been measured as a function of latitude in the summer and winter seasons. These observations are discussed in detail in Section 10.1.11. Although these data provide valuable information, they do not reveal the changes in the altitude distribution in the stratosphere.

Altitude distributions of nitric oxide and other trace species have been measured at latitudes between 50 and 54 °N over western North America in winter (Ridley *et al.*, 1984; Knight *et al.*, 1982; Evans *et al.*, 1982a; McFarland *et al.*, 1985). Several rocket flights at 38 °N and one at 50 °N have been reported for the winter season by Horvath *et al.* (1983). The winter balloon experiments were inspired by the unique observations by Noxon (1979) concerning the variation with latitude and season of the column abundance of nitrogen dioxide.

Figure 10-6 shows observations of NO by McFarland *et al.* (1985) for December 15, 1982 near 50 °N. NO_2 was also observed to be greatly reduced below 28 km relative to summer observations. The seasonal change is in agreement with observations made earlier by Ridley *et al.* (1984). Both Knight *et al.* (1982) and Solomon and Garcia (1983a, b) suggested that the reduction of nitric oxide and nitrogen dioxide was likely to be due to the formation of N_2O_5 at northern latitudes in winter under certain meteorological conditions. Evans *et al.* (1982a) suggested that heterogeneous conversion to nitric acid might also contribute to the reduction. It is unfortunate that no winter profiles below 30 km have been obtained at more southerly latitudes. Such observations could provide further information on the role of N_2O_5 in winter.

Solomon and Garcia (1983a, b) and further work by Noxon and co-workers (1983) have demonstrated in detail the sensitivity of the winter distribution of nitric oxide and nitrogen dioxide to the variances in winter dynamics at high latitudes over North America.

10.1.2 Nitrogen dioxide (NO_2)

A variety of airborne and ground-based measurement programs have established some aspects of the latitudinal, seasonal and diurnal variability of stratospheric NO_2. The column abundance of NO_2 increases with increasing latitude, and summertime high latitude column amounts are a factor of three more than equatorial column amounts. The latitude distribution also depends on season with high latitude winter column amounts a factor of 2 to 3 less than summer abundances. Diurnal variations have also been observed; sunrise column amounts and altitude profiles are about a factor of two to three lower than sunset abundances. The situation during the transition from night to day (sunset or sunrise) is not well defined. There is also evidence that large scale air motions can alter the NO_2 abundance by a factor of two in a few days.

To establish a complete picture of stratospheric NO_2, measurements are required at many latitudes, for many times during a year, throughout the day. All these measurements, of course, have not been made. Observations tend to cluster at the locations of balloon launch facilities. For legitimate comparison we must group measurements with regard to location and time.

Table 10-2 lists most of the balloon-borne observations of NO_2. Most of the methods employ long-path optical techniques, either infrared (IR) emission or visible or IR absorption. Most of the absorption methods use the rising or setting sun as the light source (solar occultation). Since the 1981 WMO assessment, several *in situ* methods have been used to obtain daytime observations.

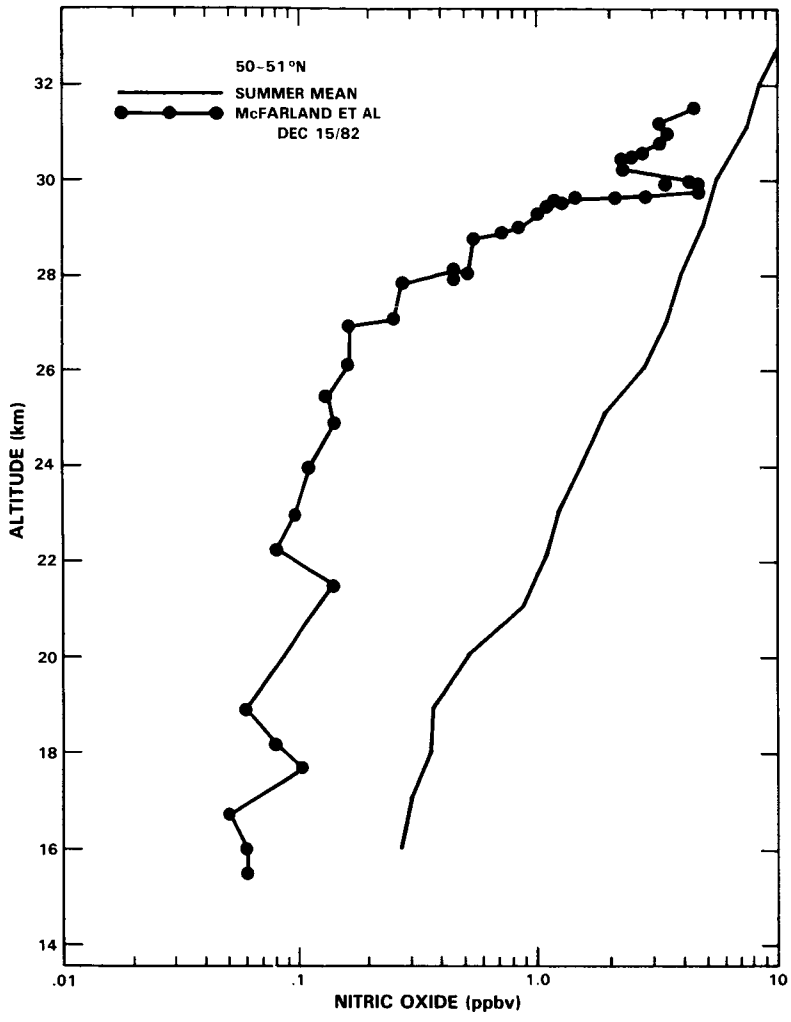

Figure 10-6. Summer and winter NO profiles by the same technique showing seasonal variability.

Figure 10-7 contains sunset vertical profiles from a number of techniques in the latitude range of 30-35 °N. Equator wards of about 40 °N there is little seasonal variation so measurements from all seasons may be compared. Since the 1981 assessment there was an extensive international measurement program, the Balloon Intercomparison Campaign (BIC 1 in September and October 1982 and BIC 2 in June 1983) which provided a number of remote observations of NO_2. A new technique using a gas correlation radiometer in a solar occultation mode (Fischer *et al.*, 1985a) has produced two sunset profiles which are included in Figure 10-7. The solid curve is a hand drawn mean from the values presented in WMO 1981 from visible and infrared absorption techniques at sunset. In general, the uncertainties are ± 20% for values between 28 and 38 km.

BIC results are not yet published and some obvious systematic instrumental differences have not been resolved. One suggestion of the BIC results is a decrease in the NO_2 during BIC 1 as compared to the BIC 2 time period, which may have been due to abnormal stratospheric conditions caused by the eruption

Table 10-2. Measurements of Profiles of NO_2 from Balloons

O=solar occultation SR=sunrise BIC 1=Sep/Oct 82, 32°N, SS N=night
E=thermal emission SS=sunset BIC 2=Jun 83, 32°N, SS

Group	Instrument	Flights	Reference
IASB	grille	May 74, 44°N, SS	Ackerman *et al.* 1978/79
ONERA	spectrometer,	May 78, 44°N, SS	Borghi *et al.* 1983
ONERA	1600cm^{-1},O	Apr 79, 32°N, SS	Borghi *et al.* 1983
ONERA	1600cm^{-1},O	Sep 80, 44°N, SS	Louisnard *et al.* 1983
ONERA	1600cm^{-1},O	May 82, 44°N, SR	Louisnard *et al.* 1985
ONERA	1600cm^{-1},O	BIC 2	—
Denver U	spectrometer,	Dec 67, 34°N, SS	Murcray *et al.* 1973
Denver U	1600cm^{-1},O	Oct 79, 33°N, SS	Blatherwick *et al.* 1980
NPL	cooled spectr,	May 81, 32°N, pm	—
NPL	1600cm^{-1},	BIC 1, pm	—
NPL	wideband, E	BIC 2, pm	—
Oxford U	PMR, 1600cm^{-1},E	Jun 75, 44°N, am+N	Drummond & Jarnot 1978
Oxford U	PMR, 1600cm^{-1},E	Sep 78, 32°N, pm	Roscoe *et al.* 1981
Oxford U	PMR, 1600cm^{-1},E	Oct 80, 32°N, pm+N	Roscoe *et al.* 1985a
Oxford U	PMR, 1600cm^{-1},E	May 81, 32°N, pm+N	Roscoe *et al.* 1985a
Oxford U	PMR, 1600cm^{-1},E	BIC 1, pm+N	Roscoe *et al.* 1985a
Oxford U	PMR, 1600cm^{-1},E	BIC 2, pm+N	Roscoe *et al.* 1985a
Met Inst, Munich	gas correlation,	Jul 78, 48°N, SR	Fischer *et al.* 1985b
	1600cm^{-1},O	Feb 79, 32°N, SS	Fischer *et al.* 1985b
	1600cm^{-1},O	May 79, 32°N, SS	Fischer *et al.* 1985b
York U	laser, *in situ*	Jul 83, 51°N, pm	Hastie *et al.* 1985
NOAA,	chemilumines,	Nov 81, 32°N, pm	McFarland *et al.* 1985
Boulder	*in situ*	Jul 82, 32°N, pm	McFarland *et al.* 1985
Boulder	chemilumines	Aug 82, 51°N, pm	McFarland *et al.* 1985
Julich	matrix isol,	Sep 83, 44°N, am	Helten *et al.* 1984a, b
Julich	ESR, *in situ*	Sep 83, 44°N, N+am	Helten *et al.* 1984a, b
Denver U	scanning	Feb 77, 33°N, SS,	Goldman *et al.* 1978
Tokyo U	spectrometer,	May 78, 40°N, SS,	Ogawa *et al.* 1981
Tokyo U	440nm, O	Nov 82, 67°S, SS+SR	—
Tokyo U	440nm, O	BIC 2	—
CNRS	440nm, O	Sep 79, 44°N, day	Pommereau 1982
CNRS	440nm, O	BIC 2	—
U PM. Curie	440nm, star O	Sep 79, 44°N, N	Naudet *et al.* 1984
U PM. Curie	440nm, star O	Sep 81, 44°N, N	Naudet *et al.* 1984
AES	fixed	Jul 74, 58°N, SS	Kerr & McElroy 1976
AES	spectr,	Aug 75, 5°N, SS+SR	Kerr & McElroy 1976
AES	440nm, O	Aug 75, 5°N, SS+SR)	Kerr *et al.* 1982
AES	440nm, O	Aug 76, 5°N, SS+SR	Kerr *et al.* 1982
AES	440nm, O	Aug 76, 5°N, SS+SR	Kerr *et al.* 1982
AES	440nm, O	Aug 77, 5°N, SR	—
AES	440nm, O	Dec 77, 32°N, SS	—
AES	440nm, O	Nov 78, 32°N, SS	—
AES	440nm, O	Oct 80, 32°N, SS	—
AES	440nm, O	Oct 79, 34°S, SR	—
AES	440nm, O	Oct 79, 34°S, SS	—
AES	440nm, O	BIC 1	

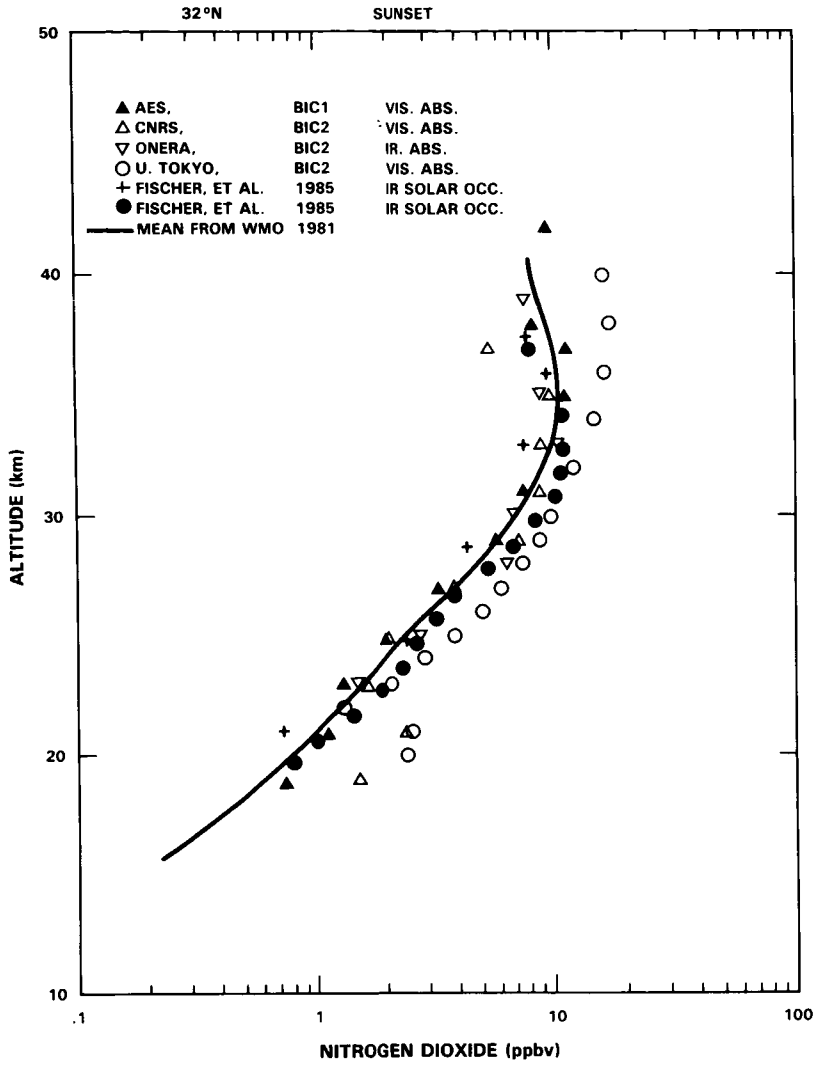

Figure 10-7. Sunset NO_2 profiles from a number of techniques in the latitude range 30–35°N.

of the volcano El Chichon in April 1982. The difference (a factor of 1.5 to 2) is supported by ground based and aircraft measurements of the NO_2 column. The possibility of such sporadic and apparently temporary effects adds another dimension to the variability in stratospheric NO_2.

In situ and emission measurements made during the day should represent a lower NO_2 amount at every altitude as compared with a sunset determination (up to a factor of two less at 30 km). Figure 10-8 contains daytime NO_2 profiles from a number of sources. The daytime profiles are significantly less than sunset profiles, as expected. Variation in the profiles is nearly encompassed by the measurement uncertainties. To strictly compare daytime measurements consideration must be given to the exact time of day of the measurements.

It is clear from observations, especially those of the AES group (Kerr *et al.*, 1982), that sunrise NO_2 ($\chi = 90°$, am) is about a factor of two lower than sunset NO_2 ($\chi = 90°$ pm). Observations during a

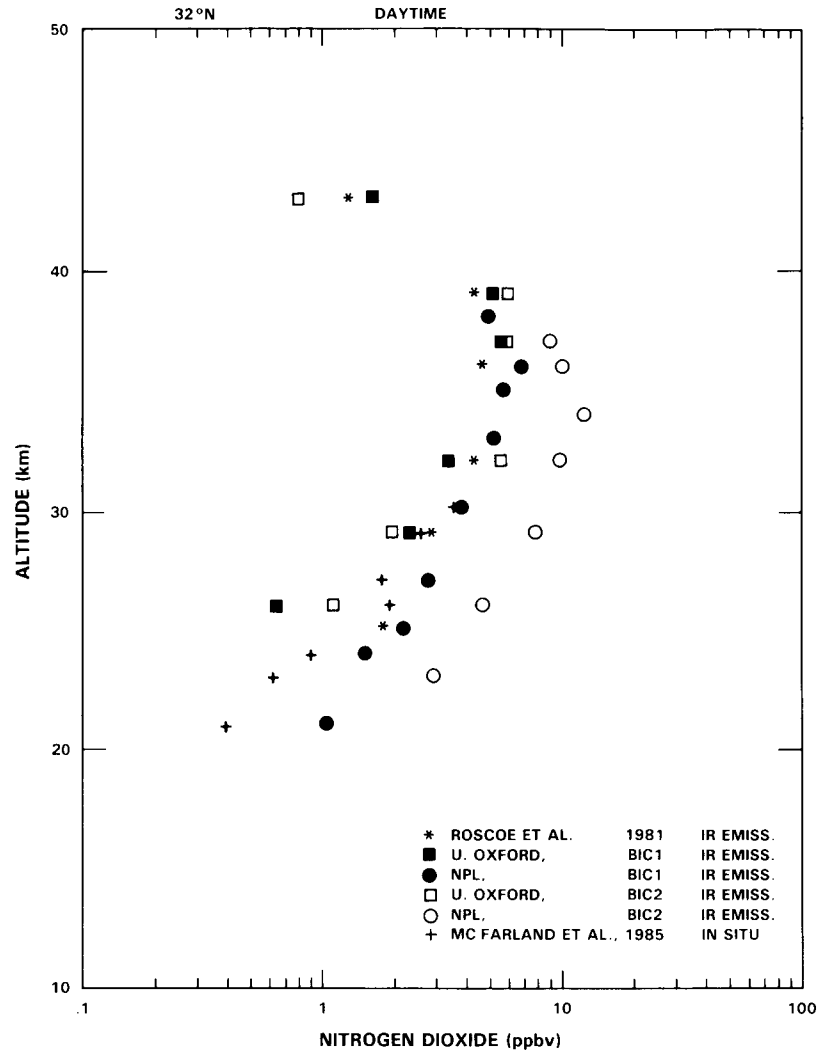

Figure 10-8. Daytime NO_2 profiles near 32°N.

day with the same instrument have shown slow diurnal changes in NO_2 amounts (Roscoe *et al.*, 1981; Pommereau, 1982; Flaud *et al.*, 1983). As discussed in the previous Section (10.1.1) several factors may contribute to this daytime variation. First, release of NO and NO_2 from nighttime reservoirs, especially N_2O_5, would cause a daytime increase of NO and NO_2. Little is known about the stratospheric abundance of N_2O_5 and the photolysis rate of N_2O_5 is a strong function of altitude. Second, due to multiple scattering and the change in the contribution of surface or cloud albedo with zenith angle, the photodissociation coefficient of NO_2 (J_{NO_2}) exhibits a diurnal dependence. From noon to sunset, J_{NO_2} is expected to decrease especially as $\chi \rightarrow 90°$. Third, the atomic oxygen concentration at higher altitudes also exhibits a strong zenith angle dependence. Consequently, NO_2 is expected to increase in the afternoon towards sunset at the expense of NO. Considerable debate remains as to the magnitude of the change in NO_2 at a given altitude as sunset is approached; models are not consistent in their treatment of multiple scattering and albedo for curved earth geometry. Nevertheless, observations made near local noon are not expected to agree with sunset solar occulation measurements that are equivalent to a solar angle of 90° (cf. Rinsland

et al., 1984c). Thus careful attention must be given to the time (solar angle) of the measurements if observations from different techniques are to be intercompared. The same attention must be given to comparisons of observations with predictions from photochemical/transport computer models.

Figure 10-9 shows daytime and sunset NO_2 measurements which have been reported since WMO 1981 in the latitude range of 40 to 50 °N. The open symbols (Louisnard *et al.*, 1983) are from infrared solar occultation measurements at sunset using a grille spectrometer, the solid line is a hand drawn mean of the measurements reported in WMO 1981 by the same spectrometer in earlier years. A recent development is an *in situ* measurement of daytime NO_2 using a matrix isolation ESR spectroscopy technique (Helten *et al.*, 1984a, b). The agreement between the *in situ* and remote occultation measurements is encouraging. *In situ* measurements are not susceptible to the uncertainties in NO_2 photochemistry which affect the retrieval of remote occultation measurements. Future, more numerous comparisons of *in situ* and remote observations would make a valuable contribution to our understanding of the NO_2 data base.

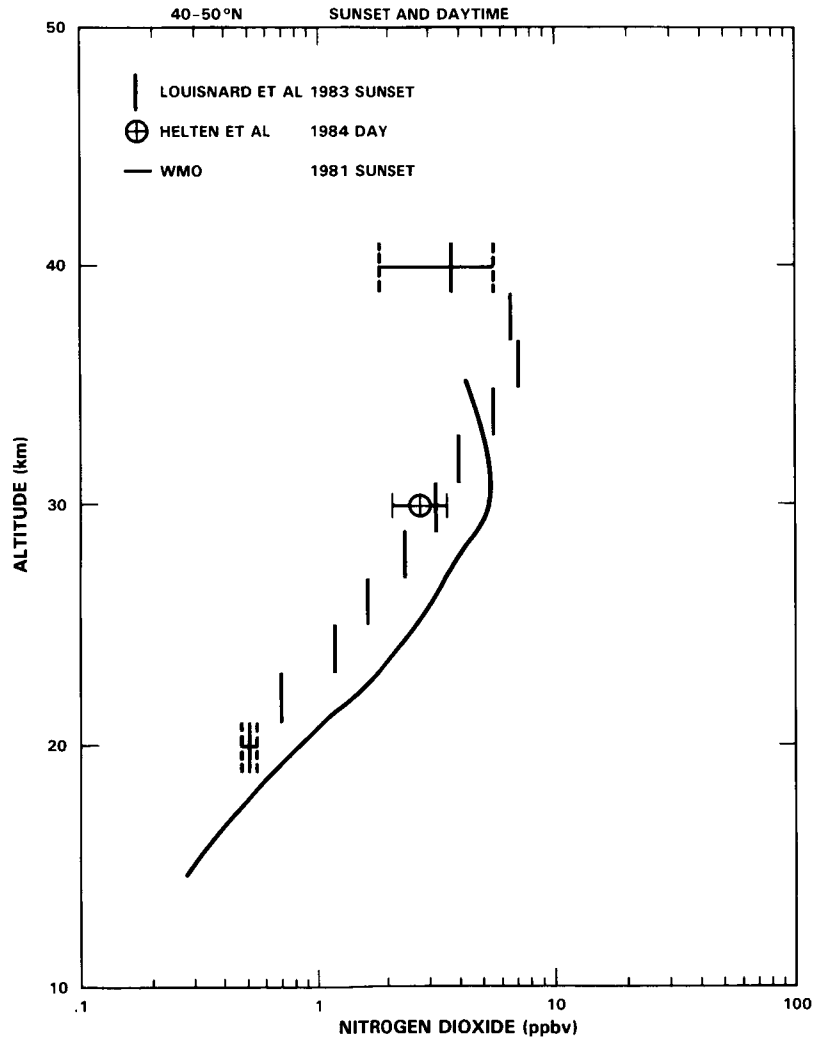

Figure 10-9. Daytime and sunset observations of NO_2 from 40 to 50 °N latitude.

NITROGEN SPECIES

New measurements reported from 50 to 60 °N are from an *in situ* technique based on infrared tunable diode laser absorption spectroscopy (Hastie and Miller, 1985) and an *in situ* profile determined using a chemiluminescence technique (McFarland *et al.*, 1985). Figure 10-10 shows the daytime *in situ* measurements and a remote sunset profile published in 1982 (Kerr *et al.*, 1982) which are essentially the same data presented in WMO 1981. At these higher latitudes one must distinguish measurements made in different seasons. The observations in Figure 10-9 were all in summer and no profile measurements have been made at high latitudes in winter to test the seasonal variability calculated by models. As was the case at lower latitudes the noontime profile is uniformly less than the sunset profile.

As described above, measurements of sunrise NO_2 should not be the same as nighttime measurements. Figure 10-11 contains the relatively few observations of nighttime and sunrise NO_2 profiles. The two sunrise observations agree well and are rather less than most of the nighttime observations as our understanding of nighttime photochemistry would predict. Profiles produced for sunrise and sunset by visible absorption spectrometry (Kerr *et al.*, 1982) indicate a factor of two increase from sunrise to sunset at all altitudes; the magnitude of the increase is in agreement with column measurements from aircraft (Coffey *et al.*, 1981a).

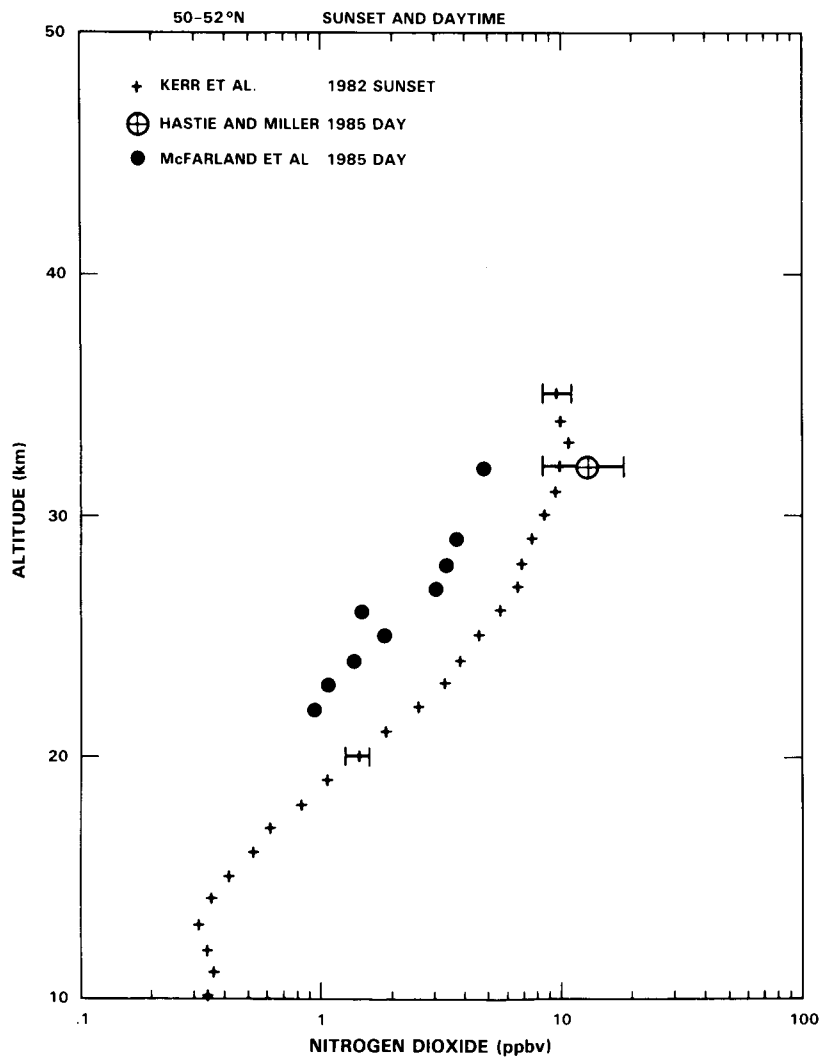

Figure 10-10. Daytime and sunset observations of NO_2 from 50 to 52 °N latitude.

Having examined each of the latitudinal groups of measurements one may attempt to discern a latitudinal trend in the NO_2 vertical profile. Figure 10-12 contains a representative sunset profile from each of the latitude ranges. Some liberty has been taken in selecting a profile in the 30 to 35 °N range since there may have been unusual effects in the BIC 1 results due to perturbations resulting from the El Chichon eruption. Also plotted in the figure are summertime profiles for various latitudes from the LIMS and SAGE satellite-borne instruments. The LIMS measurements are appropriate to a local time of 13:00 hours, the SAGE profiles are for sunset so our simple model implies that the LIMS profile should show less NO_2 than SAGE. Figure 10-12 shows that the NO_2 vertical profile does not change substantially in shape or magnitude from 30 to 45 °N but the profile at 60 °N is considerably different. Reasonable agreement is shown between the balloon and satellite observations over much of the range of overlap, though the substantial differences at 50-60 °N need to be explained.

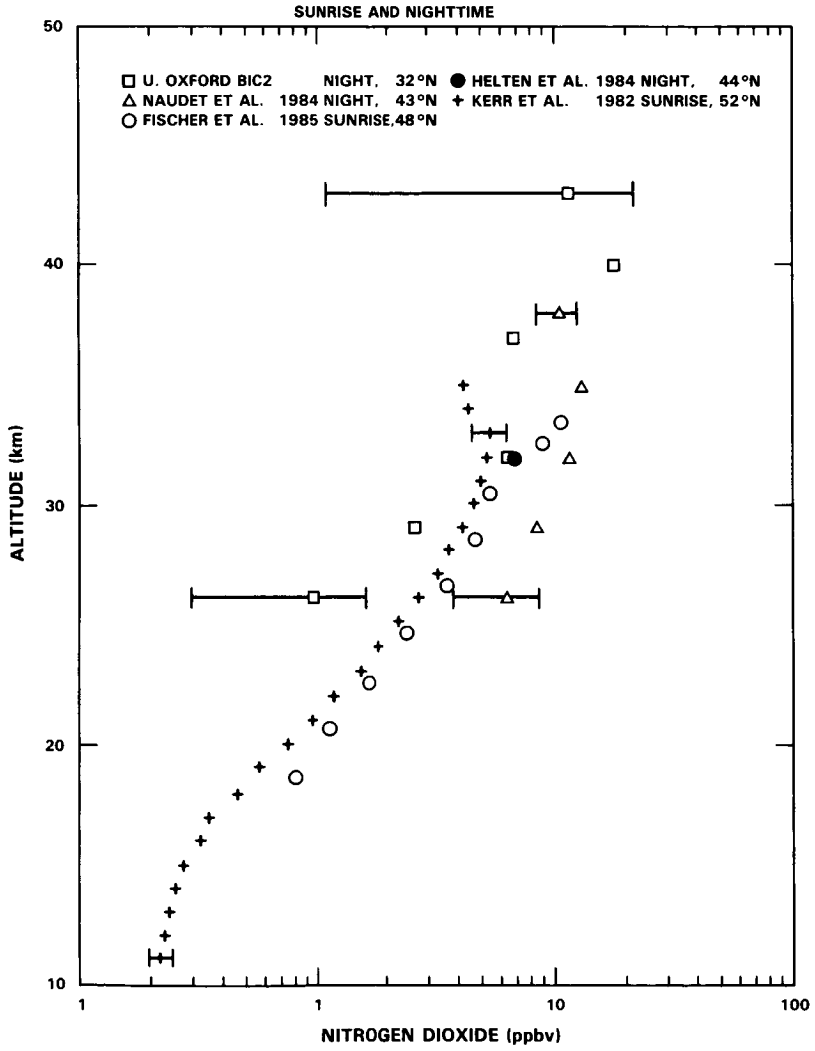

Figure 10-11. Nighttime and sunrise observations of NO_2 from all latitudes.

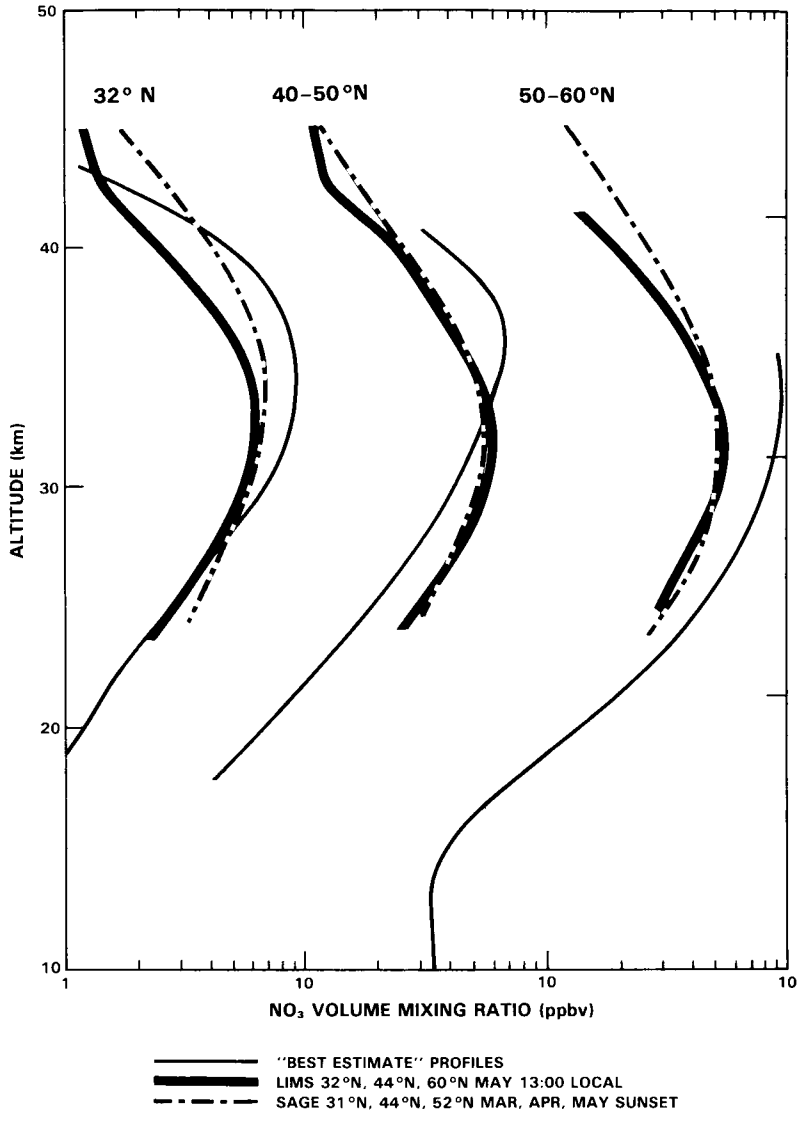

Figure 10-12. Best estimate of NO_2 profiles in three latitude ranges from non-satellite techniques compared with observations by the satellite-borne instruments LIMS and SAGE.

10.1.3 Nitric Acid (HNO_3)

A nearly complete listing of balloon-borne measurements of stratospheric HNO_3 profiles is given in Table 10-3. Most of the measurements have been performed with remote sounding instruments. The compilation also includes measurements with the filter collection and ion-sampling techniques. The list of University of Denver (DU) measurements and Atmospheric Environment Service (AES) measurements is not complete.

The two Balloon Intercomparison Campaigns (BIC) provided a good comparison for understanding instrumental differences. Firstly, some systematic errors were discovered. The profile measured by the ONERA grille spectrometer exhibits significantly greater concentrations in the lower stratosphere than those measured by other instruments (errors could be as large as 50%). The absence of spectroscopic

Table 10-3. Measurements of Profiles of HNO_3 from Balloons

O=solar occultation
E=thermal emission

SS=sunset

BIC 1=Sep/Oct 82, 32°N, SS
BIC 2=Jun 83, 32°N, SS

Groups	Instrument	Flights	References
AES	Filter	Jul 74, 59°N	Evans *et al.* 1976
AES	radiometer,	Aug 76, 51°N	Ridley *et al.* 1984
AES	880cm^{-1}, E	Feb 77, 8, 9, 54°N	Ridley *et al.* 1984
AES	ascent	BIC 1+2	—
Denver U	ascent	May-Nov 70, 33°N	Murcray *et al.* 1973
Denver U	ascent	71-75, 64°N	Goldman *et al.* 1976
Denver U	Cooled spectr,	June 74, 33°N	Murcray *et al.* 1983
Denver U	880cm^{-1},E,asc.	BIC 1+2	
NPL	Interfer, far IR	Sep 74, 44°N	Harries *et al.* 1976
NPL	Cooled spectr,	May 81, 32°N	Louisnard and Pollitt, 1985
NPL	880cm^{-1},E	BIC 1+2	—
Wuppertal	Cooled spectr.	Sep 83, 44°N	Rippel 1984a, b
GHSW	880cm^{-1},E		
Met Inst.	Filt radiometer	Feb 79, 32°N, SS	Fischer *et al.* 1985a
Munich	880cm^{-1},O	May 79, 32°N, SS	Fischer *et al.* 1985a
NOAA	Spectrometer,	Jun 82, 32°N, SS	Weinreb *et al.* 1984
Washington	880cm^{-1},O		
Denver U	Interferometer,	Mar 81, 33°N, SS	Goldman *et al.* 1984c
Denver U	880cm^{-1},O	BIC 2	—
ONERA	Grille spectr,	May 78, 44°N, SS	Borghi *et al.* 1983
ONERA	1325 cm^{-1},O	Apr 79, 32°N, SS	Girard and Louisnard, 1984
ONERA	1325 cm^{-1},O	Sep 80, 44°N, SS	Louisnard *et al.* 1983
ONERA	1325 cm^{-1},O	BIC 2	—
MPIH	Ion measure	Nov 77, Oct 82+3, 44°N	Arnold and Qui, 1984
MPIH	*in situ*	1984, 48-50°N	Knop and Arnold, 1985
NCAR	Cellulose	Spring 71, 34S-64°N	Lazrus and Gandrud, 1974
NCAR	filters,	Spring 72, 34S-64°N	Lazrus and Gandrud, 1974
NCAR	*in situ*	Spring 73, 34S-32°N	Lazrus and Gandrud, 1974

line parameters at 1320 cm^{-1} is probably responsible for this discrepancy, since the temperature dependence of the absorption is unknown. The laboratory calibration which was used is now under reinvestigation. The AES group has improved their data evaluation procedure by taking into account the CFC-11 and CFC-12 absorption. This increased the HNO_3 mixing ratio retrieved below 20 km by 1×10^{-9}; above 20 km, the increase decreases linearly to zero at 30 km (Evans, private communication). All previous profiles published by the AES group must be similarly corrected. Secondly, after reanalysis,

the profiles measured by different instruments in the campaigns showed agreement within ± 30%. However, not all groups listed in Table 10-3 were able to participate in the BIC intercomparisons. Thus it is not clear how much of the remaining differences are caused by instrumental effects including data processing. As stated in WMO 1981 the *in situ* measurements of Lazrus and Gandrud (1974) yield lower HNO_3 values than the other techniques, in particular in the lower stratosphere. The reason for this discrepancy has still not been found.

Due to the known latitudinal variation of HNO_3, the balloon-borne measurements are divided into sets made in different latitude ranges. A large number of the profiles were measured at 32 °N. Since no noticeable change in the HNO_3 concentration as a function of the time of the day has been observed and, since there is no evidence to support a significant seasonal variation at latitudes less than 40 °N (Murcray *et al.*, 1975; Coffey *et al.*, 1981a), the balloon profiles measured at 32 °N should be comparable. Several groups have measured similar HNO_3 profiles at 32 °N at different times and in different years (e.g. NPL, Met Inst., Munich). Figure 10-13 shows a selection of typical profiles from different groups. The agreement between all of the profiles is good around 25 km. The high HNO_3 values of the ONERA profile below 24 km are suspect as discussed above. The University of Denver profile measured during BIC 2 is representative of profiles measured during this campaign and can therefore be used for comparison with the other results. Above 30 km most of the profiles show a rapidly decreasing HNO_3 concentration; only the NOAA group have deduced high values, but with large error bars (Weinreb *et al.*, 1984).

All measurements available for 40-50 °N are presented in Figure 10-14. Most of them were measured in the autumn. The large discrepancy between remote sounding and filter collection results is obvious

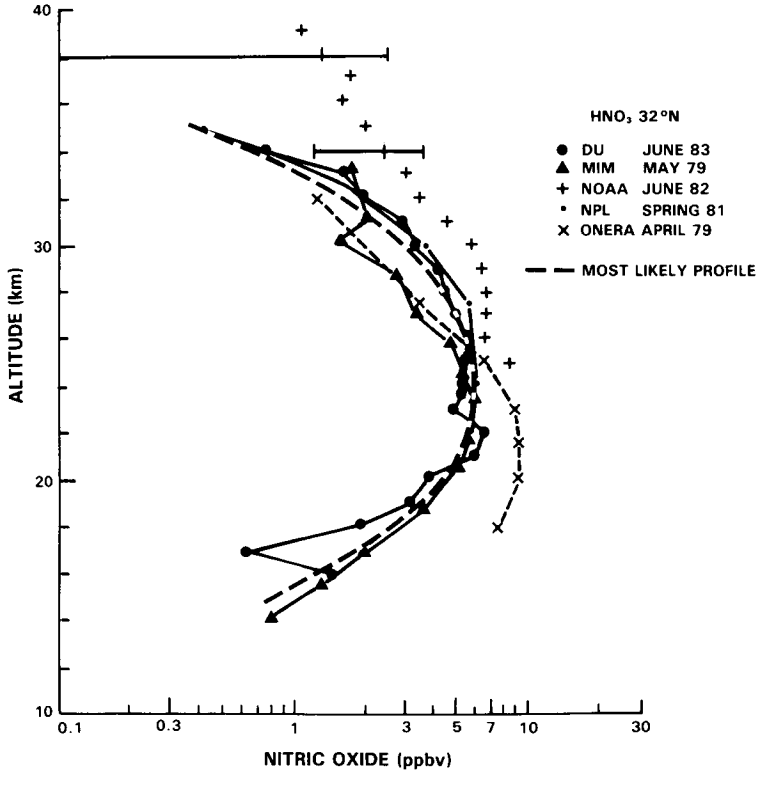

Figure 10-13. Observed HNO_3 profiles from a number of groups near 32 °N latitude.

while the HNO_3 values evaluated from measurements with the ion technique agree with the remote sounding results. The Wuppertal measurements with a cooled grating spectrometer show relatively high HNO_3 mixing ratios at levels above 30 km; possibly because these measurements were made after the El Chichon eruption and the radiance measurements may be contaminated by aerosol emission.

A comparison between Figures 10-13 and 10-14 shows that the HNO_3 values at the maximum and in particular above the maximum are greater at 40-50 °N than at 32 °N. This was already noted by Louisnard *et al.* (1983, ONERA) who have carried out measurements at 32 °N and 44 °N.

At high latitudes, HNO_3 profiles have been measured by two groups, in the latitude belt between 50 °N and 55 °N by AES and around 64 °N by University of Denver (Figure 10-15). A comparison between a summer profile at 51 °N and a profile at 54 °N averaged from two measurements in February 1978 and February 1979 shows clearly the seasonal variations at these latitudes (Ridley *et al.*, 1984). It should be recognized that the increase of the HNO_3 mixing ratios takes place at all altitudes. A similar picture of the seasonal changes is given by the averaged profiles at 64 °N (D. Murcray, private communication). A comparison of the results of the two groups below the HNO_3 maximum shows a considerable difference (see Figure 10-15). The difference appears to be consistent with the rapid increase of the vertical column amount with increasing latitude.

Some of the spread in the HNO_3 profiles is due to atmospheric variability. This is illustrated by the results of several groups which have performed measurements at different times at the same location. Thermal emission measurements at different azimuth directions have shown significant differences around 29 km which lead to the conclusion that there is a mesoscale spatial variability in HNO_3 concentration (Pollitt, *et al.*, 1984).

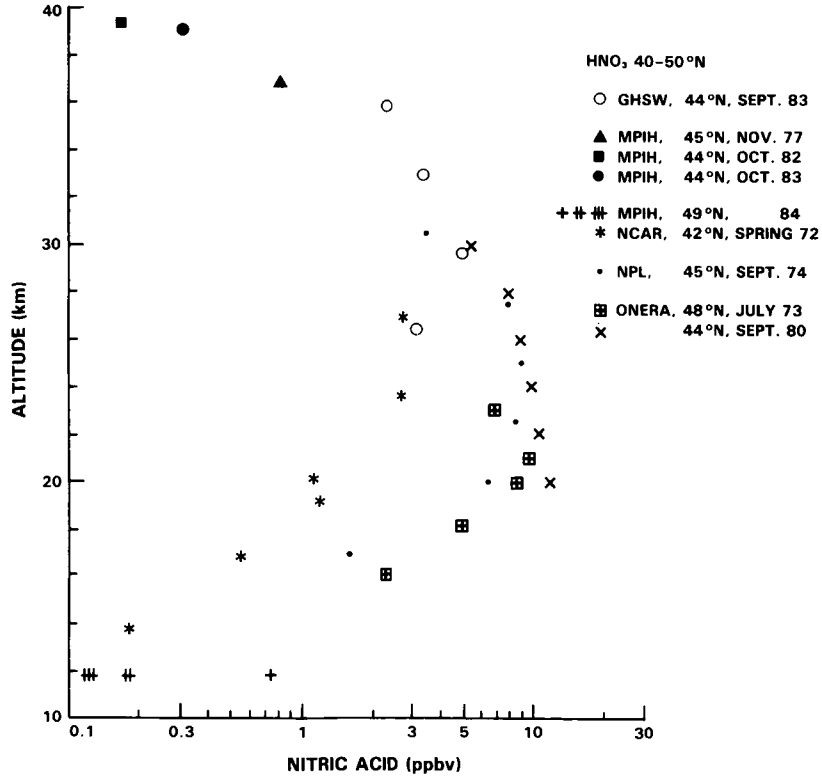

Figure 10-14. HNO_3 observations in the 40 to 50 °N latitude range.

The most likely profile for HNO_3 at 32 °N is deduced from the data presented in Figure 10-13, not taking into account the more suspicious points of the ONERA and the NOAA profiles.

Our knowledge of the HNO_3 profile has increased since the WMO assessment report of 1982. The balloon measurements have contributed to this in the following way:

1. Most of the more recent balloon measurements have confirmed that calculations overestimate HNO_3 concentrations above 25 km. The balloon measurements show HNO_3 mixing ratios above 32 km which are on average lower than the LIMS satellite measurements.

2. Taking into account our more recent experience about systematic errors in some of the balloon results, some features of the latitudinal variation in the HNO_3 profile become obvious. Between 32 °N and 45 °N the HNO_3 mixing ratios increase with latitude at and above the altitude of maximum mixing ratio. Between 45 °N and 64 °N there is a distinct increase of HNO_3 mixing ratios with latitude in the lower stratosphere.

3. The seasonal variation has been identified at latitudes above 50 °N. The HNO_3 mixing ratios are larger at all altitudes in winter than in summer.

4. HNO_3 profiles show spatial variability at 32 °N in the altitude region around 30 km.

5. Several HNO_3 profiles measured during ascent show a layered structure. At the moment it is not clear whether this structure is real or an artifact of the data evaluation.

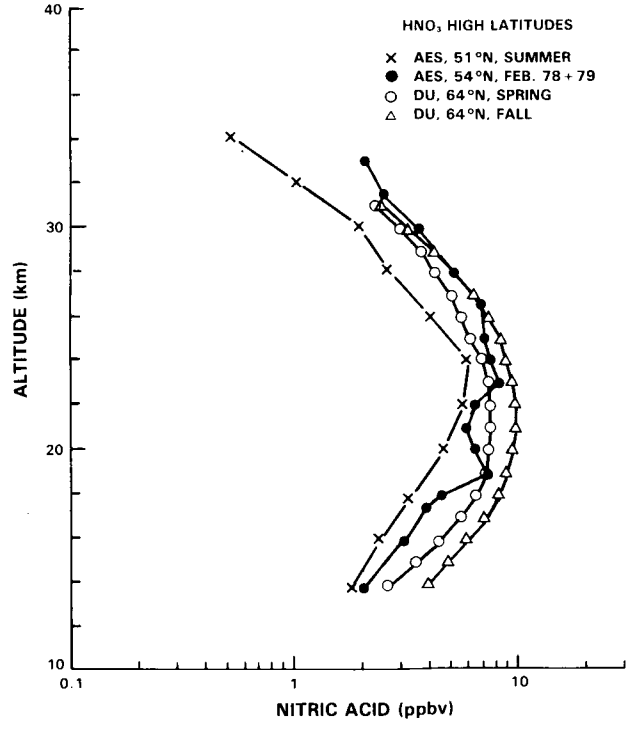

Figure 10-15. High latitude observations of stratospheric HNO_3.

10.1.4 Nitrous Oxide (N_2O)

Our understanding of the behavior of stratospheric N_2O has not changed substantially since the WMO 1981 assessment. There is a rapid decrease in mixing ratio with altitude and, at a given altitude above the tropopause, there is less N_2O at midlatitudes than at the equator. Figure 10-16 shows mean curves drawn through the observations represented in WMO 1981 for tropical and midlatitude conditions. Also shown in Figure 10-16 are the more recent measurements by an infrared grille spectrometer flown on Spacelab (Laurent *et al.*, 1983, Ackerman *et al.*, 1985). These solar occultation measurements, applicable to 43 °N latitude, support the rapid decrease in N_2O amount above about 20 km and extend the measurements to more than 50 km.

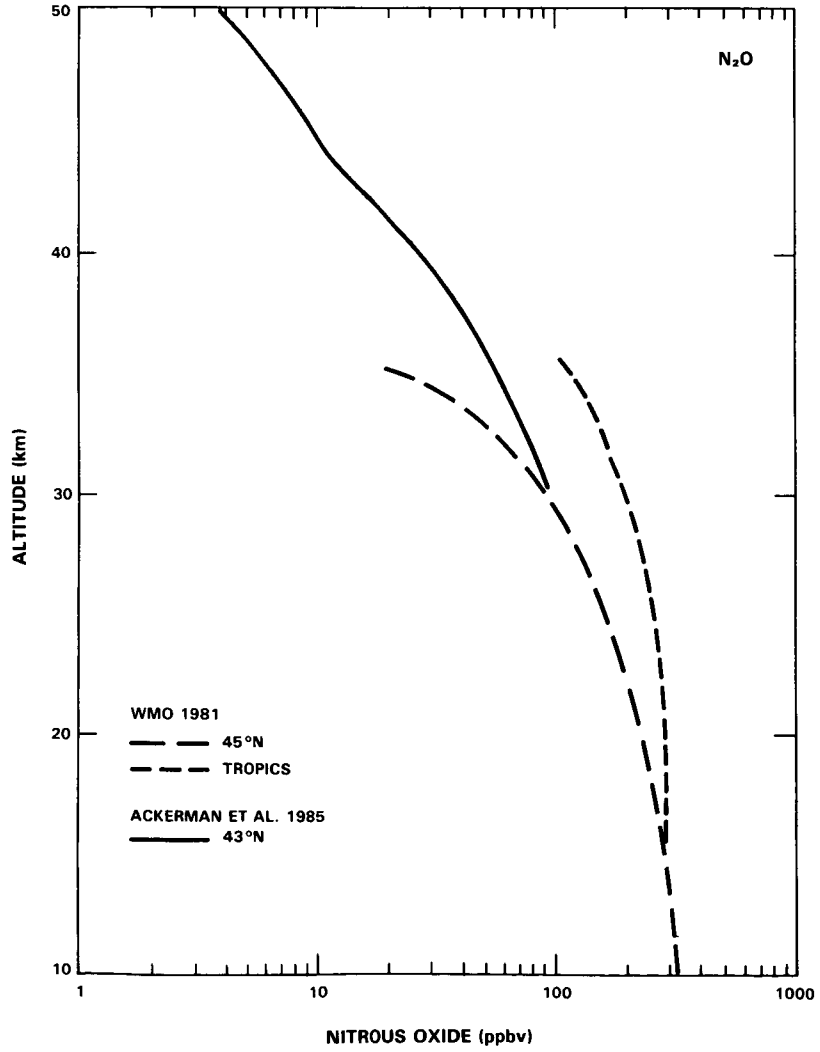

Figure 10-16. Observed stratospheric N_2O profiles.

10.1.5 Nitrogen Trioxide (NO_3)

Visible absorption spectroscopy near 600 nm with the moon or a star as a light source is used to measure NO_3 in the stratosphere. As there is still some uncertainty in the absorption cross section the results have been scaled to a value that is assumed to be temperature independent: 1.7×10^{-17} cm^2 given by Ravishankara and Wine (1983).

The total column abundance at night has been measured over a 5 year period at 40 °N from a ground-based station by Norton and Noxon (1985). They observed a maximum of stratospheric NO_3 in April/May and usually found it to be below their detection limit during the rest of the year. The latitudinal variation of the NO_3 column abundance (Norton and Noxon, 1985) is shown in Figure 10-17.

Nighttime profiles at 44 °N have been obtained from a balloon platform at 38.8 km in fall 1980, 1981, 1983 and in spring 1982 (Rigaud *et al.*, 1983; Pirre *et al.*, 1985) looking at the setting star Arcturus or at the rising planet Venus (Figure 10-18).

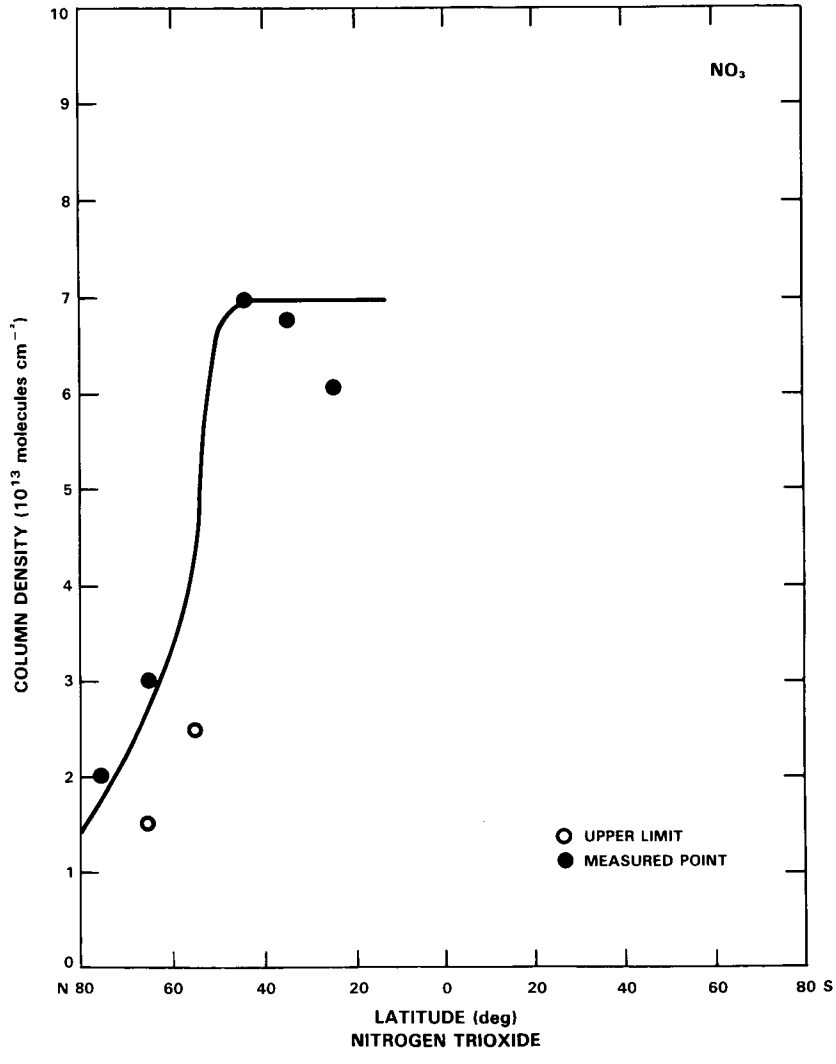

Figure 10-17. Latitude variation during Spring of column abundance of NO_3 from ground-based visible absorption spectroscopy.

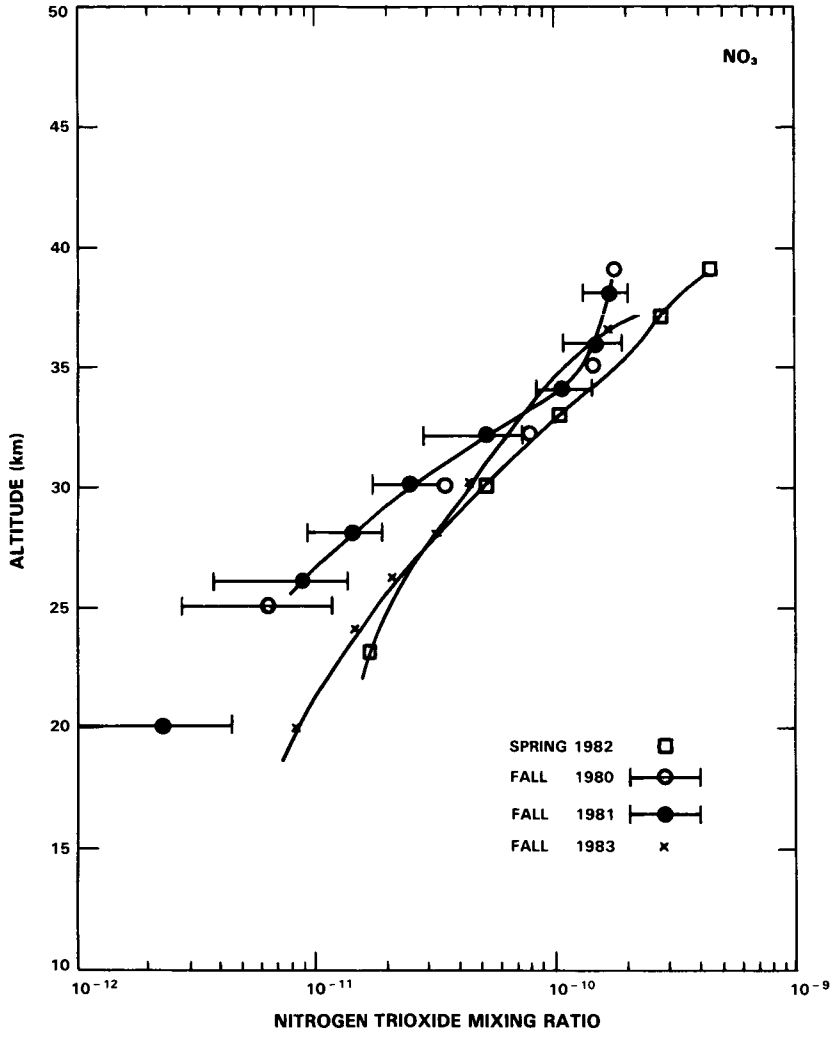

Figure 10-18. Nighttime profiles of NO_3 near 44°N.

In situ diurnal variations at sunrise have recently been measured by Helten *et al.* (1984b) using matrix isolation and electron spin resonance spectroscopy from a balloon platform at 32.7 km. The nighttime mixing ratio is 2×10^{-10}. About 30 minutes before sunrise the mixing ratio decreases to a value below 2×20^{-11} (the detection limit). These values tend to be about a factor of two larger than those from visible spectroscopy.

10.1.6 Dinitrogen Pentoxide (N_2O_5)

This important molecule still has not been definitively measured in quantitative manner in the stratosphere. A tentative measurement by Roscoe (1982) suggests a mixing ratio of $1.2 \pm 0.5 \times 10^{-9}$ at 32 km. Both the profile, shown in Figure 10-19 and the measured nighttime increase are fully consistent with predictions by the model of Fabian *et al.* (1982a). The recent first mission of the ATMOS spectrometer has yielded a clear detection of N_2O_5, though data are not available at the time of writing this report.

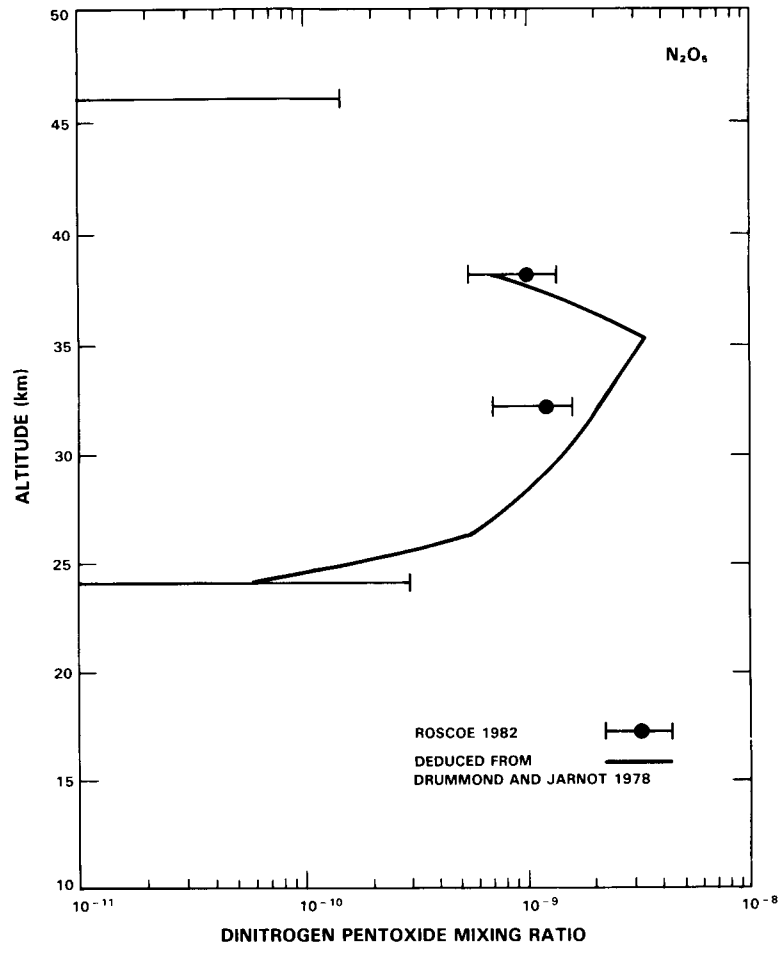

Figure 10-19. Tentative observation of stratospheric N_2O_5 near 32°N.

Fabian *et al.* (1982a) deduced N_2O_5 from the change of daytime [NO + NO_2] to nighttime [NO_2] measured by Drummond and Jarnot (1978). Although the deduced profile is fully consistent with that measured by Roscoe (1982), the error bar is large enough to encompass zero. Similarly, measurement of the nighttime decay of NO_2 by Roscoe *et al.* (1985b) is consistent with the N_2O_5 of Roscoe (1982), but again with a large error bar (see Section 10.2.2). For the purpose of deriving N_2O_5, measuring the change in NO_2 during the night should be more accurate than measuring the change in NO plus NO_2 across sunrise since the total error must be smaller.

The column of N_2O_5 can be deduced from changes in the columns of NO_2 and NO from sunrise to sunset. These have been measured by Coffey *et al.* (1981a), Ridley *et al.* (1984), and by Girard *et al.* (1983).

10.1.7 Chlorine Nitrate ($ClONO_2$)

This important stratospheric molecule still has not been definitively detected. However, tentative detections have been reported by the University of Denver group (Murcray *et al.*, 1979; Rinsland *et al.*, 1985b). If confirmed, these measurements would correspond to a mixing ratio of $1.1 \pm 0.7 \times 10^{-9}$ at 28 km. For a more detailed discussion, see Chapter 11, Section 11.3.

10.1.8 Peroxynitric Acid (HNO_4)

Although this molecule awaits a definitive detection in the stratosphere, the University of Denver group have observed a weak feature, just above noise level, at the frequency of one of its Q-branches near 802 cm^{-1} (D. G. Murcray, private communication). Assuming the line intensity measured by Molina (private communication) this would correspond to an upper limit of 0.5×10^{-9} at 28 km.

10.1.9 Hydrogen Cyanide (HCN)

Hydrogen cyanide is present in the stratosphere as a result of surface emission due to biomass burning and industrial activity (Cicerone and Zellner, 1983). According to the observations by Rinsland *et al.* (1982a), the tropospheric mixing ratio of HCN is of the order of $170 \pm 50 \times 10^{-12}$. The observations of Coffey *et al.* (1981b) and Carli *et al.* (1982) indicate a slightly lower mixing ratio in the stratosphere.

10.1.10 Methyl Cyanide (CH_3CN)

Methyl cyanide (or acetonitrile) has been postulated to be one of the ligands of positive stratospheric ions (Arnold *et al.*, 1978; Arnold and Henschen, 1978) and should thus be present in the atmosphere. The stratospheric abundance of this molecule has been inferred from balloon and rocket borne ion mass spectrometric observations; the deduced mixing ratio is smaller than 10×10^{-12} above 25 km.

10.1.11 Latitudinal, Diurnal and Seasonal Variations

Most non-satellite observations of stratospheric NO_x reported since the 1981 WMO assessment have not substantially altered our understanding of latitudinal and seasonal variations in NO, NO_2, and HNO_3. An important exception to this general statement is provided by balloon data characterizing high latitude NO variations.

Observational techniques that lend themselves to latitudinal surveys or long term monitoring for seasonal variation are ground- and aircraft-based, and, more recently, the extensive temporal and spatial measurements by satellite-borne instruments. Various techniques are summarized in Table 10-4.

No *in situ* measurement surveys of NO versus latitude have been made since the 1981 WMO assessment. The measurements of Loewenstein *et al.* (1978b) reproduced in Figure 10-20 still represent our best understanding of the variation of NO concentration versus latitude at a pair of selected altitudes.

Figure 10-21 shows the column measurements of NO. Open symbols represent data reported at the time of WMO 1981; closed symbols represent measurements reported since the 1981 assessment. Measurements since 1981 were during summer or early autumn conditions and tend to support a nearly uniform distribution of the NO column between the equator and 70 °N in summer with a value near 3×10^{15} molecules cm^{-2}.

The difference in magnitude between the NO column derived by Girard *et al.* and those derived by Coffey *et al.* is probably not significant, as their error bars overlap. Mean NO vertical profiles from summer and autumn measurements at three latitudes (Section 10.1.1) show no significant variation with latitude and indicate a symmetric distribution in the two hemispheres. One may integrate the mean profile, assuming no NO above 52 km to derive a vertical column. This yields a column amount of 3.95×10^{15} molecules cm^{-2}, and is plotted in Figure 10-21 at the three latitudes of those measurements; 38 °N, 51 °N and 34 °S.

Table 10-4. Techniques for Observation of Latitudinal and Seasonal Variations of NO, NO_2 and HNO_3

Investigator	Technique	Molecule	Accuracy
Loewenstein *et al.* (1978b)	aircraft *in situ* chemiluminescence	NO 18.3, 21.3 km	±25%
Rinsland *et al.* (1984b)	ground-based	NO	
Noxon (1979a)	ground-based vis. absorption spectrometer	NO_2	±20%
McKenzie and Johnston (1982)	"	NO_2	±20%
Syed and Harrison (1981)	"	NO_2	±20%
Elansky *et al.* (1984)	"	NO_2	±20%
Coffey *et al.* (1981a)	aircraft IR Fourier transform spectrometer	NO NO_2 HNO_3	±20% ±20% ±20%
Girard *et al.* (1978/79)	aircraft IR Grille spectrometer	NO NO_2 HNO_3	±30% ±15% ±25%
Murcray *et al.* (1975)	aircraft IR emission	HNO_3	±25%

Profile measurements reported since the 1981 assessment for nitric oxide at high latitude in winter and summer (Ridley *et al.*, 1984, to be published, 1986) have confirmed a decrease of NO mixing ratio in winter below 28 km. The 1981 interpretation of a decrease in NO column north of 50 to 60 degrees in winter remains unchanged.

Previous observations of the NO_2 column abundance established a diurnal variation from sunrise to sunset of about a factor of two (Noxon, 1979; Syed and Harrison, 1981), presumably due to photolysis of N_2O_5 and $ClONO_2$ formed at night. Since NO_2 and NO are in photochemical equilibrium in the sunlit atmosphere, a substantial diurnal increase in NO should also be anticipated.

The early measurements of Girard *et al.* (1978/79) showed no diurnal change in NO. Results for NO are not reported for subsequent flights of the Girard spectrometer in STRATOZ 1 and 2. Further comparison of NO columns measured by Coffey and Mankin confirms that NO increases by a factor of two between early morning and late afternoon. Note that their measurements, while close to sunrise or sunset,

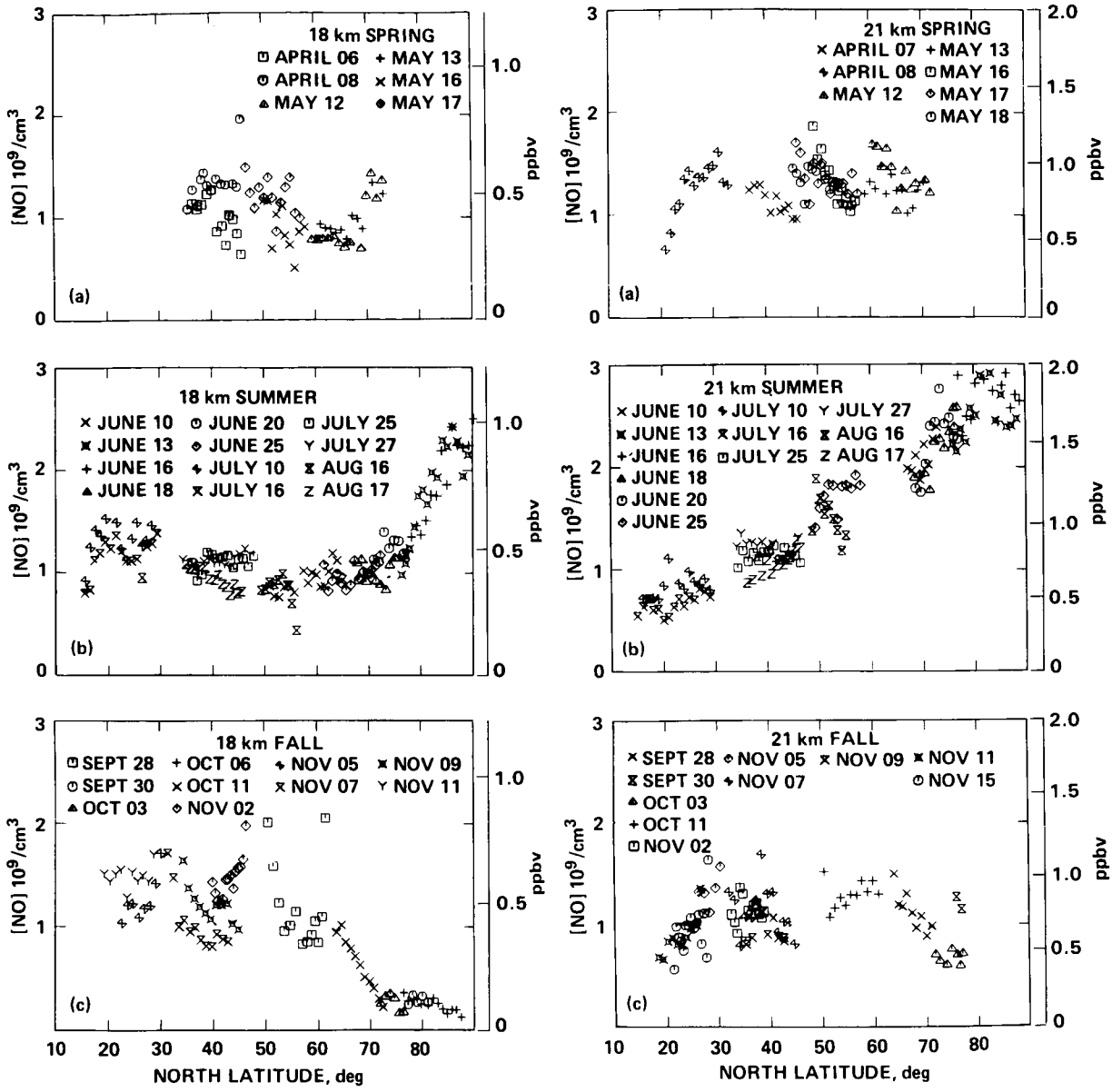

Figure 10-20. Variation of NO at 18 and 21 km versus latitude and season (Loewenstein *et al.*, 1978a, b).

are made when the solar zenith angle is in the range 75 to 85°. Roscoe *et al.* (1985a, b) have also observed diurnal changes in NO and NO_2 profiles, as discussed in section 10.3.2.

A number of important developments have occurred since the 1981 WMO assessment in the observation of stratospheric NO_2. Firstly, three exciting data sets have become available from satellite-borne limb viewing instruments, discussed in Section 10.2. Secondly, long term ground-based measurements of stratospheric NO_2 columns have been reported by Elansky *et al.* (1984) at 44°N, Syed and Harrison (1981) at 50°N and by McKenzie and Johnston (1982) at 45°S. Since the 1981 assessment further latitudinal measurements of NO_2 column amounts have been made by the aircraft mounted instruments of Girard *et al.* and Coffey *et al.*

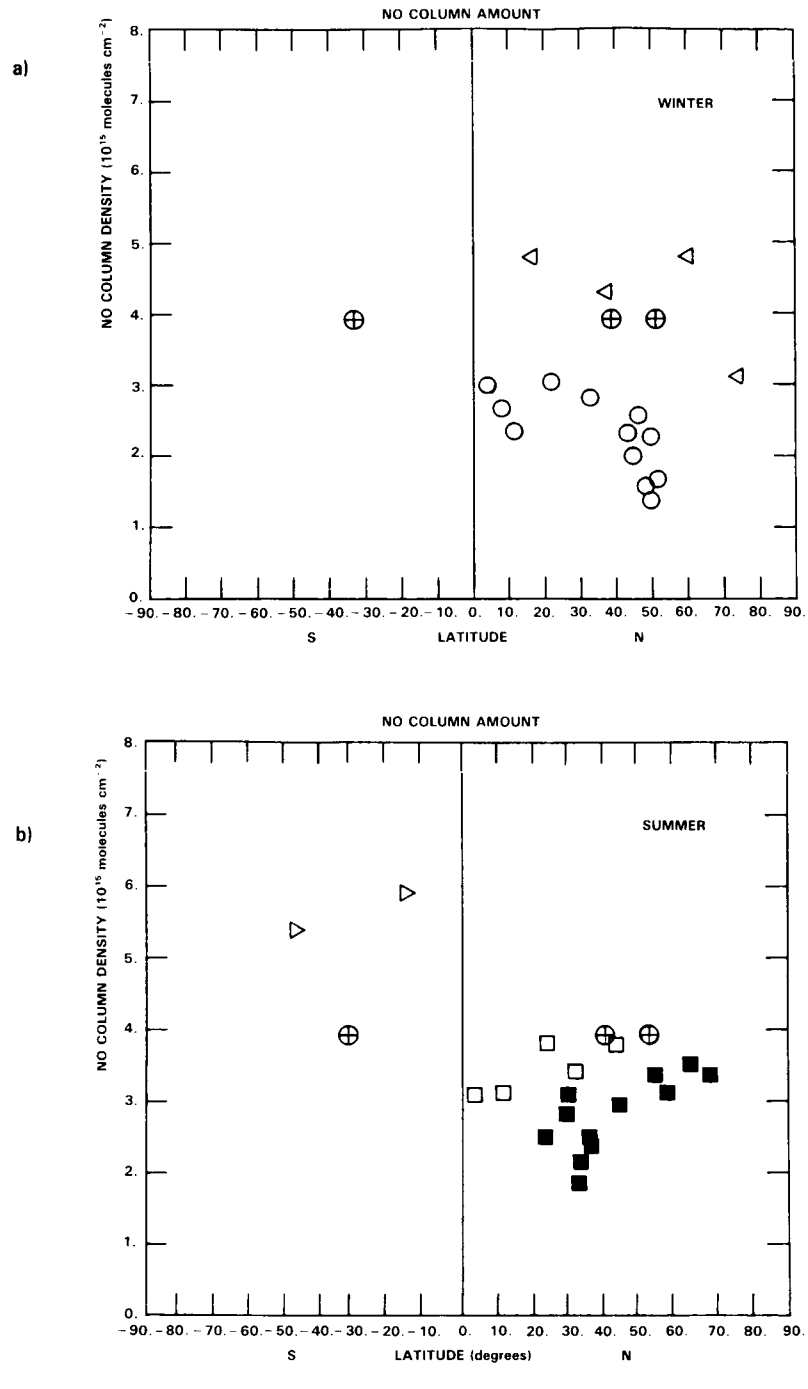

	(a)	(b)
Girard *et al.*, 1978/79:	◁ - winter;	▷ - summer
Coffey *et al.*, 1981:	○ - winter;	□ - summer
Coffey *et al.*, 1985:		■ - summer
Integral of mean profiles:	⊕ - summer and winter	

Figure 10-21. Vertical column of daytime stratospheric NO versus latitude.

The main features of the latitudinal distribution of NO_2 are not changed from that presented in WMO 1981. A general increase occurs with latitude in both hemispheres in winter and summer up to near 30 degrees of latitude. At higher latitudes a sharp decline is observed in winter NO_2 columns. Figure 10-22 shows NO_2 vertical columns for sunset conditions from a number of sources. Open symbols are from the 1981 WMO assessment, solid symbols are observations reported since 1981.

As has been observed by Noxon and others, the NO_2 vertical column may change by as much as a factor of two in the time span of a few days at a given location. This effect probably accounts for much of the spread of observed NO_2 columns between 40 and 60 °N latitude in Figure 10-22.

Extensive ground-based measurements of NO_2 have been reported. Figure 10-23 shows the variation over a year for a number of latitudes. The pioneering work of Noxon has been supplemented by studies near 50 °N (Syed and Harrison, 1981) and at 45 °S (McKenzie and Johnston, 1982) latitudes. Column measurements at 43.7 °N from 1979-1984 by Elansky *et al.* (1984) show a behavior very similar to the 40 °N panel of Figure 10-23.

The behavior is consistent at all latitudes with a minimum column in winter and a maximum in summer with a less pronounced annual variation near the equator, as expected.

The basic features of the latitudinal and seasonal variations of HNO_3 are not substantially different from those described in WMO 1981. Since the 1981 assessment a wealth of data has become available from the infrared radiometer LIMS on the Nimbus 7 satellite, and is discussed in Section 10.2.

There is a strong increase in the vertical column of HNO_3 with increasing latitude in both hemispheres. Figure 10-24 shows the results from a number of investigations. The measurements indicate that there may be an asymmetry about the equator with a steeper increase with latitude in the Southern Hemisphere.

There appears to be a decreasing gradient in column HNO_3 at high latitudes in summer. Above about 50 degrees latitude in the Northern Hemisphere and 30 degrees latitude in the Southern Hemisphere, the summertime HNO_3 column amounts reported by Murcray *et al.* (1975, 1978) and Coffey *et al.* (1985) do not increase with latitude as they do in the lower latitudes and at higher latitudes in winter.

Aircraft and ground-based measurements have shown no evidence for a diurnal change in HNO_3 columns.

10.2 SATELLITE DATA

Introduction

Satellite observations of the global distributions of several of the nitrogen species are one of the major recent developments in the study of the stratosphere. Since 1981 there have been presentations of three sets of observations of NO_2, one of HNO_3 and one of N_2O. These must be regarded as major technical and scientific achievements, since these gases are present in concentrations from a few to a few hundred parts per billion by volume (ppbv). These observations provide a wealth of information on the temporal and spatial variations of these species that was not previously available.

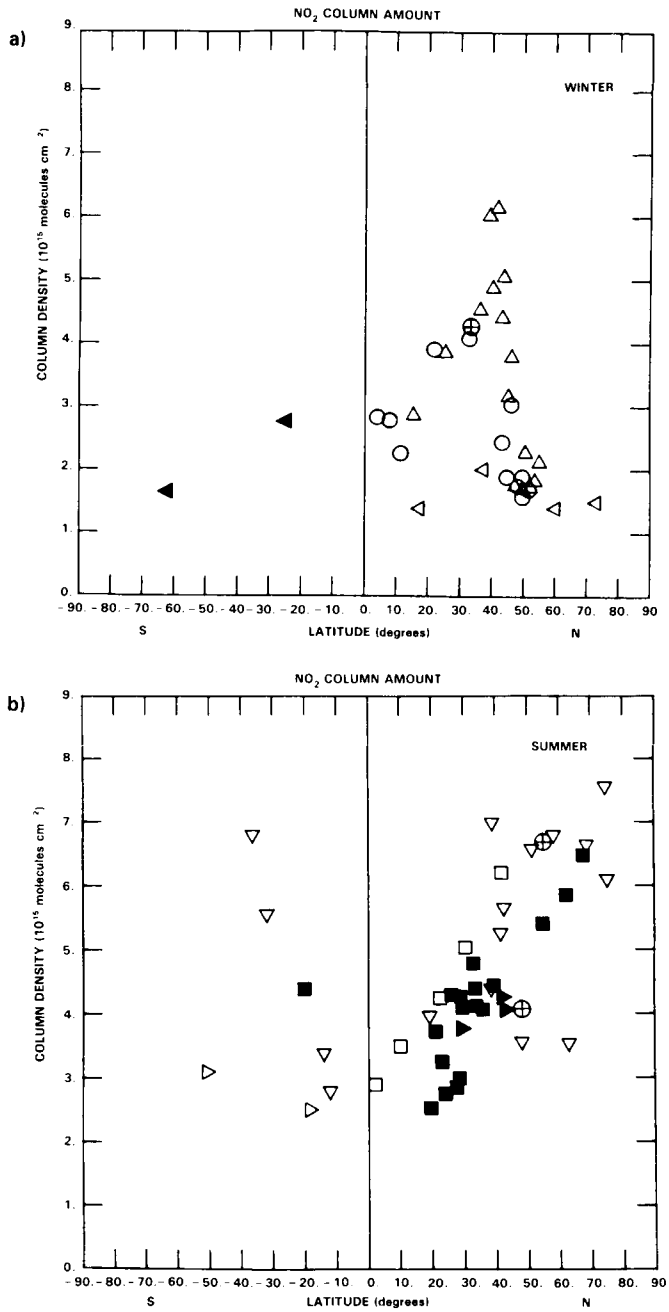

	(a) winter	(b) summer
Girard *et al.*, 1978/79:	◁ - winter;	▷ - summer
Girard *et al.*, 1983:	◀ - winter;	▶ - summer
Noxon, 1979	△ - winter;	▽ - summer
Coffey *et al.*, 1981a	○ - winter;	□ - summer
Coffey *et al.*, 1985:		■ - summer

Integral of WMO 1981 profiles: ⊕ - winter and summer

Figure 10-22. Vertical column of daytime NO_2 versus latitude.

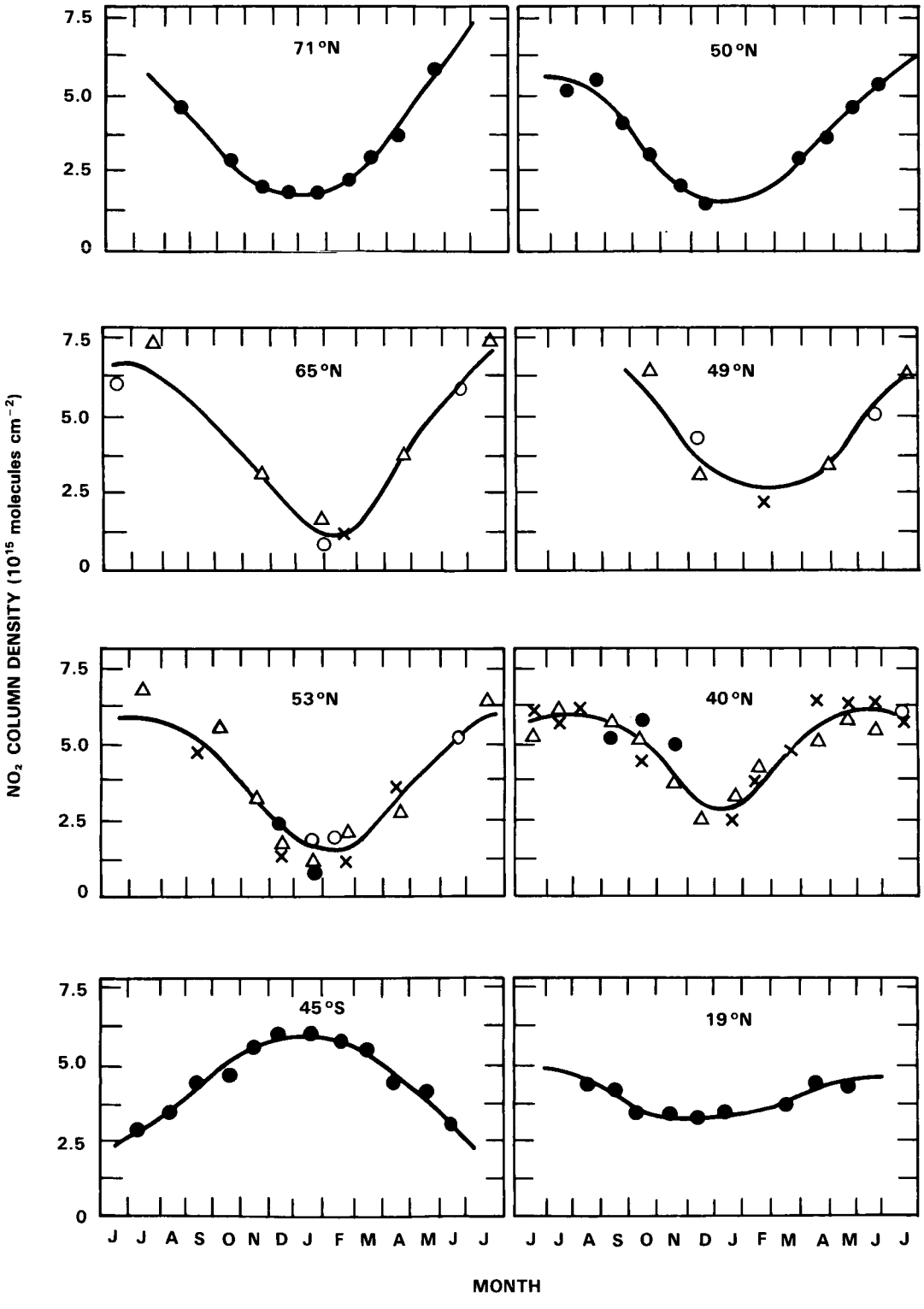

Figure 10-23. Variation over a year of the daytime NO_2 vertical column at various latitudes. Latitude 50°N is from Syed and Harrison (1981), 45°S is from McKenzie and Johnston (1982), all other latitudes are from Noxon (1979) and Noxon *et al.* (1983).

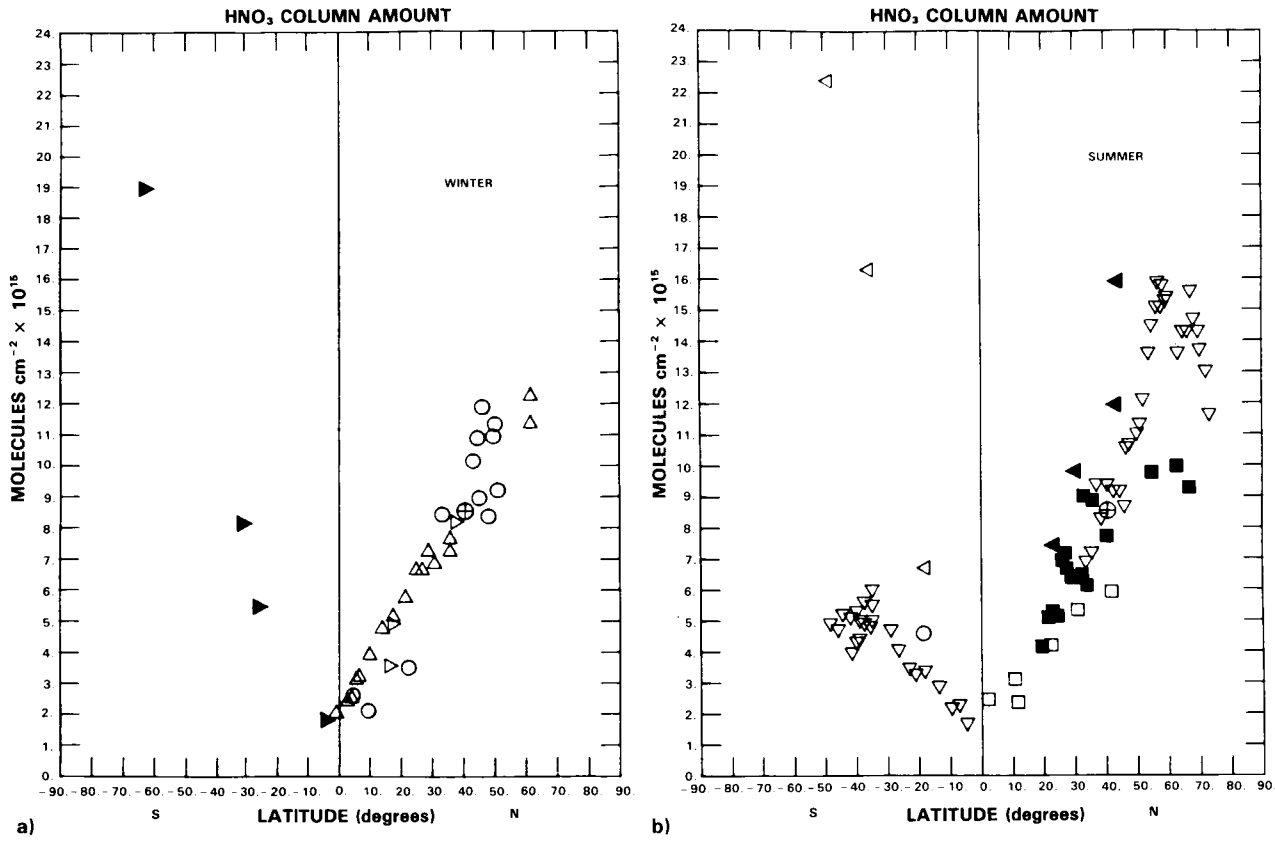

Figure 10-24. Vertical column of stratospheric HNO_3 versus latitude.

	(a) winter	(b) summer
Murcray *et al.*, 1975, 1978:	△ - winter;	▽ - summer
Girard *et al.*, 1978/79:	▷ - winter;	◁ - summer
Girad *et al.*, 1983:	▶ - winter;	◀ - summer
Coffey *et al.*, 1981a	○ - winter;	□ - summer
Coffey *et al.*, 1985:		■ - summer
Integral of WMO 1981 profiles:	⊕ - winter and summer	

In the following section, the experiments and the data validation are briefly described, since most of this has been published. The results of the measurements are then described, with emphasis on the scientific questions which they address, and the uses to which the data can be put.

10.2.1 Nitrogen Dioxide (NO_2)

Measurements of NO_2 have been obtained by three different instruments, LIMS, SAGE and SME, measurements being made at five different local times during the day, using three different techniques. Their results are described below. Because NO_2 varies with time of day, an intercomparison between the measurements is more easily done in conjunction with a model, and is discussed in the modelling section.

10.2.1.1 LIMS Measurements of Nitrogen Dioxide

The LIMS Experiment

The Limb Infrared Monitor of the Stratosphere (LIMS) has been described in the Special Introduction to Chapters 8, 9, 10 and 11. The instrument and its performance in orbit, the data reduction, and examples of the results, are described by Gille and Russell (1984). Earlier descriptions are given by Russell and Gille (1978) and Gille *et al.* (1980a).

Gille and House (1971) mentioned some of the advantages of limb viewing. These include the long horizontal path through the atmosphere, giving greater sensitivity to gases present in trace amounts, and the dark background behind the atmosphere, which aids in signal detection and interpretation. By making measurements in the thermal infrared, observations can in principle be obtained at any local time. The geometry also allows good vertical resolution, if a narrow field of view is used in the instrument and the sampling is sufficiently frequent in the vertical. Because clouds along the line of sight block any signal from the lower atmosphere, the long horizontal path also precludes the soundings from extending into the troposphere on a regular basis.

Two instrumental details affect the data discussed here. To achieve a high radiometric signal to noise ratio with narrow fields of view, the LIMS detectors were cooled to 63 K by a subliming solid methane cryogen. This was designed for a seven-month lifetime, resulting in a LIMS data span from 25 October 1978 to 28 May 1979.

To prevent sunlight from directly entering the LIMS aperture, the instrument viewed off the plane of the orbit. This resulted in latitudinal coverage from 64 °S to 84 °N. The local times of overpass were close to 1 PM and 11 PM over a wide range of latitudes, but changed rapidly at high latitudes near the terminator. These times are shown in Table 10-5.

Table 10-5. Tangent Point Local Time, as a Function of Latitude (From Gille & Russell, 1984)

	Local time. Hours	
Latitude °N	Ascending Part of Orbit	Descending Part of Orbit
80	14.76	21.23
60	13.03	22.97
40	12.85	23.15
20	12.90	23.11
0	13.06	22.94
−20	13.38	22.62
−40	13.97	22.03
−60	15.77	20.24

Each retrieval provides a profile with a vertical resolution of about 3 km. Retrievals were performed every 4 degrees of latitude from 64 °S to 84 °N, resulting in about 1000 profiles per day for the life of the experiment. The results at each latitude were then treated as a time series, and Kalman filtered to provide an optimal estimate of the zonal mean and the amplitudes and phases of the first six harmonics around the latitude circle, as described by Rodgers (1977) and Kohri (1981). This procedure provides data smoothing, in that noise and small scale geophysical features are reduced, and explicitly provides a time interpolation to standard map times, which are taken to be 12 UT daily. These mapped data provide the basis for the data presentations that follow.

Evaluation of the NO_2 Results

The radiances, data reduction, and error assessment for the NO_2 observations are described in detail by Russell *et al.* (1984a). The methods by which the precision and accuracy were assessed are briefly summarised, and some particular features of these data are noted here.

The measured radiance decreases with altitude, eventually approaching the noise level, which sets the upper altitude limit of the retrievals. For single scans of the NO_2 channel, this occurs slightly below 1 mbar (48 km). However, by averaging scans together, altitudes as high as 70 km can be reached (Russell *et al.*, 1984b). The lower limit can be set by clouds, but also by the large opacity in this spectral interval due to water vapour and the pressure induced absorption of molecular oxygen. A calculation of the NO_2 signal coming from a given pressure level indicates poor signal to noise ratio below 30 mbar. The operational retrieval is extended to 100 mbar and below, but these levels are strongly influenced by climatological NO_2 input profiles: data below 30 mbar will not be considered.

At 6.2 μm, the NO_2 channel is on the steep, high frequency end of the Planck function for atmospheric temperatures, and signal strength drops rapidly for low temperatures. During northern winter, the temperatures in the polar region were often so low that no retrievals of single profiles were attempted, resulting in some data loss under those conditions.

The precision (repeatability) has been estimated by a forward propagation of errors, and from the data themselves. Observationally, a series of 7 sequential radiance scans in a meteorologically undisturbed situation were retrieved independently, and the standard deviation calculated. This is a measure of the end-to-end repeatability of the retrievals, and resulted in values between 0.1 and 0.5 ppbv, depending on altitude. Numerical simulations, calculating the response of the retrievals to the random noise sources, radiometer noise, and random temperature errors (from Gille *et al.*, 1984a), are in excellent agreement with the observations. The observational results do not depend to any great extent on the meteorological situation. The results are noted in Table 10-6 below.

The accuracy has been estimated by two complementary methods. Several sources of systematic errors were identified, and their magnitudes estimated. These included errors in the radiometric calibration, in the size of the field of view effects, uncertainties in their removal, errors in the LIMS temperatures and water vapour concentrations which enter into the NO_2 retrievals, and uncertainties in the spectral data for NO_2 and O_2. The effect of these errors on the results was estimated by numerical simulations; the results are shown in Table 10-6.

To make sure that no major source of error had been omitted, and to relate the LIMS results to other measurements which have been made in the past, four balloon underflights to measure NO_2 with spectroscopic instruments were made. All of the measurements were obtained as the sun set, which complicates

Table 10-6. LIMS NO_2 Channel Systematic Error Sensitivity Study

Error Parameter	NO_2 Mixing Ratio Error. %					
	50 mbar	30 mbar	10 mbar (≈ 30 km)	5 mbar	3 mbar	1 mbar (≈ 50 km)
1. Temperature profile. ± 2 K	36	22	14	12	7	8
2. O_2 absorption coefficient. ± 20%	68	37	5	1	0	0
3. H_2O mixing ratio. ± 30%	32	20	10	8	9	30
4. IFOV side lobe integrated area, ± 0.8%	1	2	4	1	2	1
5. NO_2 spectral parameters. ± 10%	10	10	10	10	10	10
6. Retrieval algorithm	5	5	5	5	5	5
7. RSS of 1 through 6 with 6% systematic radiometric error and 5% error due to IFOV removal	84	49	23	20	18	34

The random NO_2 error is estimated to be 10% for 25 mbar < P < 100 mbar; 5% for 3 mbar < P < 25 mbar; 30% for P < 3 mbar

the comparison because of the large diurnal changes in NO_2 concentration. A model was used to adjust the sunset measurements to LIMS overpass times. The mean difference between LIMS and the correlative measurement data in the 5 to 30 mbar region is 15%, which is much smaller than the combined error bars of the balloon determinations and LIMS. The LIMS data were also shown to lie within the envelope of previous measurements presented in WMO 1981 (1982), and with the model results presented there.

Daytime Values

Zonal Cross Sections of NO_2

One of the most straight-forward ways to display the results is as latitude-altitude cross sections of the zonally averaged quantities. In these, the longitudinal variations are averaged out, but the larger variations with altitude and latitude are shown. Similarly, monthly averages are displayed to smooth out short period temporal variations. Distributions under both day and night conditions are presented.

Zonally averaged monthly mean cross-sections of the NO_2 measurements obtained for daytime conditions are presented in Figure 10-25 for the months, October, January, April and May (the closest to northern summer conditions available). Note that the latitudes in daylight vary as the terminator moves with the season.

The standard deviations (in per cent) of the daily cross section values are shown in Figure 10-26 for January and April. The day-to-day variations are < 0.3 ppbv away from the terminator, or < 5% in

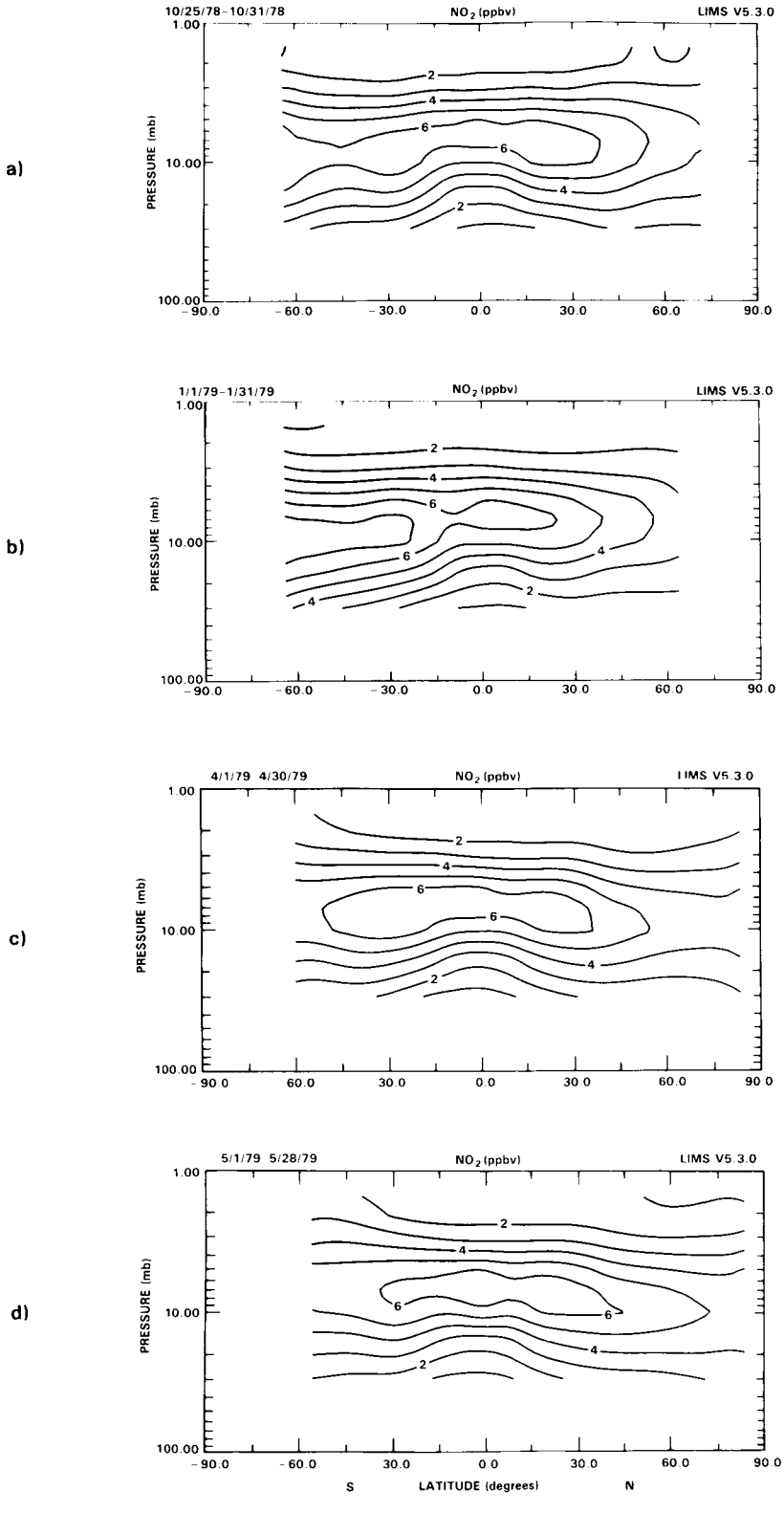

Figure 10-25. Monthly average zonal mean cross-sections of daytime NO_2 for (a) October (last 7 days), (b) January, (c) April and (d) May (first 28 days).

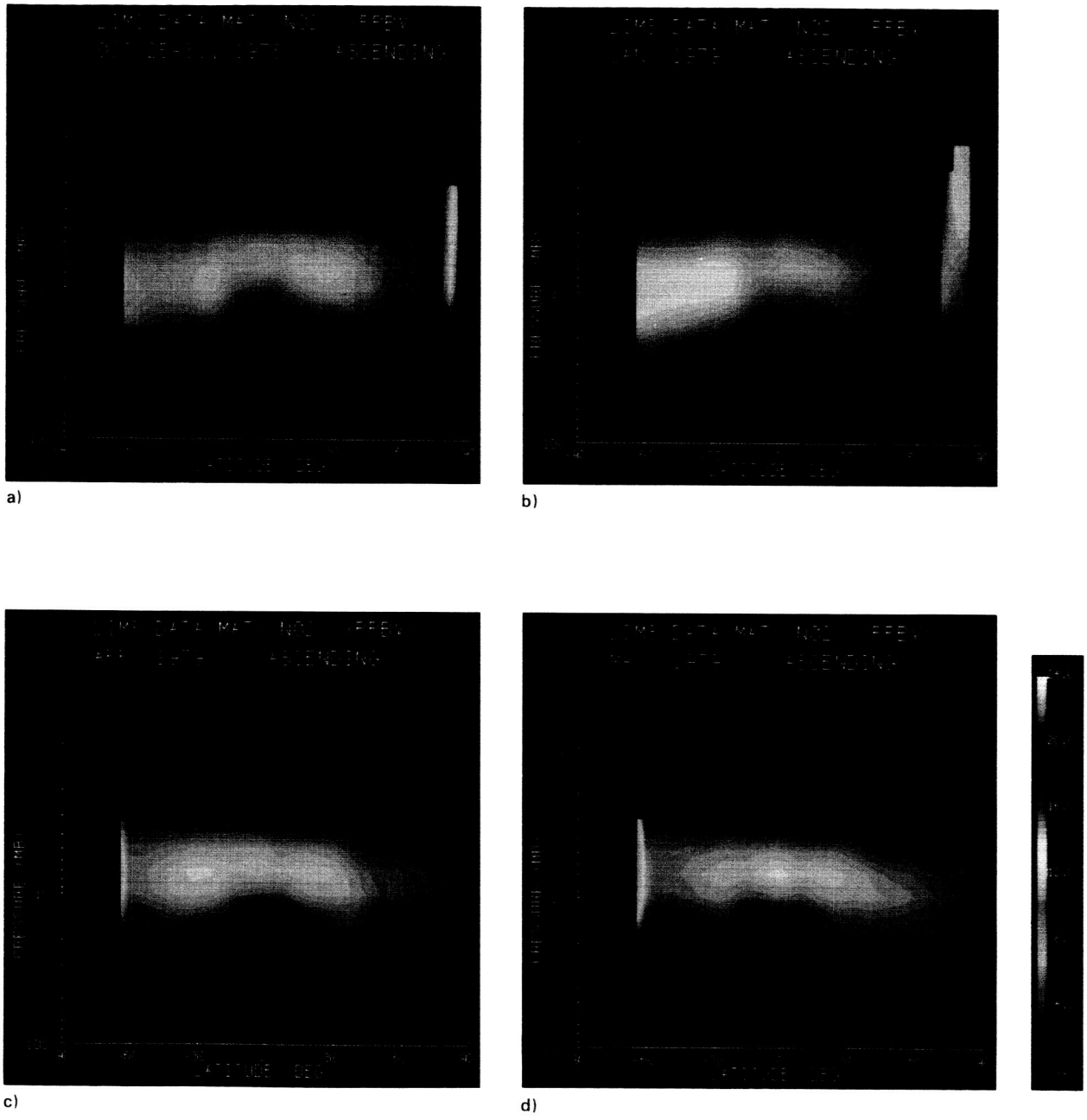

Figure 10-25. (Color) Monthly average zonal mean cross-sections of daytime NO_2 for (a) October (last 7 days), (b) January, (c) April and (d) May (first 28 days).

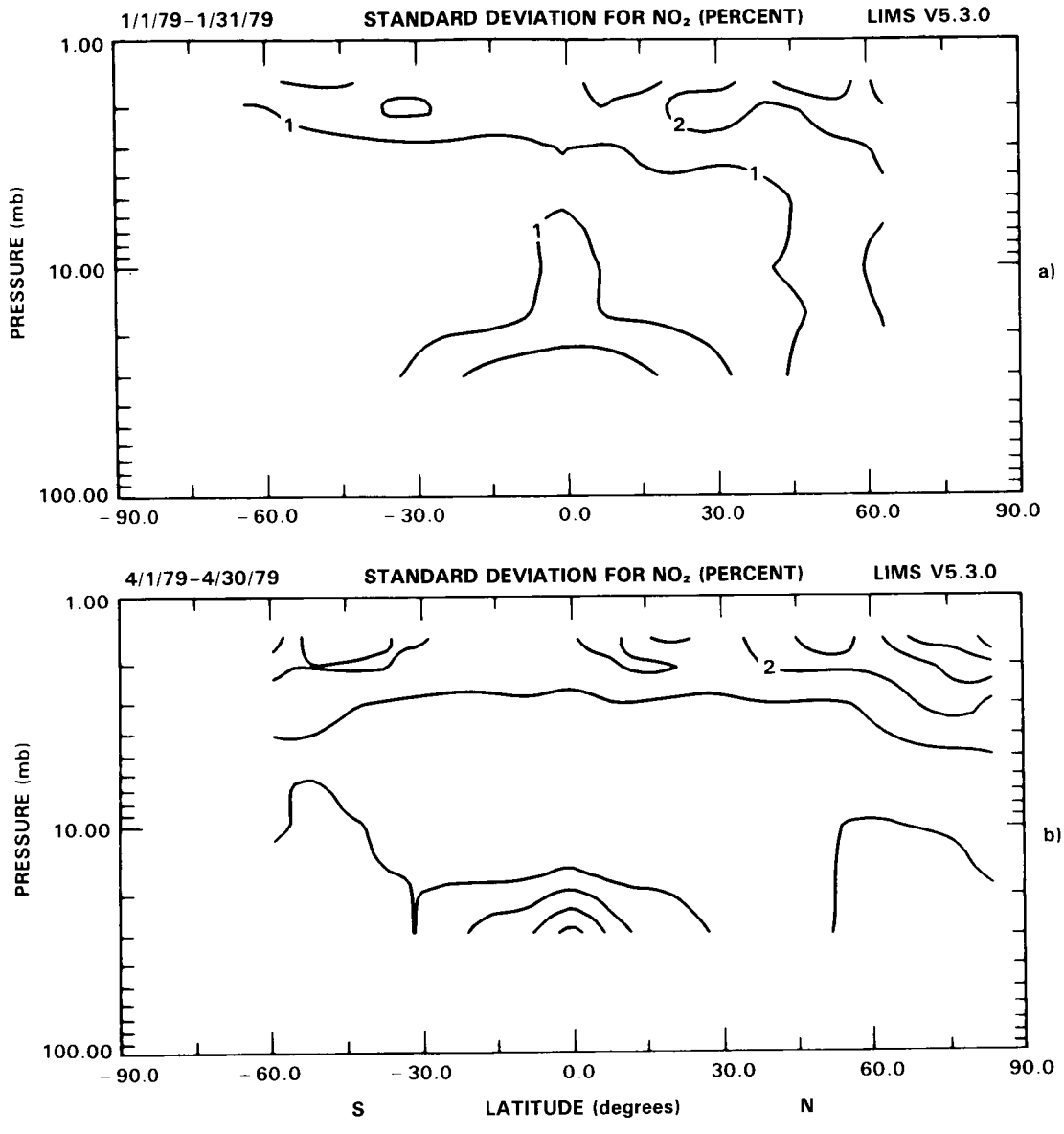

Figure 10-26. Standard deviation of daily values of daytime NO_2 cross-sections for (a) January and (b) April. Contour interval is 1 percent.

most cases, indicating that the means are quite stable, that the latitudinal and vertical structure is consistently present, and that the differences between months are statistically significant.

The general features of the NO_2 distribution can be seen in the January cross-section. There is a layered structure, with maximum values of 7 ppbv at 10 mbar in the summer hemisphere, decreasing toward the winter hemisphere, and toward the northern terminator. At lower altitudes there is a minimum in the tropics resulting from the injection of NO_2-poor air from the troposphere. As N_2O is oxidised in this upward moving air, the NO_2 concentration increases. Above the maximum, there is very little variation with latitude.

The distribution is the same in the other months, but becomes more symmetric with latitude in April and May. There is also a tendency for the level of maximum values to slope down towards the summer pole.

Vertical Profiles

Prior to the satellite observations, a large fraction of the available data were as vertical profiles obtained from balloon-borne measurements. The LIMS data can also be displayed in this way for comparison with balloon measurements most of which are made during the day (or at sunrise or sunset, which are also close to day conditions). This presentation clearly shows the seasonal variations, since the large number of observations allows the random error to be reduced to a very small value, and subtle changes to be seen.

As discussed in the introduction, formation and loss of N_2O_5 probably plays a major role in determining spatial and temporal variation in NO_2 densities, particularly at high latitudes. N_2O_5 is formed in large amounts in the lower stratosphere at night (destroying NO_2) and photolyzed slowly on a time scale of hours to days in the sunlit atmosphere (reforming NO_2). Thus the altitude and magnitude of the NO_2 maximum abundance should be expected to vary greatly between high latitude summer and winter, as the balance between the sunlit and dark portion of the day changes.

Monthly average zonal mean vertical profiles for 5 latitudes are shown in Figure 10-27. At 60 °S, the peak value increases from 7 to 8 ppbv from spring to summer but the levels of the distributions are quite similar. The peak value decreases in the fall, and the shape of the curve is altered, presumably due to the short length of day near the terminator. The summer maximum at the peak level can also be seen at 32 °S, again with larger values in the fall at the high levels. There is rather little seasonal variation at the equator, especially above and below the maximum.

The Northern Hemisphere latitudes show the same type of behaviour, shifted by 6 months. At 32 °N there is a winter minimum at the peak altitude, but not the usual behaviour above the maximum. At 60 °N the winter value is lower at the level of the maximum, which here is at a higher altitude than under summer conditions, again, presumably because of the shorter day and shorter span of time between sunrise and the measurement time. The values are larger and lower in late spring.

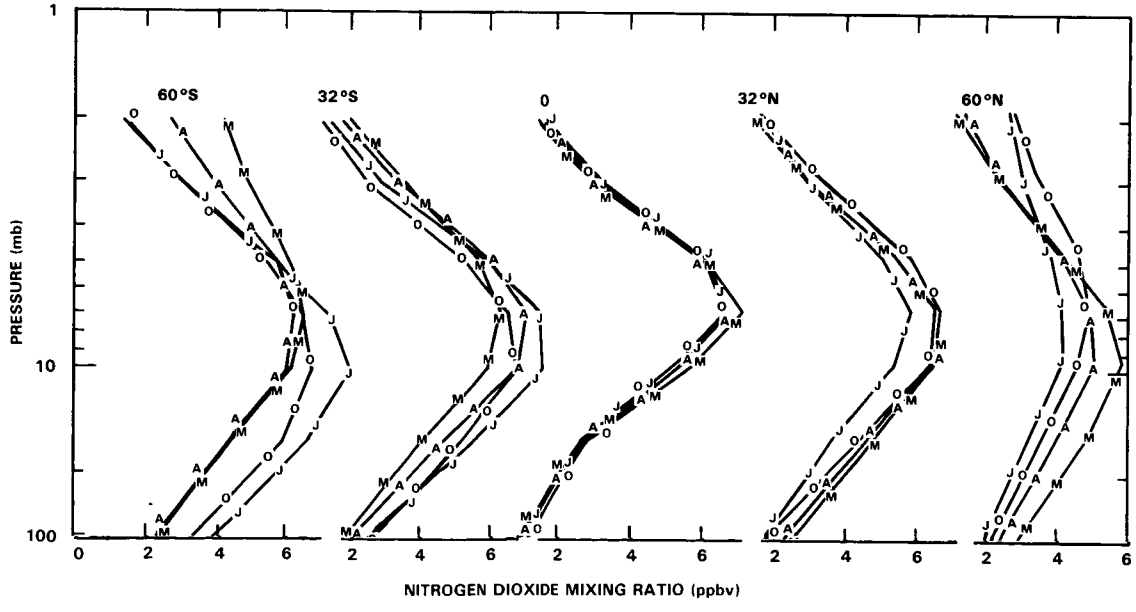

Figure 10-27. Vertical profiles of daytime NO_2 showing seasonal variation at several latitudes. O - October, J - January, A - April, M - May.

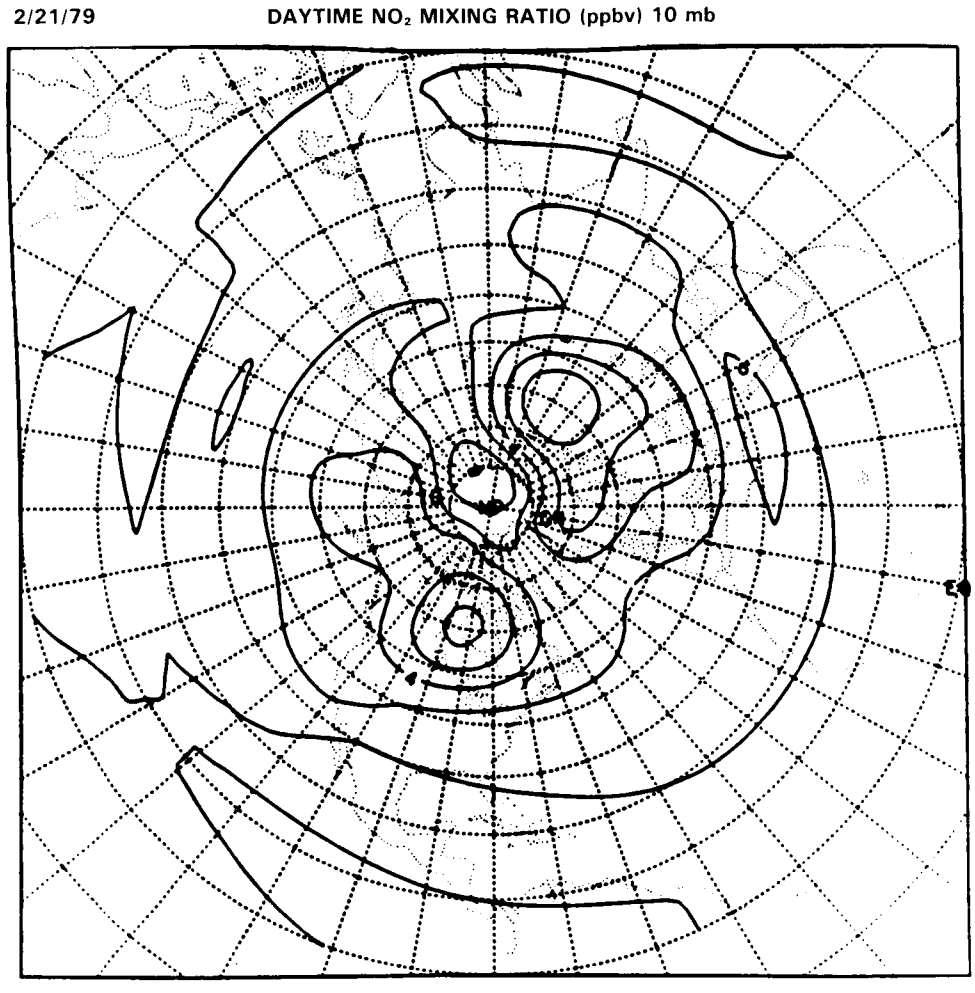

Figure 10-28. Map of NO_2 mixing ratio (ppbv) on the 10 mbar surface ($\sim$ 30 km altitude) for February 21, 1979.

It should be noted that the standard deviations about these profiles are rather small, indicating that in any month the zonal mean changes slowly. The question of variations at particular balloon launch sites is discussed below.

Overburden Measurements

The LIMS values can be vertically integrated to provide a measure of the total column amount of NO_2. Using a ground-based technique, Noxon (1979) observed very rapid decreases of NO_2 column amounts toward the pole during the winter, a phenomenon referred to as the Noxon "cliff". Figure 10-28 presents a map of the LIMS NO_2 mixing ratio on the 10 mbar surface for 21 February. This is during a sudden warming disturbance, and two regions of low mixing ratio can be seen near 60 °N, 90 °W and 70 °E. The column amount above 30 mbar (24 km) is shown as a function of latitude for 90 °W in Figure 10-29, where it is compared with the zonal average. The zonal average shows a small decrease from 30 °N to 60 °N, beyond which there is an increase near the terminator. Along 90 °W, there is a much steeper drop, by a factor of two, from 40 °N to 60 °N. There is a similar variation at 70 °E. This is not as steep as those

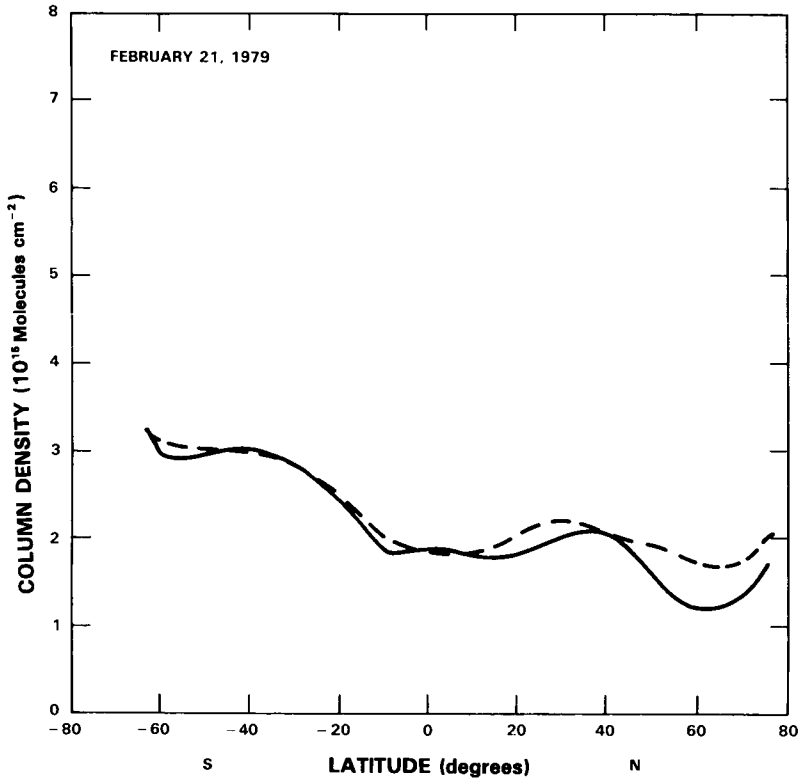

Figure 10-29. Total column amount of NO_2 above 30 mbar as a function of latitude for 90°W (solid line) and the zonal mean (dashed line), for February 21, 1979.

seen on some occasions by Noxon; the differences may be due to differences in the meteorological and measurement situation. Note that Noxon's measurements were obtained at sunset after the NO_x has built up over the entire day; which would be expected to result in a steeper gradient. Callis *et al.* (1983b) calculated larger gradients in the nighttime cliff observed by LIMS. These data show in some detail how the effect depends on the advection of air from the polar cap that is low in NO_2, as Noxon suggested.

Nighttime Values

Zonally Averaged Cross-Sections

The zonally averaged monthly mean values of NO_2 are displayed in Figure 10-30 for the same months as were shown for the daytime values. Regions which were in daylight for all or some of the days have been left blank.

The standard deviations of the daily values are shown in Figure 10-31. Although these are larger than for the daylight values, the percentages are again $< 5\%$ in most locations, indicating that there is rather little day-to-day variability, and that the means are quite stable.

The nighttime distribution also shows a layered structure, with maximum values of approximately 17-19 ppbv, now centred near 4-5 mb. There is a maximum over the equator in October, with a region of high values in the Southern Hemisphere near the southern terminator. In January the equatorial maximum has shifted appreciably toward the south, and the peak values are larger. At the same time, the

a) October (last 7 days)

b) January

c) April

d) May

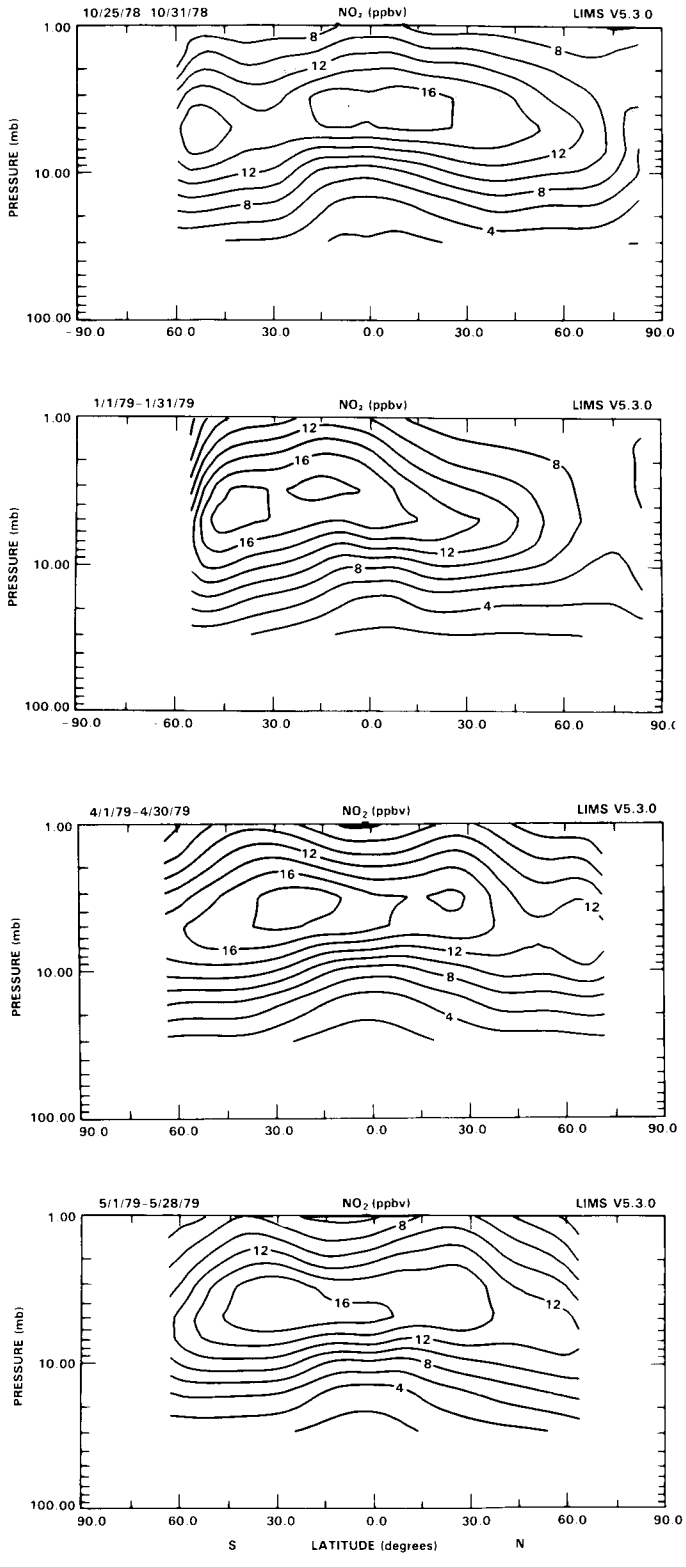

Figure 10-30. Monthly average zonal mean cross-sections of nighttime NO_2 for a) October (last 7 days), b) January, c) April, and d) May (first 28 days).

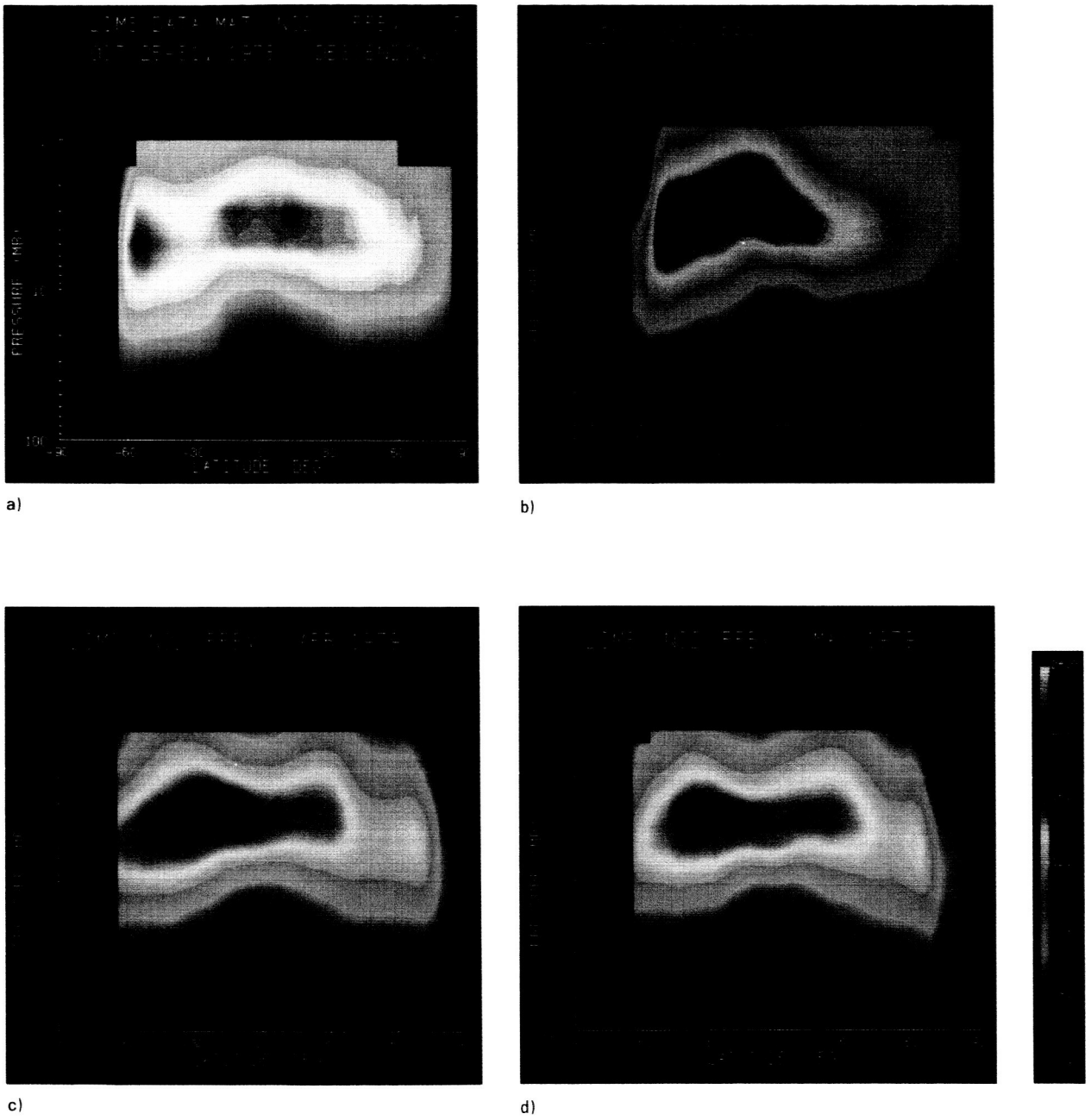

a)

b)

c)

d)

Figure 10-30. (Color) Monthly average zonal mean cross-sections of nighttime NO_2 for a) October (last 7 days), b) January, c) April, and d) May (first 28 days).

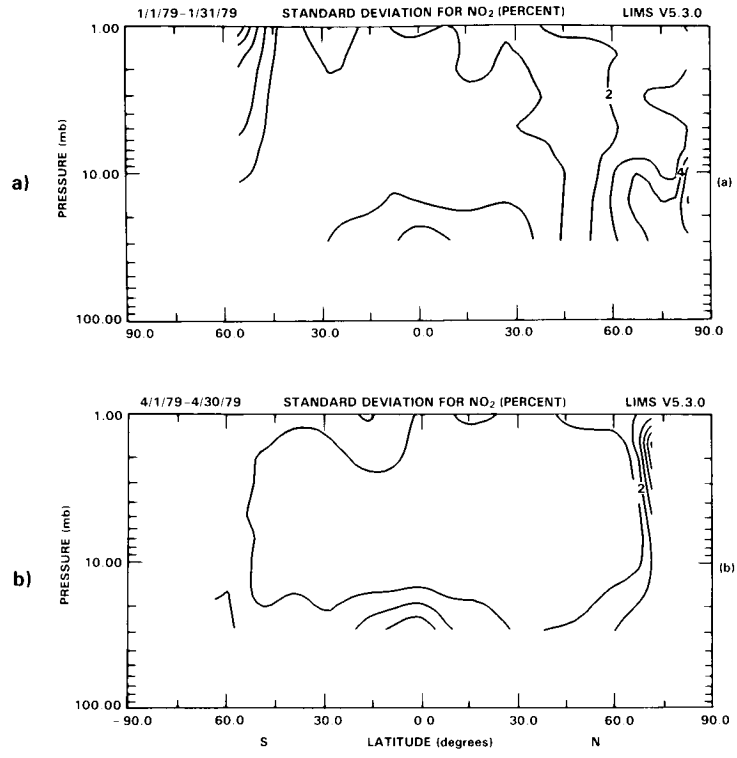

Figure 10-31. Standard deviation of daily values of nighttime NO_2 cross-sections for (a) January and (b) April. Contour interval is 1 percent.

values in the Northern Hemisphere polar night are quite low. April is characterised by a maximum still in the Southern Hemisphere, but a small local maximum in the Northern Hemisphere. These weaken in May. One feature that stands out in these plots is the tendency for there to be more NO_2 at the level of the maximum in the Southern Hemisphere night.

The interpretation of these data is in its early stages. However, it is clear that they should be invaluable in studies of the photochemistry of the nitrogen species, and their interactions with transport processes.

10.2.1.2 SAGE Measurements Nitrogen Dioxide

SAGE Instrument and Techniques

The Stratospheric Aerosol and Gas Experiment (SAGE) instrument has been described in the Special Introduction to Chapter 8, 9, 10 and 11, and is reported in McCormick *et al.* (1979) and Chu and McCormick (1979).

Measurement Errors and Validation

The estimated SAGE NO_2 measurement errors are tabulated in Table 10-7 for the altitude range from 25 to 45 km. Since the SAGE instrument measures the absorption due to atmospheric NO_2, noise in the measurement will directly affect the inferred number density of NO_2. Therefore, the estimated random

Table 10-7. SAGE NO_2 Profile Measurement Error Estimates

A. Systematic Errors

NO_2 Absorption Cross-section	10%
Instrument Wavelength Calibration	2%
Rayleigh Correction	4%

B. Random Error

	Altitude - km	Number Density molecules cm^{-3}
Noise (Measurement and inversion)	25	7×10^8
	30	5×10^8
	40	2×10^8
	45	1×10^8

errors for the SAGE NO_2 profiles are given as number density at selected altitudes. For a typical mid-latitude sunset observation, they correspond to approximately 25 percent error between 30 to 40 km altitude, and higher error above and below.

Since there were no correlative measurements of NO_2 during SAGE's lifetime, SAGE data have been compared with previous measurements of NO_2 from either balloon or aircraft platforms which have been summarised in the previous WMO assessment report, WMO 1981 (1982). Figures 10-32 (a) and (b) show some of the previously reported NO_2 profiles at sunset compared to the SAGE sunset measurements centered at latitude bands of 32 to 33°N and 45 to 50°N. The SAGE data are indicated by solid lines and are obtained by averaging all three year's observations during the spring season (March through May) over the corresponding latitude bands. The horizontal bars on the SAGE profile denote one standard deviation from the mean. As can be been in the figures, the agreement between SAGE observations and those of the balloon measurements is well within their respective uncertainties at these two latitude bands.

SAGE NO_2 Zonal Cross-Sections

Figure 10-33 shows the SAGE measured zonal mean NO_2 cross-sections. Data for the 34 months of SAGE NO_2 profiles have been grouped into 10-degree latitude bands for the four seasons to generate the zonal mean vertical cross-sections of NO_2 mixing ratio. The number of profiles in each latitude band varies from 40 to 500. The four seasons are represented by Northern Hemisphere winter (December through February), spring (March through May), summer (June through August), and fall (September through November). The SAGE data show that the NO_2 mixing ratio in the middle and upper stratosphere is at a maximum in equatorial regions and decreases towards high latitudes in both the northern and southern hemispheres for all four seasons. The maximum mixing ratio contour of 8 ppbv typically covers altitudes from about 32 to 36 km. The latitude of the peak mixing ratio shifts away from the equator with the sun and with the JJA peak located north of the equator while the DJF peak is located south of the equator. The NO_2 mixing ratio distribution for the spring and fall seasons is generally symmetric about the equator, while the summer and winter distributions show significantly less NO_2 in the local winter high latitude regions. An unusual feature of a MAM "bulge" at low latitudes above the peak can be seen.

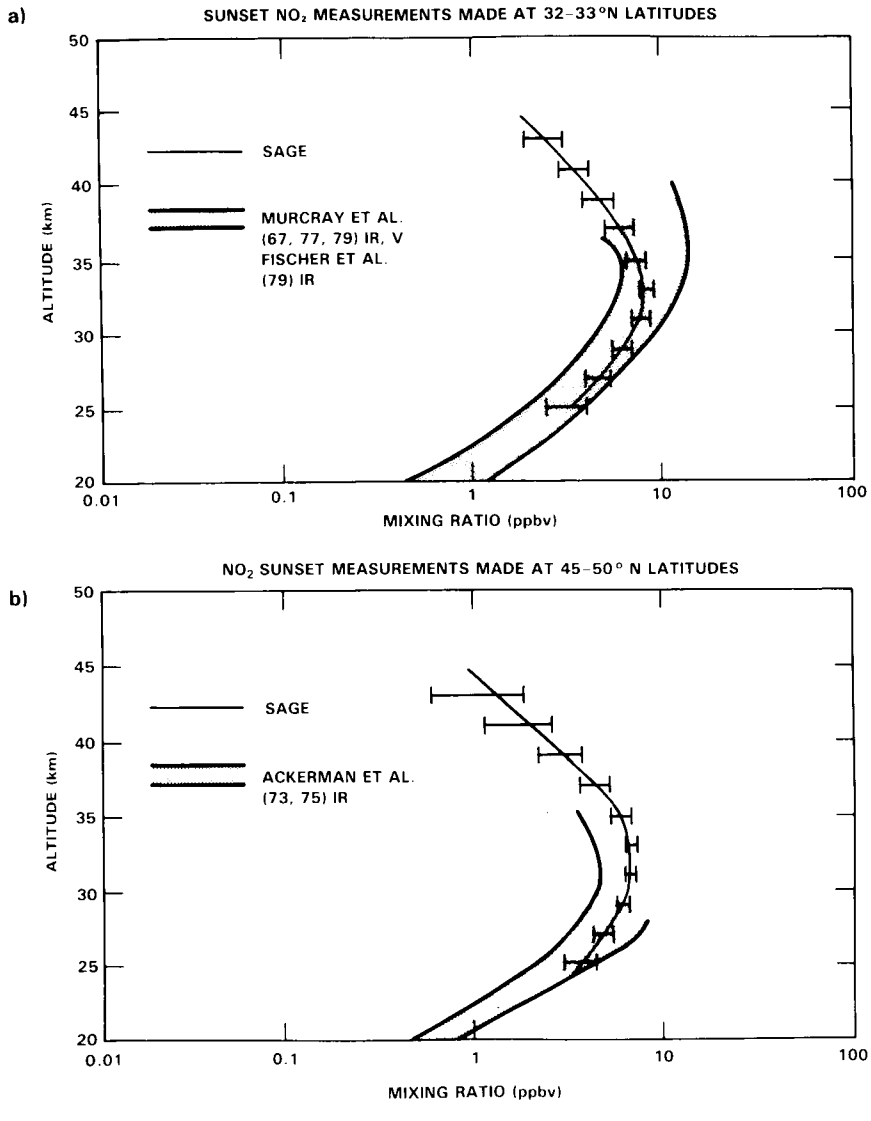

Figure 10-32. Comparison of some previous sunset measurements of NO_2 with sunset SAGE data, for (a) 32–33°N and (b) 45–50°N.

SAGE Total Column NO_2

Figure 10-34 shows the 1979 to 1981 averaged zonal mean column abundance of SAGE NO_2 integrated from 25 to 45 km altitude for the four seasons. The behaviour of the seasonal zonal mean column abundance is similar to that illustrated by the zonal mean mixing ratio cross-sections in Figure 10-33. Specifically, for all four seasons, there is a local minimum of NO_2 content in the equatorial region. The zonal mean column abundance distribution for the local winter versus summer season is significantly different. It shows a larger content in the local summer and a minimum in local winter with a rapid decrease to high latitudes in winter. As in the cross-sectional plots of Figure 10-33, the spring and fall column contents are almost symmetrical with indications of a double maximum, one near 30°N and the other near 20°S.

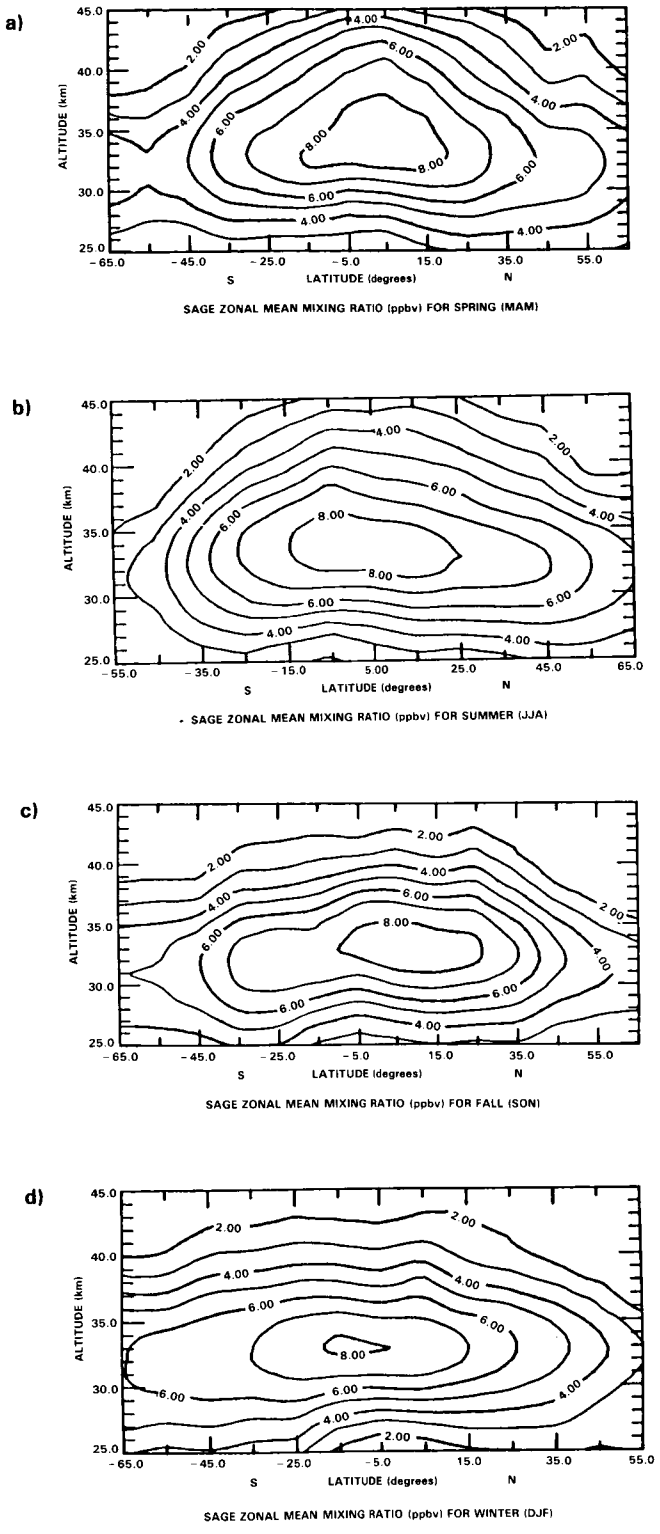

Figure 10-33. SAGE zonal mean cross-sections for NO_2 averaged for the 34 month lifetime of the experiment. (a) Spring (March, April, May); (b) Summer (June, July, August); (c) Fall (September, October, November); (d) Winter (December, January, February).

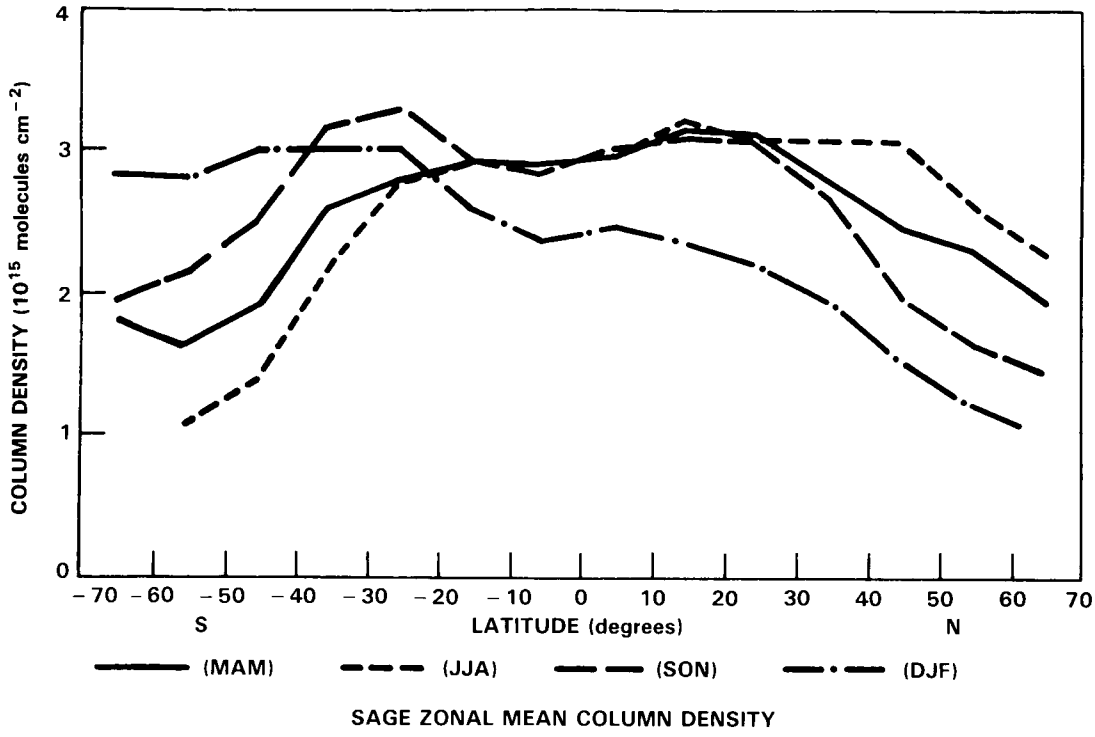

Figure 10-34. SAGE averaged zonal mean column abundance for NO_2 from 1979 to 1981, from 25 to 45 km, for the four seasons.

NO_2 Variability Near 31, 44 and 52°N

Figures 10-35 (a) through (c) show the SAGE zonal mean mixing ratio profiles for the spring season (March through May) averaged over the nearly 3 years of SAGE observations. Figure 10-35 (a) is for the latitude band from 26 to 36°N centered at 31°N. Figure (b) is for latitude band from 39 to 49°N centered at 44°N, and Figure (c) is for the latitude band from 47 to 57°N centered at 52°N. The bars denote one standard deviation from the mean. There is little variability below the peak from these northern latitudes between 31 and 52°N but significant difference above the peak for the 31°N plot which is higher in mixing ratio for all altitudes above the peak. Similar located profiles for winter (as shown in Figures 10-36 (a) through (c) show the located profiles for summer and fall (not included here) are all in between those shown in Figures 10-35 and 36.

Special Events: Noxon Cliff and Sudden Warmings

One of the most striking features of the behaviour of NO_2 is the observed sharp column density gradient (the "cliff") at high latitude during the winter season (Noxon *et al.*, 1979).

Even though the SAGE coverage does not usually penetrate into high latitudes during the winter season where cliffs are normally situated, there are occasions such as during a sudden warming event (where the polar vortex splits and/or moves to a lower latitude), when cliffs can be observed at more southerly locations. Figure 10-37 shows the SAGE observations on 23 February 1979 at 52°N. latitude during the

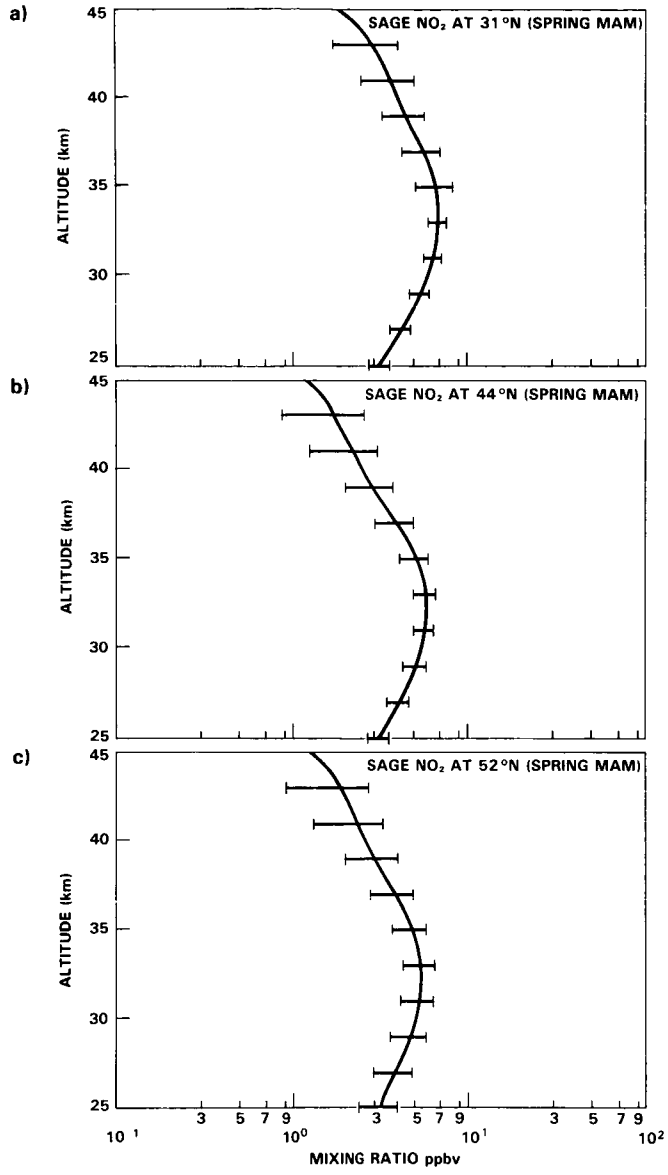

Figure 10-35. SAGE averaged zonal mean mixing ratio profiles for spring (MAM) at three latitudes, (a) 26–36°N centered at 31°N; (b) 39–49°N centered at 44°N; (c) 47–57°N centered at 52°N.

last phase of the sudden warming for this winter season. The normal single polar low was distorted and split into two lows approximately centered on the eastern and western hemispheres. Of the 13 sunrise SAGE NO_2 measurements, there are two distinct minima of NO_2 column. Positions A and B in Figure 10-37a show these on the 10 mbar isobaric height contour map. The locations of the SAGE measurement are illustrated by black dots and the heavy height contour lines around the two lows are the approximate boundaries of the two vortices based on calculations of the positions of the maximum wind field across the height contour levels. Figure 10-37b gives the corresponding SAGE NO_2 column content values. It is very clear that within the polar vortex there was significantly less NO_2 than observed outside the two vortices. These data demonstrate that one must consider dynamical as well as photochemical processes in understanding NO_2 distributions.

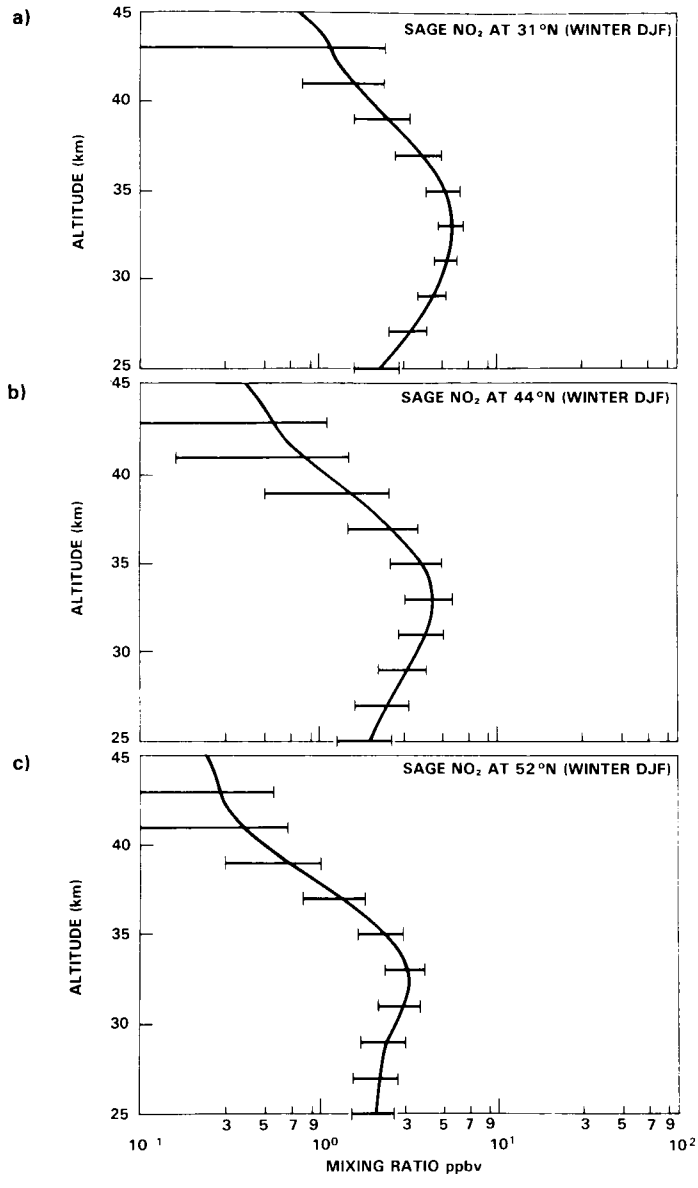

Figure 10-36. SAGE averaged zonal mean mixing ratio profiles for winter (DJF) season at three latitudes, (a) 26–36°N centered at 31°N; (b) 39–49°N centered at 44°N; (c) 47–57°N centered at 52°N.

10.2.1.3 SME Measurements of Nitrogen Dioxide

The Solar Mesosphere Explorer (SME) satellite measures stratospheric NO_2 in the 20-40 km altitude region. The instrument has been described in the Special Introduction. Detailed discussions of the measurements, which are based on the technique of Noxon (1979), are provided by Mount *et al.*, (1983, 1984).

Table 10-8 provides an estimate of the accuracy of the NO_2 observations. The largest error in determination of the NO_2 density profiles is caused by measurements of the altitude for the instrument field of view above the Earth's surface as a function of time. The absolute altitude determination is made to

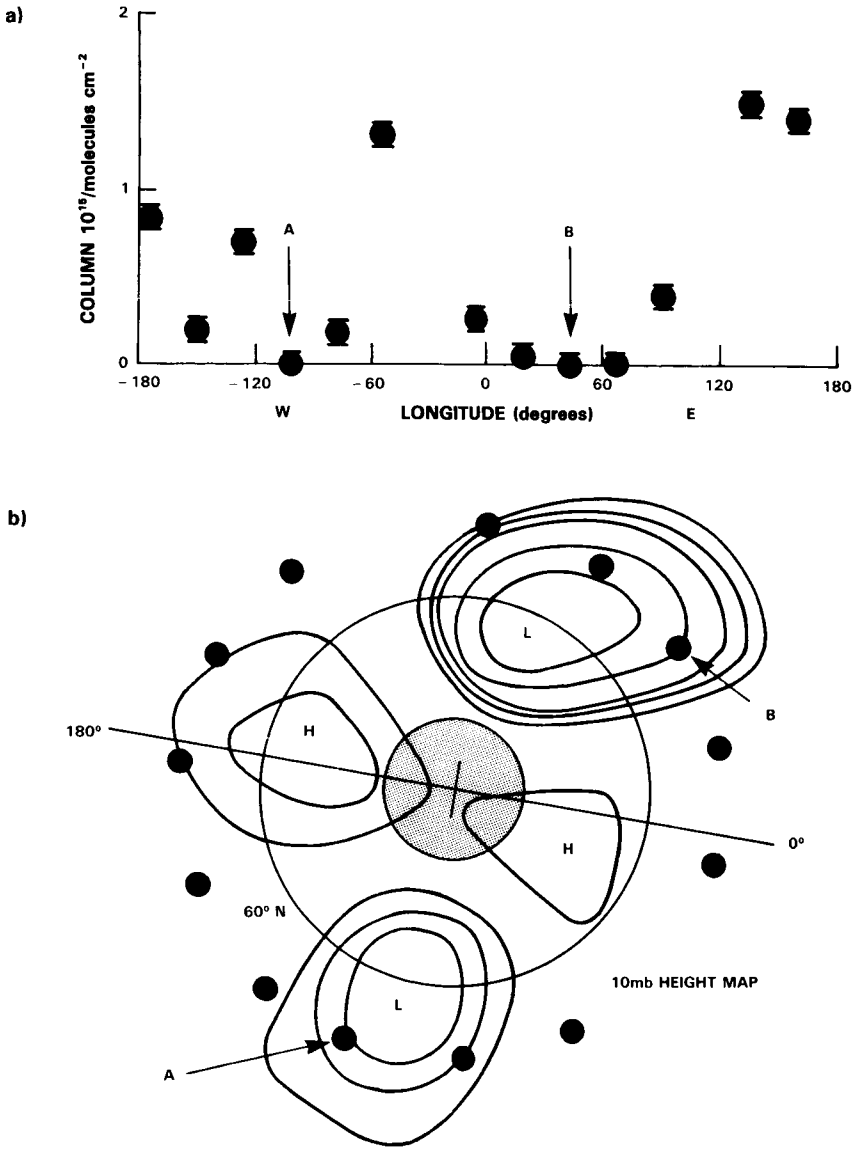

Figure 10-37. SAGE sunset measurements on February 23, 1979 at 59°N.
(a) SAGE column content integrated from 25 to 45 km.
(b) 10 mb height map. SAGE measurement locations shown by black dots.

an upper error limit of ± 1 km at the limb, and since the NO_2 scale height is about 4 km, this results in a significant error in NO_2 density determination. (See Table 10-8).

The primary NO_2 quantity measured by SME is the concentration or density (molecule/cm^3). Because of an instrument failure on board the SME spacecraft, measurements of the atmosphere neutral density are not available, and the NO_2 observations can only be converted to mixing ratio by adopting a reference atmosphere (see, Mount *et al.*, 1984; Rusch *et al.*, 1984). This introduces an additional large error in the mixing ratio products displayed here which may be as much as 20%.

Table 10-8. SME Error Analysis

Type of Error	Error	Error in NO_2 Density	
		28 km	38 km
Altitude of field of view at limb	± 1 km	5%	50%
Random error in data numbers (noise)	± <1 DN	<5%	<25%
Determination of on board differencing amplification ratio	1%	<1%	10%
Determination of relative instrument polarization	1%	<1%	10%
Determination of diode "dead" time	<1%	<1%	<1%
Error in master null set used for subtraction	<0.2%	5%	25%
NO_2 cross section (relative error between wavelength pairs)	<10%	10%	10%
Ozone correction	×2	<15%	0%
Absolute placement of instrument on spacecraft	<30 arc sec	<5%	<10%
Determination of electronic background	± <1 DN	<5%	<5%
Total rms error (quadrature sum)		± 21%	±65%

The Solar Mesosphere Explorer began taking NO_2 observations in December 1981. The eruption of the El Chichon volcano on 4 April 1982 injected a large number of scattering particles into the atmosphere, interrupting NO_2 observations. We present here results only from the first winter of observations, 1981-1982 before the eruption. Coverage of the NO_2 data is restricted to about 4 orbits over North America on a daily basis, at a local time near 3 pm. There are no coincident correlative measurements of NO_2 available for this period. Figure 10-38 shows a comparison of NO_2 vertical profiles in January 1982, in the summer hemisphere compared to several observations performed in the Northern Hemisphere summer. The comparison reveals reasonable agreement.

Figure 10-39 presents monthly and zonally averaged NO_2 mixing ratio distributions from SME for January, February and March of 1982. The most striking feature in these distributions is the sharp gradient observed near the polar night terminator. The progression of NO_2 mixing ratio near 40-80 °N from January to March reveals that NO_2 must be converted to another reservoir NO_y species during high latitude winter, as first suggested by Noxon (1978), and as shown in several other ground-based and aircraft studies (e.g. McKenzie and Johnston, 1982).

Figures 10-40 (a-c) show vertical profiles observed by SME at the equator, 35 and 55 °N. Because of the limited seasonal information, only a few statements regarding the profiles can be made. The altitude of maximum mixing ratio occurs near 30 ±1km in virtually all seasons and latitudes. The equatorial profile reveals a steep gradient below the peak, probably because of the predominance of upward transport in the tropical lower stratosphere. NO_2 abundances observed in winter at 55 °N are extremely low, and show only a very modest peak. A significant increase occurs in the peak values in March.

On many occasions, SME observed abrupt decreases in NO_2 abundances during winter in high latitudes at particular longitudes; this is the Noxon "cliff" phenomenon, discussed earlier. Note that the gradients

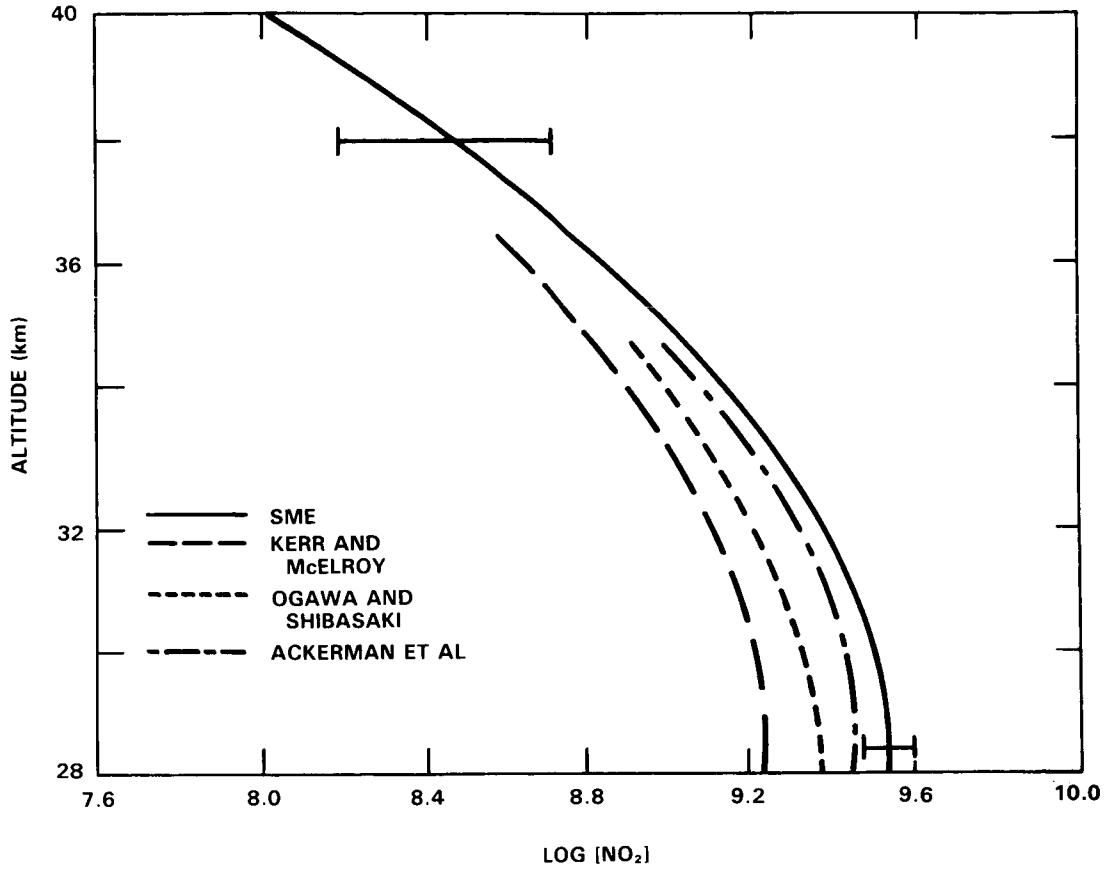

Figure 10-38. A typical NO_2 number density profile taken during January 1982 at 40°S latitude compared with measured NO_2 profiles (summer mid-latitudes) of Kerr and McElroy (1976), Ackerman *et al.* (1975), and Ogawa and Shibasaki (1980). The agreement of both shape and absolute value is acceptable, considering the lack of temporal and geophysical coincidence. The comparison of the southern summer data taken in January to published northern summer data should be reasonable. The eruption of El Chichon in April 1982 prevents a direct comparison of northern summer data for SME.

at particular longitudes were much greater than those obtained in the zonal mean as shown in Figure 10-39. Figure 10-41a shows an example of the NO_2 density gradient observed at 10 mbar on day 40 of 1982 on a single orbit, showing a decrease of a factor of 4.5 in 20 degrees of latitude. A chemistry/trajectory model calculation is also shown (Figure 10-41b). The model calculation and its implications will be discussed in Section 10.3.

10.2.2 Nitric Acid (HNO_3)

The LIMS instrument, which was described above, also made observations of the global distribution of HNO_3.

Data Quality

The HNO_3 data are discussed and evaluated by Gille *et al.* (1984b), from which the following discussion is summarised. The vertical range is again set by the region of adequate signal to noise ratio, and

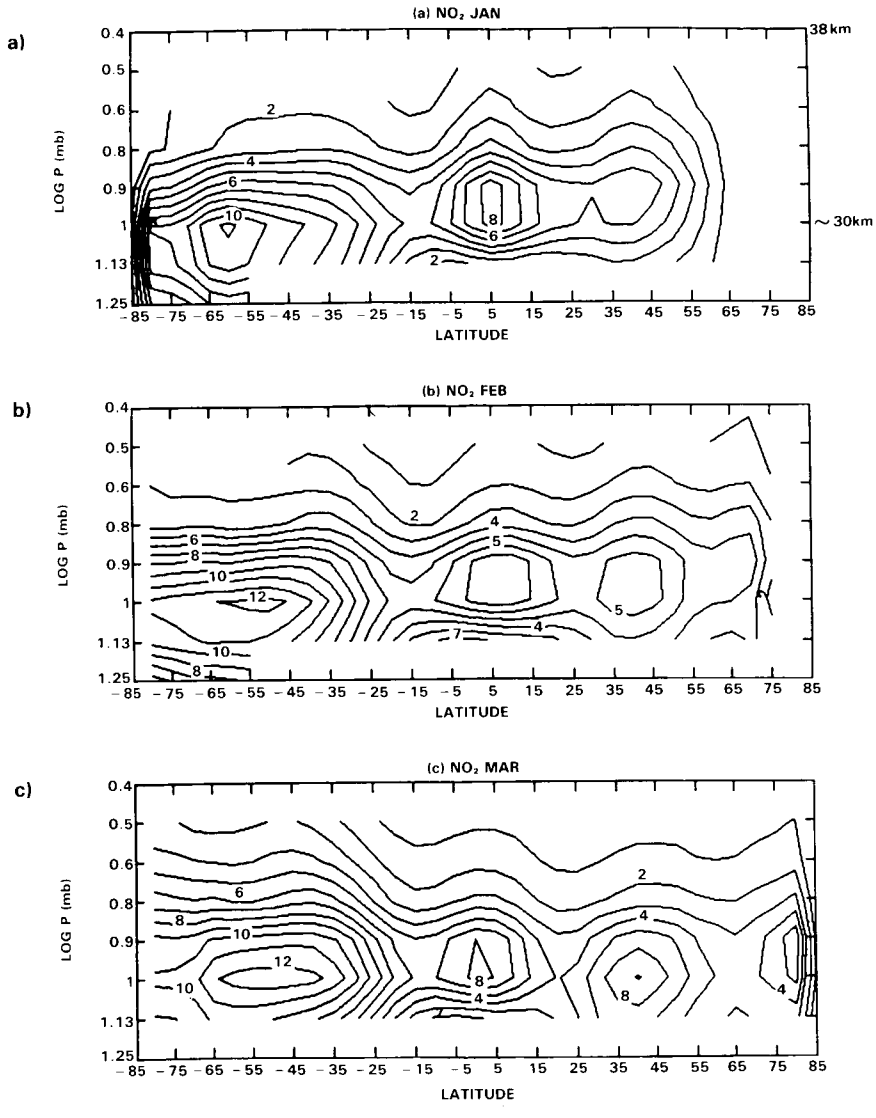

Figure 10-39. Monthly and zonally averaged NO_2 distributions from SME for (a) January, (b) February, and (c) March 1982.

at the bottom, by the frequent occurrence of clouds. For the HNO_3 signal, the upper limit occurred at about 2 mbar pressure level, or around 45 km altitude. Clouds usually interrupt the path at or above the 100 mbar pressure level in the tropics. Retrievals to lower altitude are possible at higher latitudes, but with rather small signal to noise ratios. In this discussion the lower boundary is usually taken to be 100 mbar.

The precision of the profiles or scan-to-scan repeatability, is about 0.05-0.1 ppbv in undisturbed regions, where atmospheric changes do not contribute much to the variations. This intrinsic precision is of the order of 2% up to 7 mbar rising to only 6% at 5 mbar. When natural atmospheric variability, which may incorporate real variations on scales smaller than the 100 km inter-scan spacing, is included, a repeatability at almost all latitudes and altitudes of 0.1 ppbv is found. These values are somewhat lower than the estimates presented in Table 10-9, which are based on calculations of the effects of known noise sources.

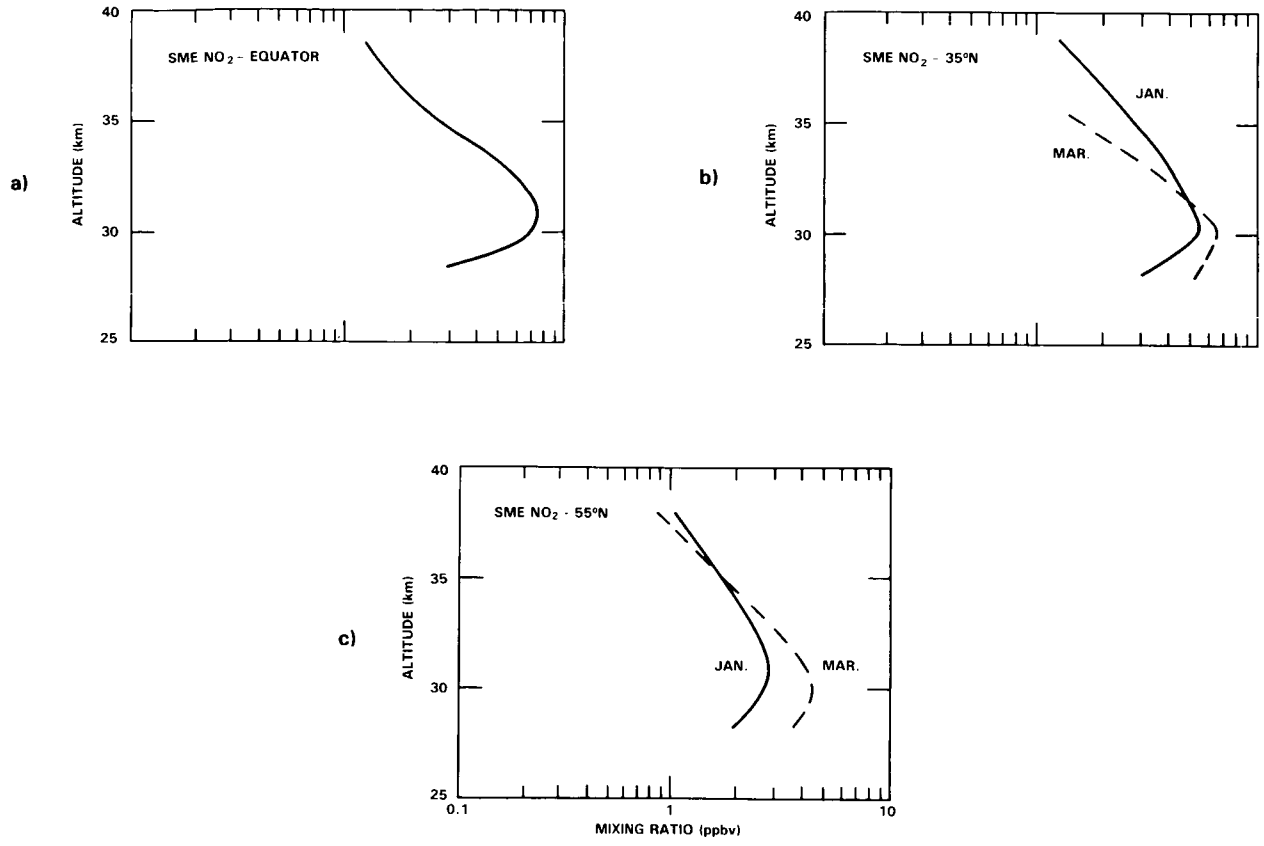

Figure 10-40. Vertical profiles of NO_2 observed by SME at (a) the equator, (b) 35°, and (c) 55°N, 1982.

The accuracy is much more difficult to establish. Table 10-9 also presents results of calculations of the effects of instrumental and data uncertainties. The errors are estimated to be 30–40% between 10 and 50 mbar rising to 65% at 3 mbar, where the signal is very close to the noise. These estimates, at least away from the top levels, are thought to be rather conservative. A second approach to estimating the accuracy is through comparison with other measurements. Mean differences of about ± 20% between LIMS measurements and 15 balloon-borne measurements were found from 100 to 10 mbar. These differences are approximately the errors associated with the balloon-borne measurements, and so form a lower limit to the differences that might be expected. However, the LIMS results become systematically larger than the correlative measurements with increasing altitude, e.g. by 7 mb the LIMS data is ~50% greater than the correlative data. There are reasons for thinking that such an effect could be due to an instrumental effect (Bailey *et al.*, in preparation). In addition, chemical consistency suggests that the original values are too large (Jackman *et al.*, 1986). Therefore, the values presented here for the upper levels should be considered as too large.

The Zonal Mean Distribution of Nitric Acid

Figure 10-42 presents monthly averaged values for the months October, January, April and May. The general features of the distribution are similar from month to month, but there are significant changes.

Table 10-9. Calculated Error Estimates for LIMS Nitric Acid Retrievals

Error Sources	Pressure Level, mbar				
	80	50	30	10	3
Random errors, ppbv					
Radiometer noise and jitter	0.25	0.27	0.29	0.16	0.09
Temperature noise	0.22	0.07	0.06	0.01	0.05
rss†	0.33	0.28	0.30	0.16	0.10
Systematic errors, %					
Calibration	1	—‡	2	1	7
Out of spectral band signal	29	29	20	7	45
Field of view side lobes	27	28	25	27	45
Temperature bias	9	1	4	1	8
Spectral data	5	5	5	5	5
Uncertainty in CFC contribution	8	1	—‡	1	1
rss†	42	41	33	28	65
Algorithm effects	5	5	5	5	5
rss†	42	41	33	29	65

†Root sum squared
‡Less than 0.5%

A knowledge of the variability of these cross-sections is necessary before they can be meaningfully discussed. Figure 10-43 presents the standard deviations of the daily values for January and April. January is the month with the largest temporal variability, which is associated with a major disturbance toward the end of the month. The standard deviation is less than 0.2 ppbv south of 45 °N, and reaches values of 1 ppbv only at the highest latitudes. The same results are presented as a percentage of the mean in Figure 10-44 which shows percentage variations for January less than 5% except for a region at high latitude. The low altitude region at the equator is spurious, resultng from the incomplete removal of cloud effects, and the low mean values present there. For other months, e.g., April (Figure 10-44b), the variability is smaller. Thus, the values at a given location are quite stable from day-to-day, and means such as those in Figure 10-42 are representative.

The general features of the nitric acid distribution are illustrated by the October data. There is a broad saddle in the tropics, centered near 20 mbar and characterised by the values of 2-3 ppbv. Mixing ratios decrease slowly above and below this level, indicating a low and relatively uniform profile. Maximum values increase toward both poles, with the altitude of the maximum decreasing to the 30 mbar level at the highest latitudes. In the Northern Hemisphere (NH) the maximum of 3 ppbv at 20 mbar and 10 °N progresses to a maximum of 12 ppbv at 30 mbar and 84 °N. The variations are similar in the Southern Hemisphere (SH) as far as they can be seen. Note also that the isolines are relatively flat on the upper side of the layer, but have fairly steep slopes on the lower side. Finally, there is an indication of an increase at high northern latitudes and high altitudes.

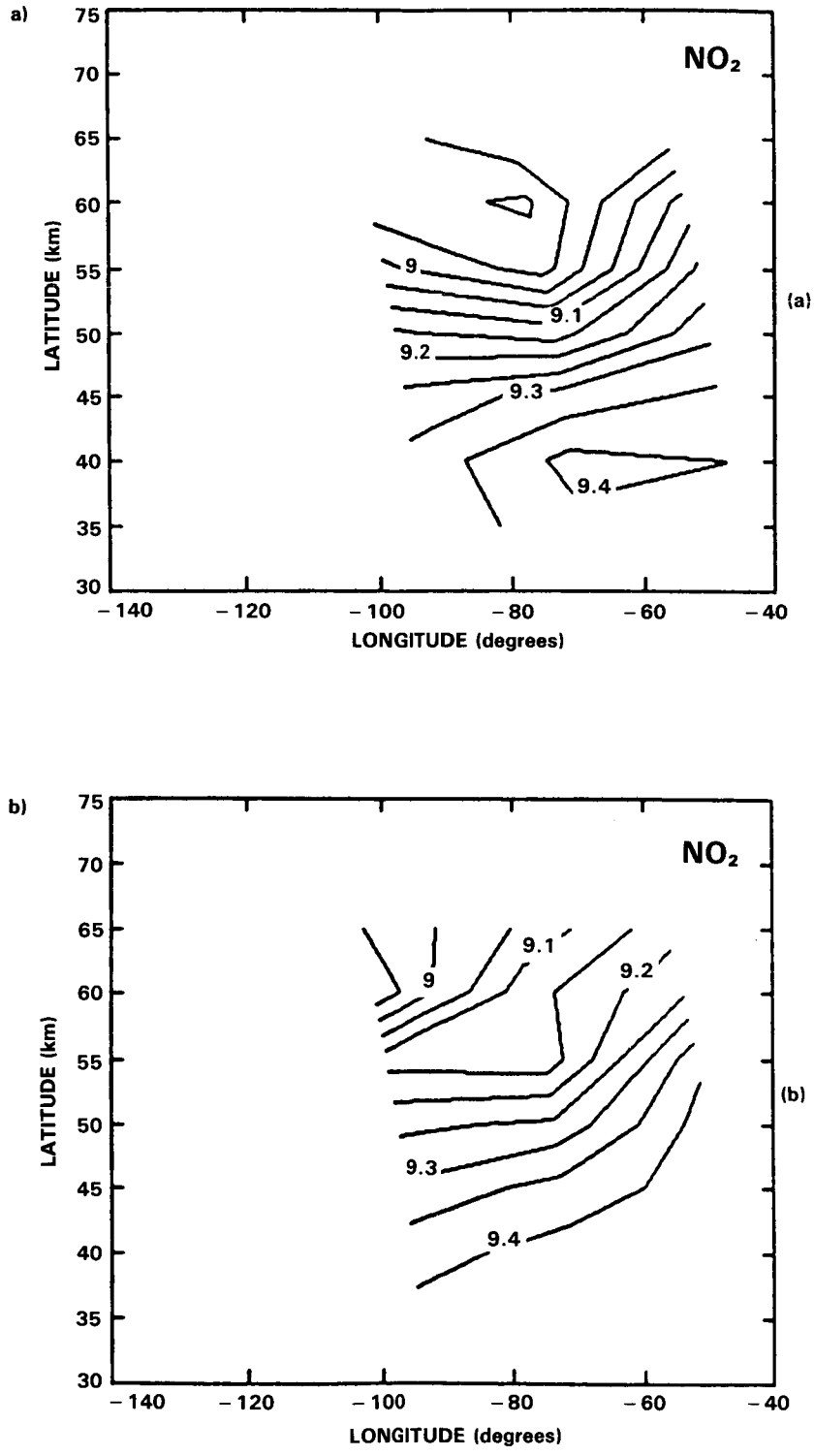

Figure 10-41. Logarithm of NO_2 density for day 40 (1982), at 10 mbar; (a) observed by SME; (b) from a 2-D coupled dynamical-chemical model.

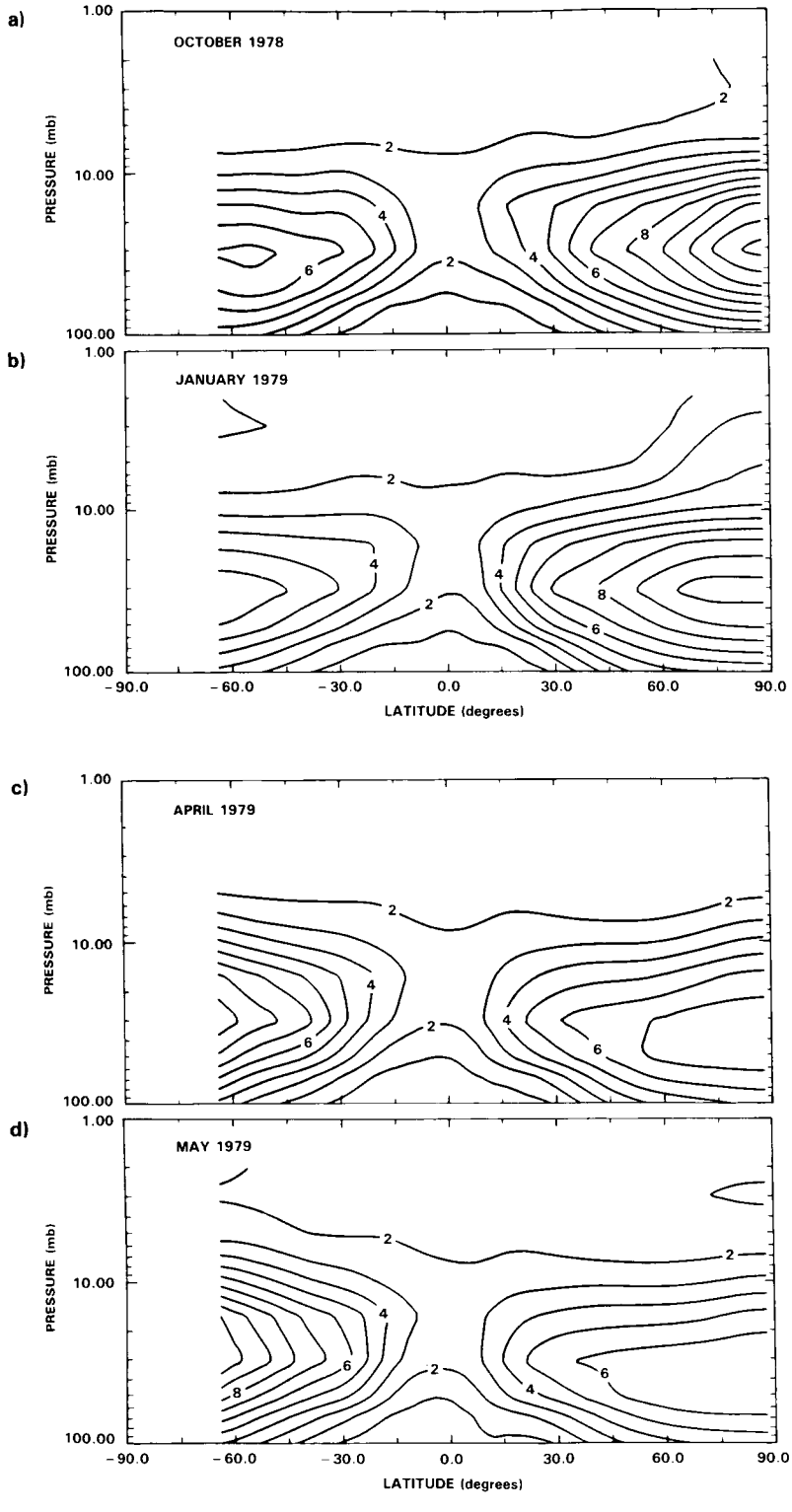

Figure 10-42. Monthly averaged zonal mean cross-sections of HNO_3 mixing ratio (ppbv) for (a) October (last 7 days), (b) January, (c) April, and (d) May (first 28 days). Note that values above 10 mb are probably somewhat too large.

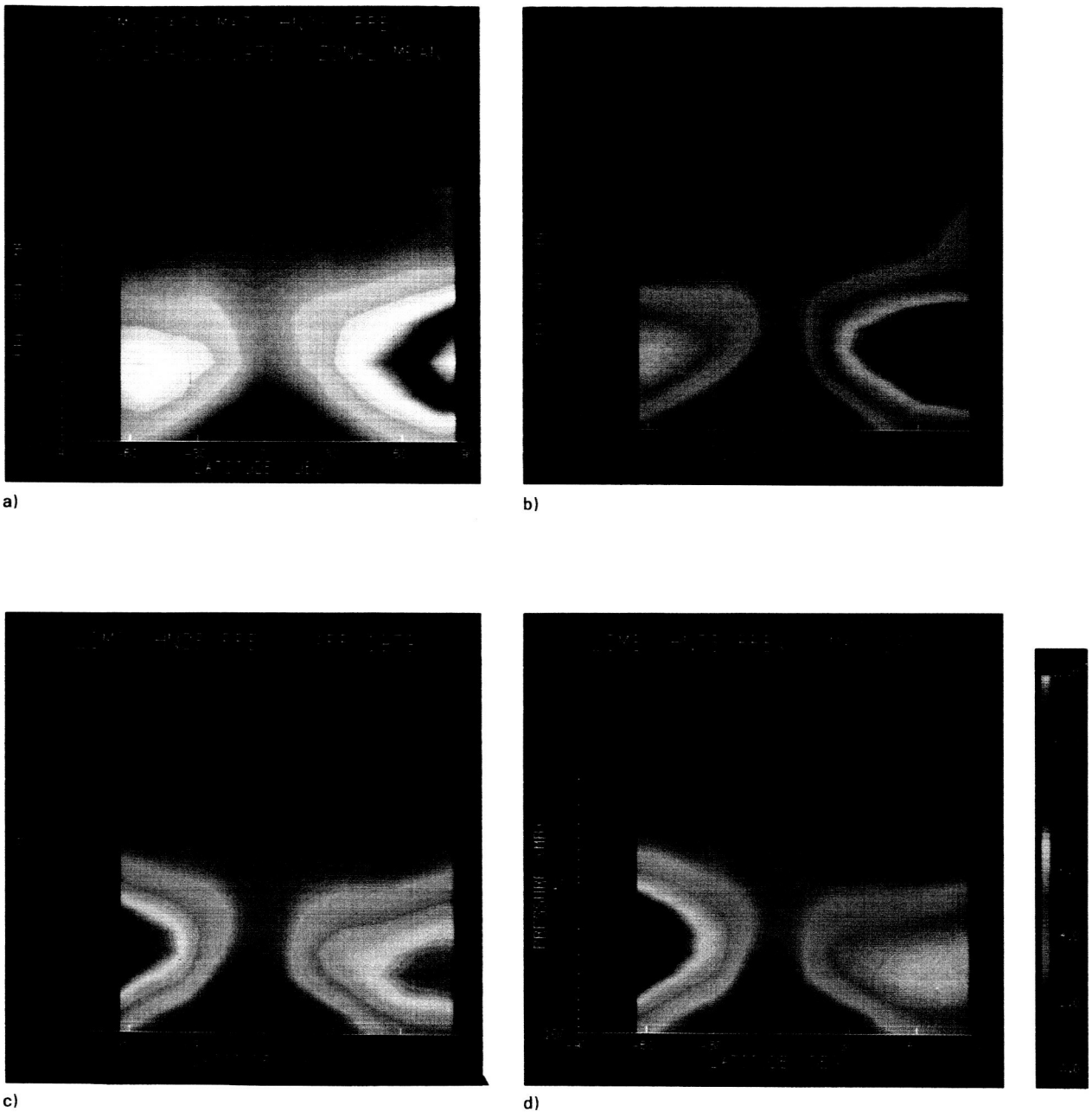

Figure 10-42. (Color) Monthly averaged zonal mean cross-sections of HNO_3 mixing ratio (ppbv) for (a) October (last 7 days), (b) January, (c) April, and (d) May (first 28 days). Note that values above 10 mbar are probably somewhat too large.

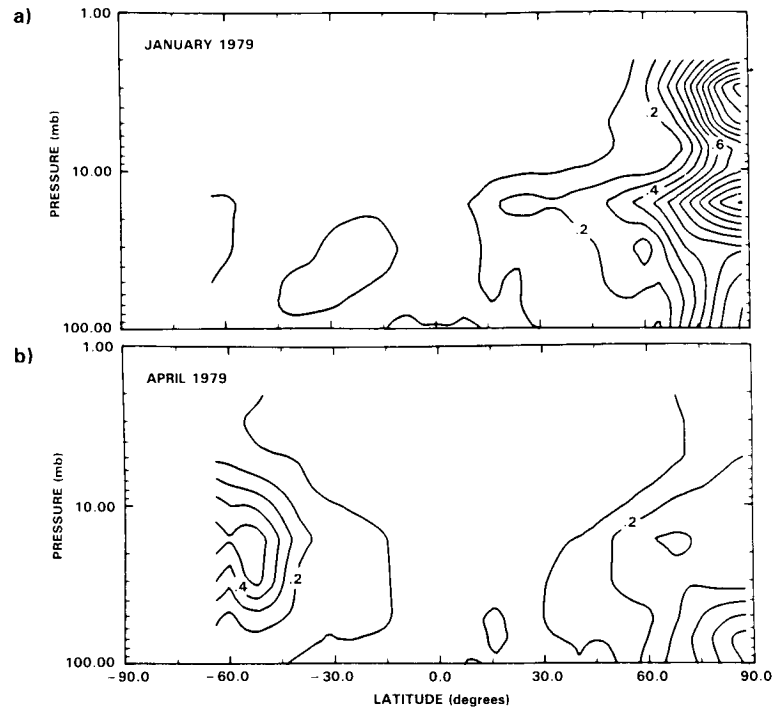

Figure 10-43. Standard deviation of daily zonal mean values of HNO_3 mixing ratio (ppbv) for (a) January and (b) April. Contour interval is 0.1 ppbv.

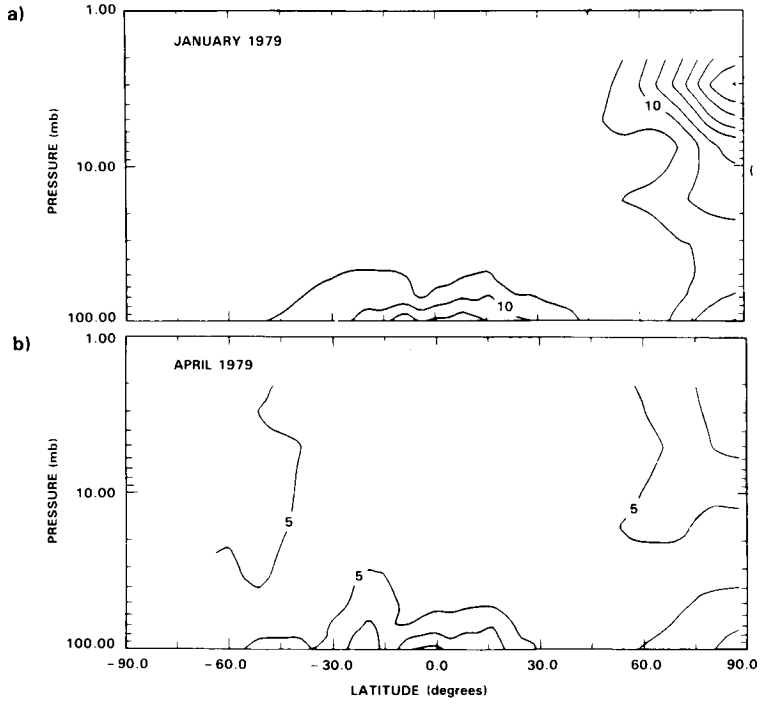

Figure 10-44. Standard deviation of daily zonal mean values of HNO_3 mixing ratio as a percent of the mean values, for (a) January and (b) April. Contour interval is 5%.

The monthly mean cross-sections in Figure 10-45 indicate that there are significant but regular changes with season. The NH maximum value at 30 mbar and 84 °N decreases from over 12 ppbv in the fall to about 7 ppbv in May. At the same time, the values in the SH are increasing. Above 10 mbar, the slope of the isolines reverses from October to May, along with the indication of higher concentrations at the winter pole.

Time-Height Cross-Sections

The temporal variation of the zonal mean is shown more explicitly by the time-height cross sections in Figure 10-45. There is an apparent semi-annual oscillation in the tropics, where the HNO_3 maxima are reached in December and (probably) June at 16 mbar, but somewhat earlier at 30 mbar and later at 10 mbar. The minimum at each level is close to the mid-point between the maxima.

At 32 °N there is an annual variation, which is approximately in anti-phase with that at 32 °S. The NH maximum occurs in late January, while the SH minimum occurs in February at 50 and 30 mbar, but somewhat earlier at higher altitudes. The patterns are similar above 30 mbar, but the spring values in the SH are larger than the NH maxima in February, suggesting a hemispheric asymmetry in the HNO_3 amounts. A striking feature is that the maximum appears to occur later at lower altitudes, as if propagating downward.

The characteristics are similar at 60 °N and S, but the NH maxima occur in January at 50 mbar, or in December at 30 mbar. This level also shows higher values in late autumn in the SH than in the NH. Again, there is a suggestion that the NH maximum occurs earlier than the SH minimum.

At 80 °N (for which a SH counterpart does not exist in the LIMS database), the maximum occurs in November. At 30 mbar the maximum of over 12.5 ppbv is reached in mid-November, after which the concentration decreases irregularly through the winter and more smoothly in the spring to a value just under 7 ppbv. The altitude of maximum values decreases from fall to winter, and rises again in the spring.

These plots clearly indicate that there are long term changes, probably due to a combination of transport and photochemical effects, and short period variations, especially during the winter, that are related to dynamical effects. There are marked decreases at high levels during the times of major disturbances in the stratosphere, which are to be expected when downward motions (which lead to stratospheric warming through adiabatic heating) bring down air that is poorer in HNO_3.

It is clear that the SH maxima and perhaps the minima have larger mixing ratios than those in the NH, indicating an asymmetry between the hemispheres in nitrogen compounds. This has also been seen in NO_2, and in estimates of the total odd nitrogen (Noxon, 1979; McKenzie and Johnston, 1982; Solomon *et al.*, 1983a; Gille, 1984b).

Vertical Profiles

Monthly and zonally averaged vertical profiles are shown in Figure 10-46 for 5 latitudes and the 4 months for which the cross-sections were discussed above. At 60 °S the largest mixing ratios are always at 30 mbar, with the lowest value in the summer, and maximum of over 10 ppbv in the late autumn. At 32 °S the values decrease from spring to summer, then increase into the autumn. There is very little seasonal variation at the equator, where the peak values are at 16 mbar. At 32 °N the seasonal variation is similar to that in the Southern Hemisphere. The smallest peak values are in the autumn, increasing into winter, and

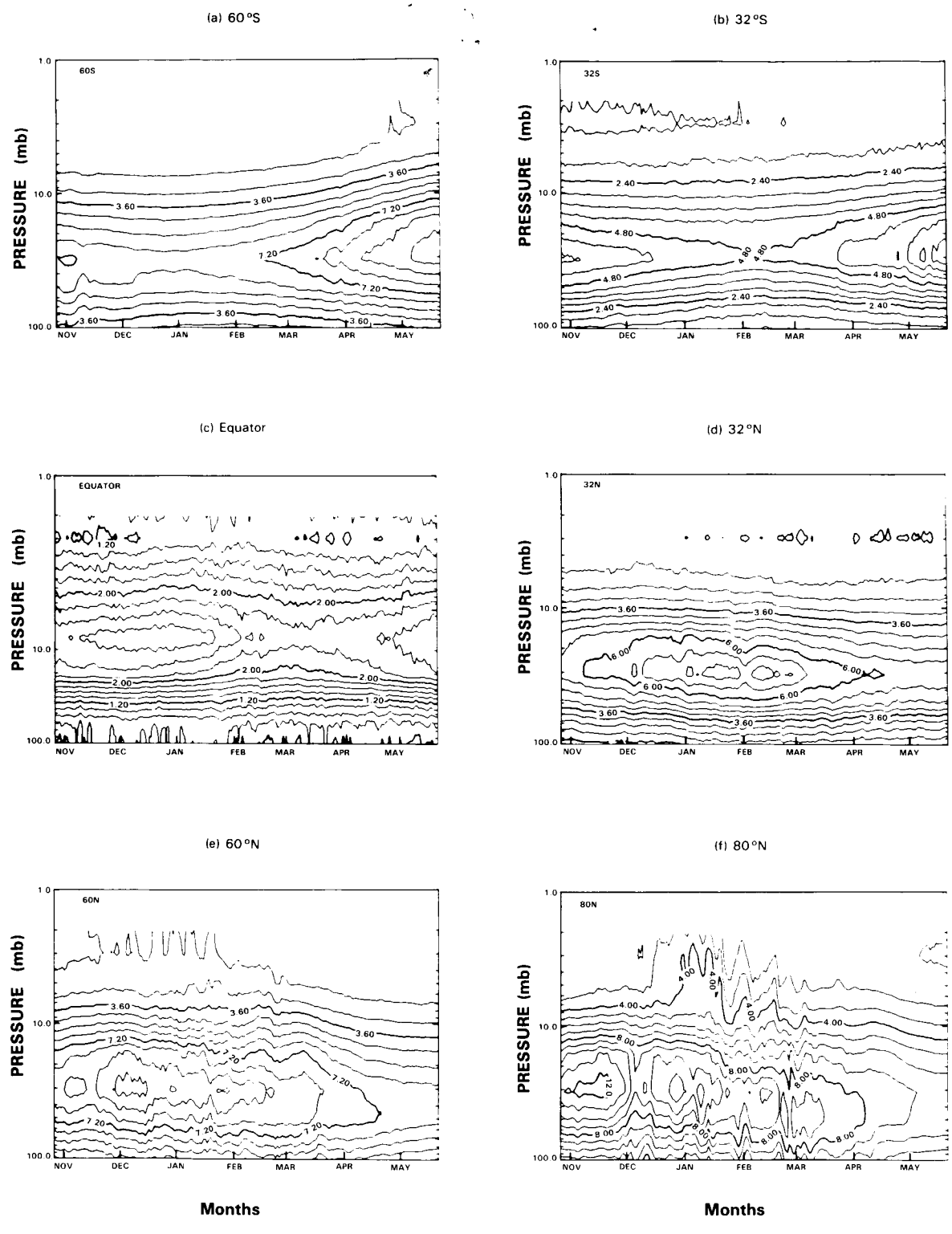

Figure 10-45. Time-height cross sections for HNO_3, for latitudes (a) 60°S, (b) 32°S, (c) Equator, (d) 32°N, (e) 60°N and (f) 80°N.

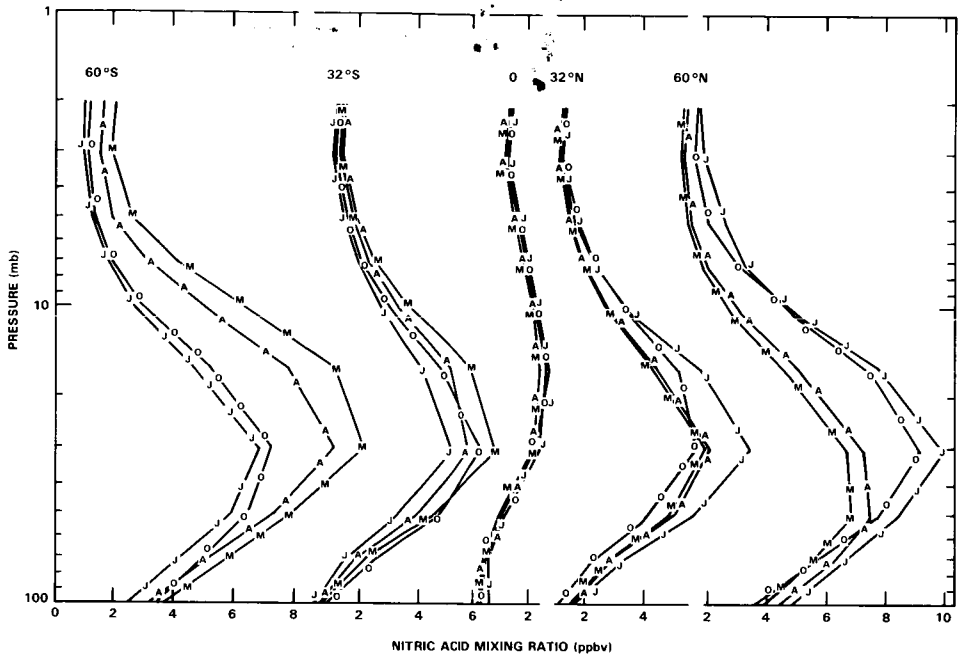

Figure 10-46. Vertical profiles of zonally and temporally averaged HNO_3 mixing ratios, at 5 latitudes for October, January, April and May. O-October, J-January, A-April, M-May.

dropping back in the spring. The same qualitative variations take place at 60 °N, but now the autumn values are almost as large as the winter value. At 84 °N the maximum value over 12 ppbv is reached in the autumn, with a continuous but irregular decrease to the late spring. Again, it should be noticed that the maximum values at 60 °S are larger than those at 60 °N, again indicating that the HNO_3 is not symmetric between the hemispheres.

10.2.3 Nitrous Oxide (N_2O)

10.2.3.1 Nitrous Oxide Mixing Ratio Measurements from SAMS

Introduction

The Stratospheric and Mesospheric Sounder (SAMS) instrument launched on the Nimbus 7 satellite in October 1978 is a multi-channel infrared limb-scanning radiometer using both "conventional" and pressure modulaton techniques to measure atmospheric temperature and the abundances of a number of minor atmospheric constituents. It is further described in the Special Introduction. In this section we present data from the nitrous oxide channel on SAMS.

Nitrous Oxide Data from SAMS

A detailed description of the SAMS instrument has been given by Drummond *et al.* (1980). Of relevance to the nitrous oxide measurements is the fact that the same optical chain is used by the methane channel on SAMS, which also shares a common detector. This meant that methane and nitrous oxide could not be measured simultaneously, and in practice this meant that measurements of the two gases were made

on alternate 24 hour periods. This, and the duty cycle of the SAMS instrument (3 days in every 4) meant that nitrous oxide measurements were made for approximately 40% of the time (approx. 12 days per month).

Details of the instrument radiometric calibration and the approach taken to deduce mixing ratio profiles from measured radiance profiles can be found in Wale and Peskett (1984) and Rodgers *et al.* (1984), respectively.

The signal-to-noise ratio of the radiances measured by the nitrous oxide channel was not in general sufficiently high to allow single profiles to be retrieved. The normal procedure was therefore to average radiances zonally before inversion. Corresponding zonal average temperature profiles were also produced by averaging the Planck function at 7.8μ (using SAMS derived termperatures). The normal procedure was to average the radiances measured over a 24 hr. period over 10 degree latitude bands and 0.2 scale height (approx 1.4 km) intervals in the vertical. Zonal mean mixing ratio profiles were then derived from the zonally averaged quantities from which daily (and of course longer term) zonal mean cross-sections could be derived.

The SAMS instrument began operation in late October 1978 and functioned until the middle of 1983 except for a period between late September 1982 and mid-February 1983. Thus a continuous record spanning in excess of three years was obtained.

The Error Budget of the SAMS Nitrous Oxide Measurements

A detailed discussion of the error budget of the SAMS nitrous oxide budget may be found in Jones and Pyle (1984). A summary of this work is given below.

Systematic errors in the retrieved nitrous oxide fields fall broadly into four categories: Uncertainties in the spectroscopy of nitrous oxide and any contaminating gases (mainly methane), instrumental uncertainties, limitations and simplifications in the retrieval method and algorithm, and inaccurate knowledge of the state of the atmosphere (mainly of the temperature structure.)

To estimate the impacts of these various error sources a synthetic radiance profile was computed from assumed typical mixing ratio and temperature profiles with all the uncertain components set to their nominal values. The simulated data set was then retrieved with each uncertain parameter offset in turn to its limit of uncertainty and the retrieved mixing ratio profile was compared each time with the original.

In addition to the systematic error sources, even with the zonal averaging there remained a significant random component to the error budget due to radiance noise. The effects of this on the retrieved mixing ratio profiles was quantified during the retrieval by means of an error covariance matrix (see Rodgers *et al.*, 1984).

A summary of the error budget of the SAMS nitrous oxide measurements are shown at various pressure levels in Table 10-10.

A detailed discussion of the various error sources may be found in Jones and Pyle (1984) and it is necessary here merely to reinforce the main conclusions found there, namely that uncertainties in retrieved temperatures have maximum impact at the profile extremities (notably at lower levels) while effects such as uncompensated Doppler shifts (due to zonal winds) have pronounced effects at upper levels. The net RSS accuracy reaches around $\pm$ 50% at most levels and is lowest (approx 20%) near 7 mbar. The random

Table 10-10. Summary of the Error Budget for the SAMS Nitrous Oxide Measurements

Pressure Level	20 mbar	7 mbar	2 mbar	0.6 mbar
1. Spectroscopy	±7%	±7%	±5%	±5%
2. Field of view	±2%	±4%	±7%	±8%
3. Mean PMC pressure	±3%	±2%	±17%	±21%
4. Uncompensated Doppler shifts	±3%	±2%	±45%	±15%
5. Zonal averaging	±8%	±8%	±8%	±8%
6. Interference of CH_4	±8.5%	±2%	±5%	±25%
7. Temperature (± 2 K)	±50%	±15%	±10%	±20%
8. Line-of-sight attitude (± 0.0006)	±4%	±8%	±12%	±3%
9. RSS of latitude and time dependent error	±51%	±17%	±48%	±35%
10. RSS of bias errors	±9%	±7%	±20%	±24%
11. Net RSS accuracy	±52%	±20%	±50%	±43%
12. Precision of monthly mean cross section	±12-20%	±6-17%	±10-24%	±50-100%

noise on a monthly zonal mean nitrous oxide cross-section was generally 10–20% except above 2 mbar where it increased dramatically. It should be noted that the precision depends strongly on the mixing ratio and temperature structure, being lowest where both high mixing ratios and high temperatures are present.

Comparison of SAMS Nitrous Oxide with Other Measurements

As was pointed out above, only zonally averaged mixing ratio profiles were derived from SAMS data. Any comparison with individual *in situ* or balloon based measurements as a means of validating the SAMS data must be regarded as of limited value. Nevertheless, it is useful to compare the SAMS data with other available measurements.

Vertical profiles of N_2O have been measured on numerous occasions over the last decade, mainly by grab-sampling (see WMO 1982). These data do not have uniform spatial coverage and for nitrous oxide are strongly weighted to equatorial latitudes and 44 °N. The data show substantial variability, far in excess of the precision of 2-5% quoted by the various experimenters, and no clear seasonal variation is discernable. For these reasons the comparison with the SAMS data have been performed by comparing all the available non-satellite measurements at each latitude irrespective of season with the SAMS nitrous oxide annual mean profile for 1979 at that latitude. These comparisons are shown in Figures 10-47 (a) and (b). Also shown are the estimated accuracies of the SAMS observations (horizontal bars) and an envelope embracing the month-to-month variability of the SAMS data.

It can be seen that the SAMS data extend to much higher levels (approx 55 km) than the *in situ* data. The SAMS nitrous oxide data give mixing ratios of around 300 ppbv at around 30 km, falling off exponentially with height to below 10 ppbv at upper levels.

At equatorial latitudes (Figure 10-47 (a)) above 30 km the SAMS measurements agree well with other measurements both in terms of vertical gradient and absolute amount. Below 30 km the SAMS measurements are biased high, but nevertheless the two data sets are consistent to within their estimated accuracies. At 45 °N (Figure 10-47(b)), although the SAMS measurements reproduce the vertical gradient suggested by the *in situ* measurements, they again appear biased high, by 20-30% at 30 km and rather more below. It is conceivable that this discrepancy is exacerbated by inaccuracies relating the geometric height scale of the *in situ* data and the pressure scale of the SAMS data. A similar comparison except using data for the three year period 1979-1981 gives very similar results (see Jones, 1984).

Overall, the SAMS nitrous oxide measurements reproduce well the gross features of the other measurements, namely the low stratosphere low latitude mixing ratio maximum and the sharp fall-off of mixing ratio with height together with a somewhat slower decrease towards high latitudes.

The Data

In Figure 10-48(a-1) are shown monthly mean zonal cross-sections of nitrous oxide mixing ratio measured by SAMS for January to December 1979. The data extend from 50 °S to 70 °N and from around 20 mbar to 0.6 mbar, covering the stratosphere and low mesosphere. Note that each monthly mean in fact comprises only approximately 12 days per month.

The gross structure suggested by these data is of a low stratosphere low latitude maximum, with the mixing ratio of nitrous oxide decreasing from around 300 ppbv at low equatorial latitudes to between 5 and 10 ppbv at high levels. Closer inspection reveals substantial differences between the various months, as slow seasonal changes progress through the year.

In January 1979 (Figure 10-48a) the distribution of nitrous oxide mixing ratio shows a marked asymmetry about the equator, with a region of elevated mixing ratios extending throughout the stratosphere, tilting from the equator at approx 20 mbar into the Southern (summer) Hemisphere, reaching 10 °S by the stratopause. This gives rise to rather sharp latitudinal gradients at high southern latitudes, with somewhat slacker gradients in the Northern Hemisphere. In the Northern Hemisphere sharp vertical gradients exist at this time in the lower stratosphere, with a more uniformly mixed region above. During February (Figure 10-48b) a second maximum began to emerge in the Northern Hemisphere at high levels. During March and April (Figures 10-48c and d) the second maximum intensified while the Southern Hemisphere maximum subsided to give by May (Figure 10-48e) an almost symmetric pattern with, on a fixed pressure surface, two low latitude maxima separated by an equatorial minimum. This evolution continued, giving by July 1979 a single maximum extending into the Summer (now the Northern) Hemisphere. The pattern during July was essentially a reversal of that of January.

The structure seen during the second half of 1979 differed in many aspects from that of the first. During August and September throughout the middle stratosphere there existed a pronounced maximum at low northern latitudes. By October (Figure 10-48j) this maximum had subsided somewhat. A region of almost uniform mixing in the vertical persisted throughout August to October at high northern latitudes in the upper stratosphere. Interestingly, the "double-peak" structure evident during May that year was not repeated. In the final months of 1979 the maximum continued to subside giving, by December, an almost symmetric distribution (Figure 10-48).

It is obviously necessary to attempt to assess how credible the month-to-month changes observed in the data are, particularly in view of the substantial random and systematic errors which may be present

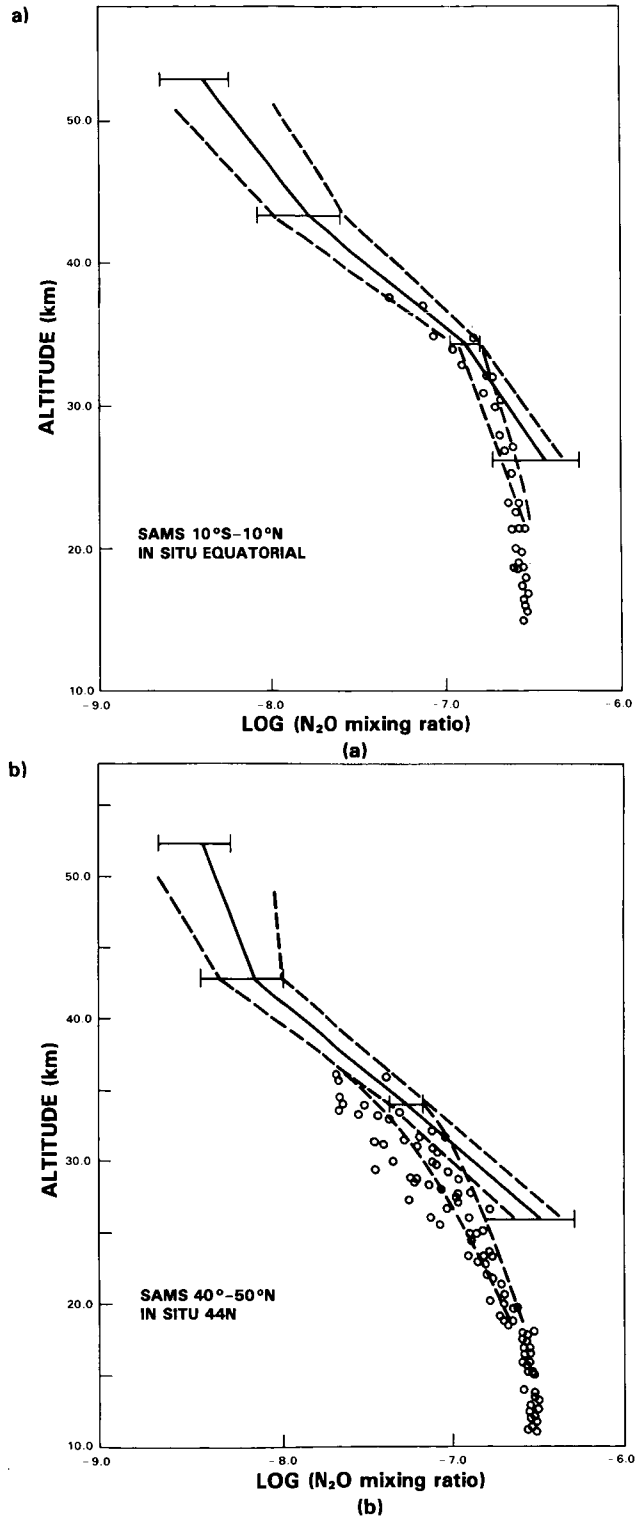

Figure 10-47. Comparison of the SAMS nitrous oxide 1979 annual mean profile (a) (Solid line) for 10°S–10°N with other measurements (circles, WMO 1982). The dashed envelope shows the standard deviation of the monthly mean profiles for the latitude band and the horizontal bars the estimated accuracy. (b) As for (a) except for 40–50°N.

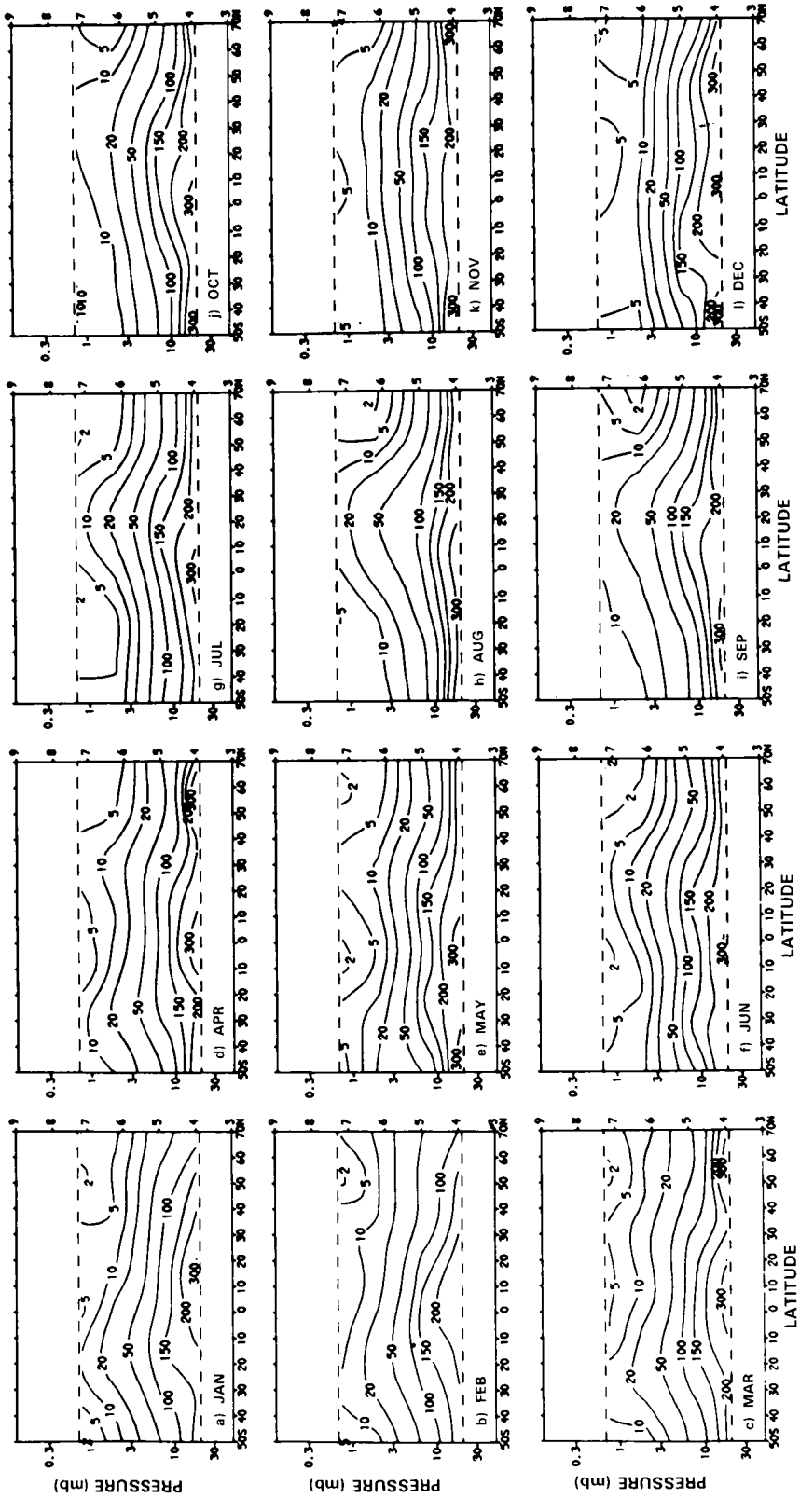

Figure 10-48. Monthly, zonal mean cross-sections of nitrous oxide (ppbv) for 1979 derived from SAMS observations.

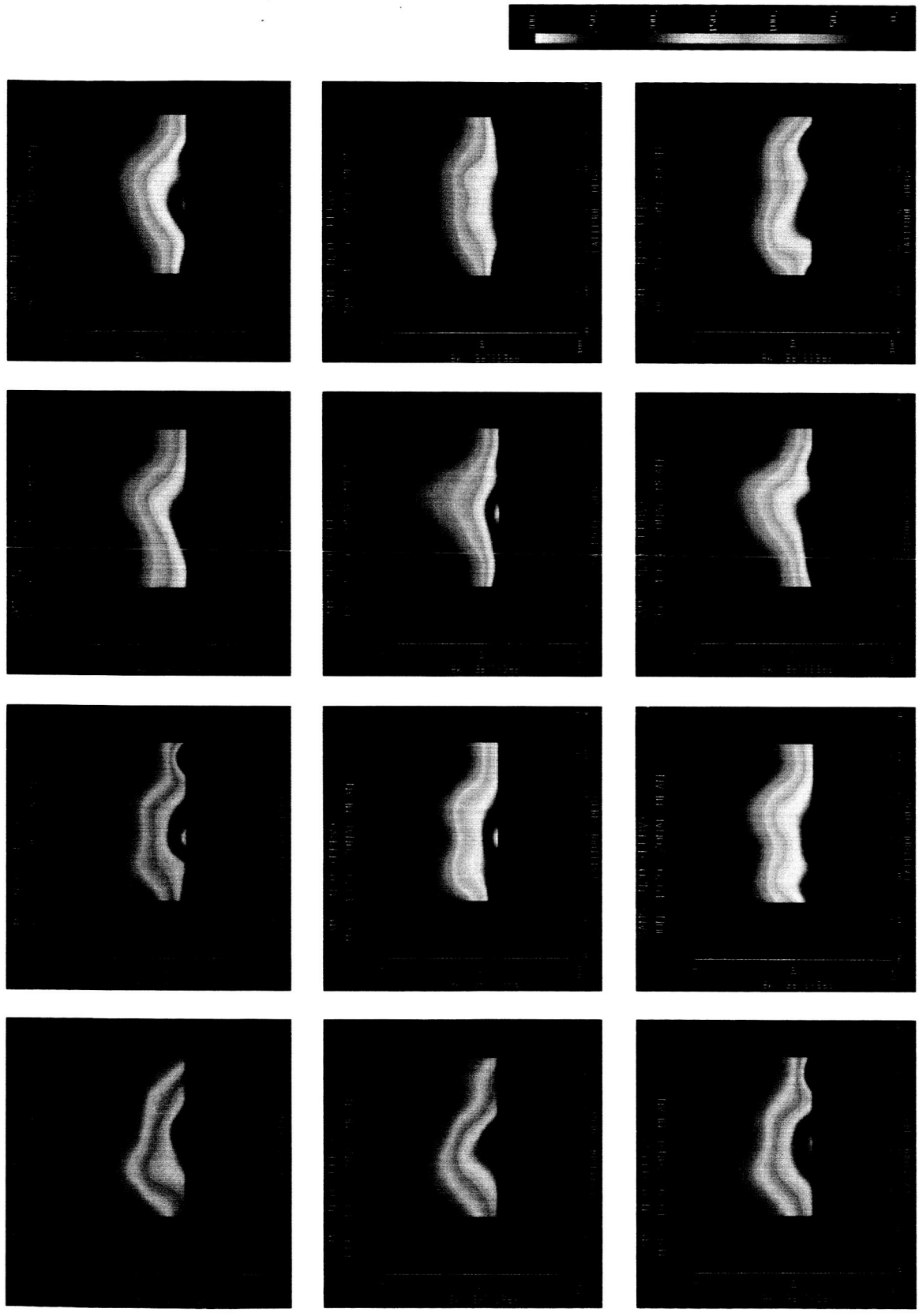

Figure 10-48. (Color) Monthly, zonal mean cross-sections of nitrous oxide (ppbv) for 1979 derived from SAMS observations.

in the data. From this point of view it it of great value to have essentially simultaneous measurements of methane made from the same instrument and in fact made using the same spectral region and optical chain. Because both methane and nitrous oxide originate in the troposphere and are destroyed with long photochemical time constants in the stratosphere, the distributions of both species are determined in large part of the same dynamical processes. The distributions, although not the gradients, of methane and nitrous oxide observed by SAMS are thus expected to be similar and this is in fact the case (Figure 10-49). Jones and Pyle (1984) argue that because of the much more rapid vertical fall-off of nitrous oxide mixing ratio, the errors required to introduce similar spurious features into the distributions of both species are quite different in percentage terms, while known error sources are very similar in percentage terms or do not influence the methane observations significantly. They suggest that the similarity of the methane and N_2O supports the thesis that features such as the "double-peak" are real and not artifacts of the retrieval method. In further support of this, it should be pointed out that independent measurements of another long lived tracer (water vapour) by the LIMS instrument on Nimbus 7 also shows many similar features including the branching seen at low latitudes at certain times of the year (see e.g. Jones *et al.*, 1985).

An equally important question is to ask whether the features seen in the nitrous oxide distributions in 1979 would appear in a long term climatology of that gas. Over three complete years of SAMS nitrous oxide data have now been retrieved and it appears (Jones, 1984) that while there are minor differences from year to year, the seasonal changes are essentially unchanged. To illustrate this, in Figures 10-50 (a-j) are shown monthly mean cross-sections for January, April, July and October for the years 1979, 1980 and 1981. These months are chosen to best emphasise the contrast between the nitrous oxide distributions observed at different times of the year. It is immediately evident that the seasonal variation observed during 1979 is broadly reproduced in 1980 and 1981. There are differences between the years; for example while the July data for 1979 and 1981 closely correspond, those for 1980 appear rather different. Nonetheless, all three years show a mixing ratio maximum extending into the Southern (summer) Hemisphere in January, a "double peak" in April/May, the July distributions mirroring those of January and a rather more quiescent distribution by the end of the year. The fact that many of the features observed during 1979 do appear in the subsequent two years suggests that the SAMS nitrous oxide data are useful as a climatology of that gas.

10.2.4 Nitric Oxide (NO)

One channel on the stratospheric and mesospheric sounder (SAMS) instrument was devoted to measuring mixing ratio of NO in the stratosphere and low mesosphere. There were, however, a number of instrumental and interpretational problems with this channel which meant that unambiguous mixing ratio fields could not be obtained. A detailed exposition of the problems encountered is given by Kerridge (1985).

10.2.5 Intercomparison of NO_2 Satellite Data

This subsection describes an inter-comparison of the NO_2 satellite data presented earlier in this section.

Comparison of the SAGE and LIMS profiles are given in Figures 10-51 a-d which show general agreement, well within the stated accuracies and temporal variability of the measurements. The data compared are zonal means for the Palestine (32 °N) and Aire sur l'Adour (44 °N) latitudes. Sunset data from SAGE for the December, January, February (February 1979-November 1981) zonal average about $32\,°N \pm 5\,°$, are compared with the LIMS 1 PM monthly average for January 1979 (Figure 10-51a). Likewise the March, April, May SAGE data for 34 months are compared with the May LIMS average in Figure 10-51b. For the 32 °N case, SAGE is, as expected, slightly higher in value (cf. Section 10.3 for diurnal effects) with about the same vertical shape except above about 35 km for the winter comparison, where SAGE tends

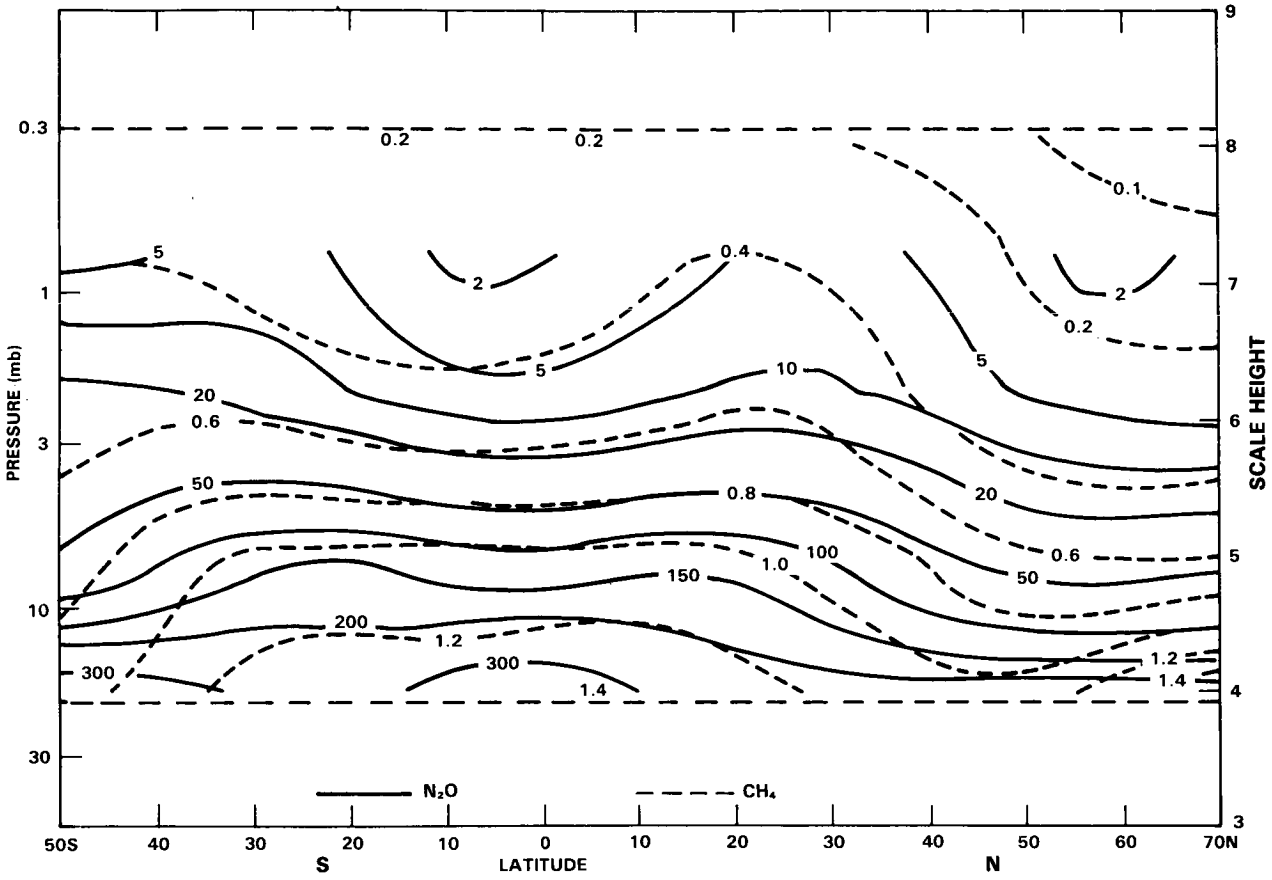

Figure 10-49. Cross-sections of methane (broken/ppmv) and nitrous oxide (solid/ppbv) for May 1979.

to be lower than LIMS which tends to turn upward. Both values are well within the accuracies of both measurements as well as within the variability shown in the three years of SAGE data.

Similarly, the data are compared for 44 °N. The comments above generally hold for this case, with the winter showing a larger difference above 35 km. The values at other altitudes and for May are very similar. Obviously, this comparison should be made for days when LIMS and SAGE were performing measurements at the same latitude. This detailed comparison is in progress.

Comparing the zonal mean cross sections show some similarities and differences but a meaningful comparison is again difficult to make due to diurnal differences (LIMS measurements are at 1 PM (Figure 10-25); SME at 3 PM (Figure 10-30); and SAGE at sunset (Figure 10-33)) and, in addition, due to temporal differences in the measurements. SME data presented in this report are for January, February, March, 1982 monthly averaged from the profiles over the U.S.; LIMS data are for the last 7 days in October, all of January and April, and the first 28 days of May 1979; and, SAGE data are for February 21, 1979 through November 1981 with data shown in this report averaged for the four seasons over three months each centered at January, April, July and October. Nevertheless it is useful to present these data and compare their gross features so that at a minimum a qualitative assessment of this new data set can be made.

All three data sets show the peak in NO_2 mixing ratio to be in the equatorial region centered at 30-36 km altitudes with the SME peak appearing slightly lower than the LIMS and SAGE peak. LIMS and SAGE

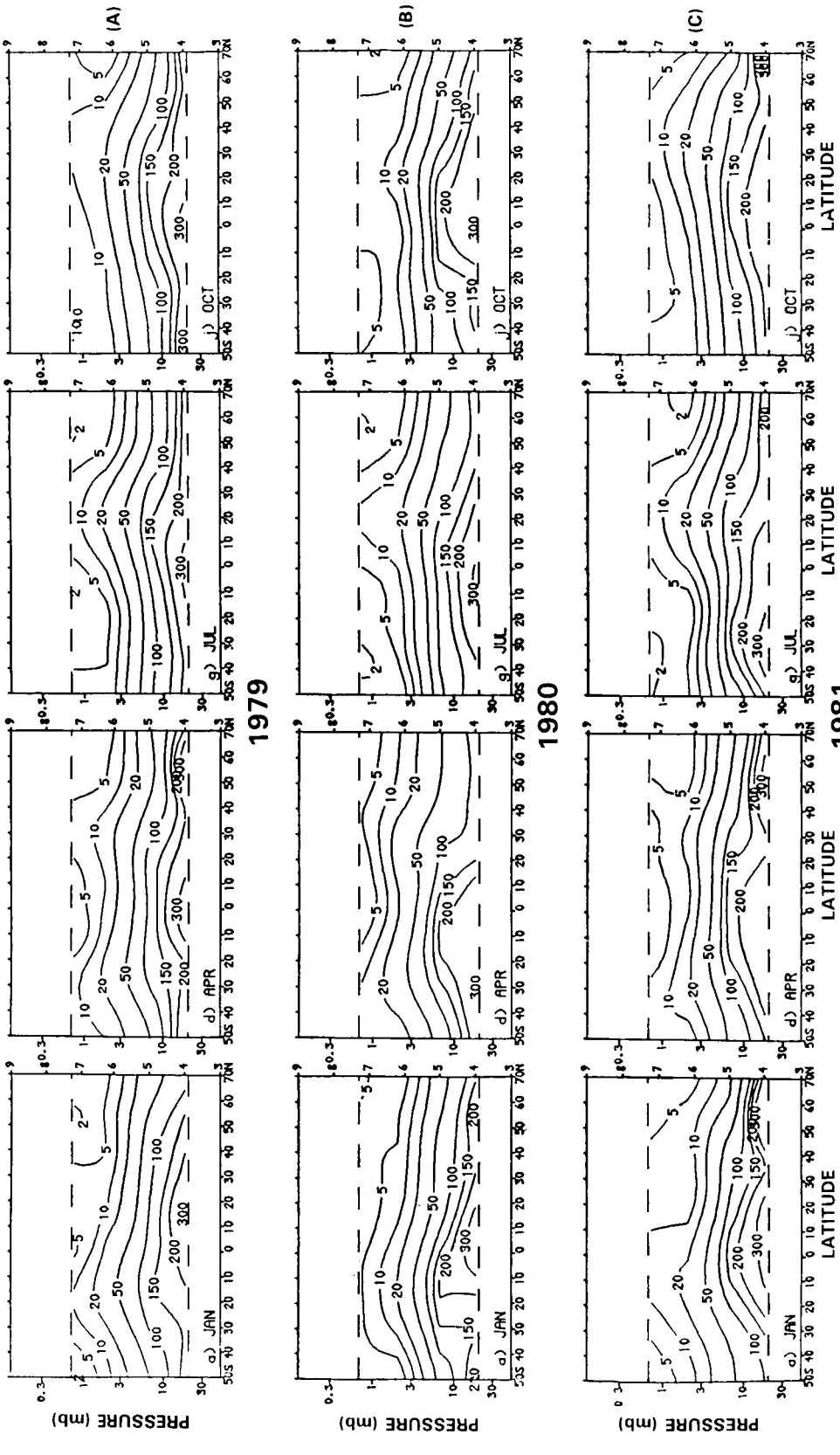

FIGURE 10-50. Monthly mean cross-sections of nitrous oxide (ppbv) for January, April, July and October, (A) is 1979, (B); 1980; (C) is 1981.

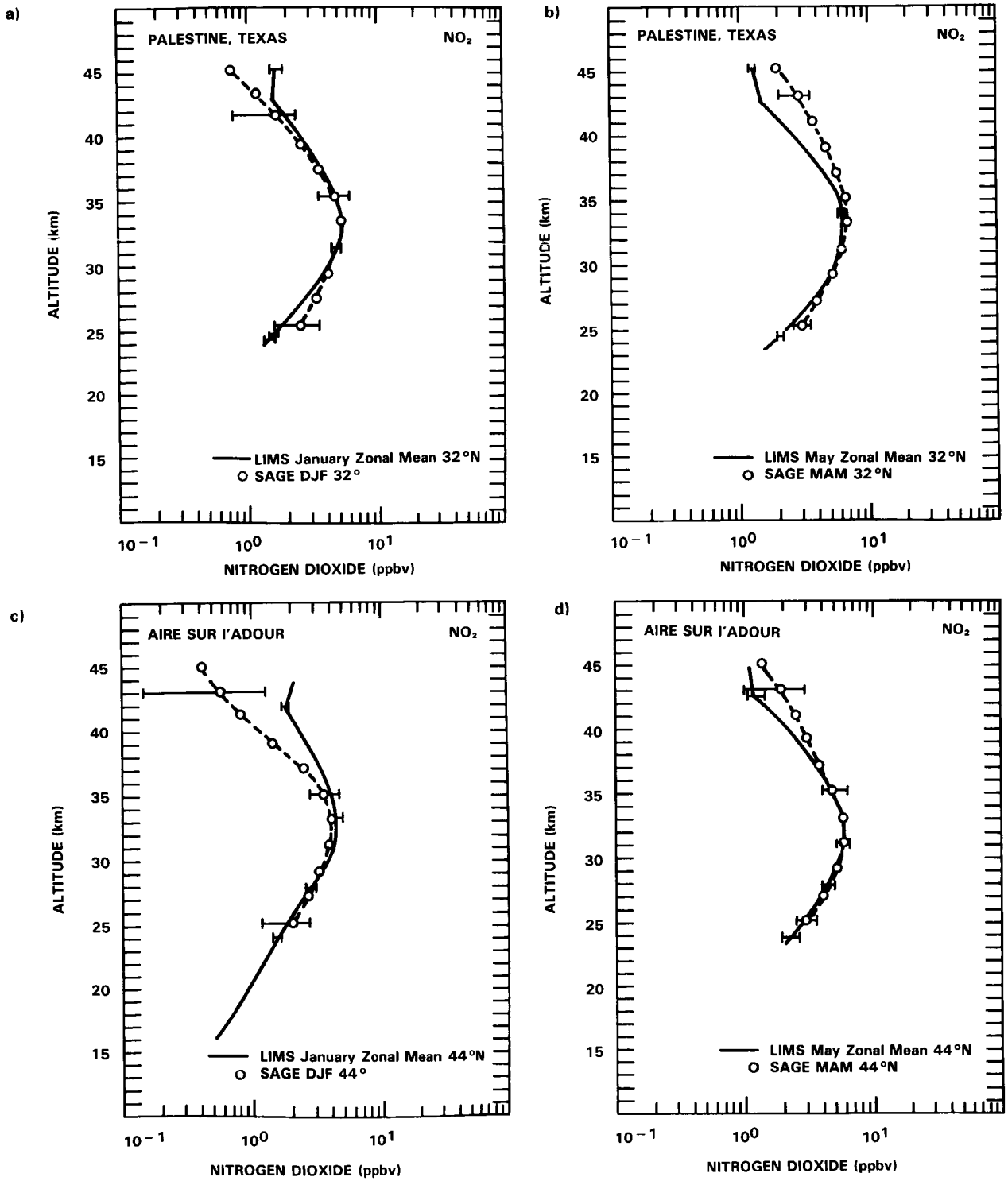

Figure 10-51. Comparison between monthly averaged LIMS profiles and seasonally (32°N) and Aire sur l'Adour, France (44°N), in January and May. Solid line LIMS, dashed line, SAGE. Bars indicate standard deviation over the averaging period. a) January, Palestine, Texas (32°N), b) May, Palestine, Texas (32°N), c) January, Aire sur l'Adour, France (44°N), d) May, Aire sur l'Adour, France (44°N).

both show decreases to higher latitudes north and south but SME shows a decrease only to the north. SME shows large peaks north and south of troughs to either side of the equatorial peak, with an especially strong peak at about 50 °S at about 1 mbar. This feature in the Southern Hemisphere or the troughs are not seen in the SAGE or LIMS data. The LIMS contours seem to be flatter above the peak than does SAGE or LIMS. Possibly this difference is due to water vapour effects in the daytime measurements. The SAGE measurements show a strong bulge above the equatorial peak in northern spring (and somewhat in summer). This is not seen in the LIMS data.

Both SAGE and LIMS show the strong summer/winter difference in profile and column content of NO_2. The data clearly show high values of NO_2 during local summer compared to winter. All three data sets show the "cliff" phenomena at high northern latitudes as described in Section 10.3

Although much more detailed comparison work needs to be done, which considers diurnal variations and other effects, the similarity of the results from these three satellite sensors (especially LIMS and SAGE where more data have been compared) utilising completely different measurement techniques (limb emission, solar absorption, and limb scattering), very encouraging.

Comparisons of LIMS and SAGE data with balloon data are presented in Figure 10-12 and show good agreement below the peak value but the balloon data are higher above the peak.

10.2.6 Representativeness of Palestine and Aire sur l'Adour Launch Sites Compatibility between Satellite and Balloon Observations

Balloon data have provided a large amount of the past and present data on the vertical distributions of trace species. The largest number of these have been made at two locations — Palestine, Texas, USA (32 °N, 95 °W), and Aire sur l'Adour, France (44 °N, 0 °W). Two questions immediately arise, namely, are these locations typical of their latitudes, and secondly, what is the seasonal and short term variation of the results at these locations, as seen in satellite observations, and how does this compare with the results of large numbers of balloon measurements.

Figure 10-52a-d compare daytime NO_2 and HNO_3 results at Palestine and Aire sur l'Adour with the zonal average for those latitudes for January and May. Clearly, these locations are very representative of the zonal averages. These values in Figure 10-52a,b agree well with the mean values for balloon based observations at the same latitudes presented in Section 10.1. Since quite different techniques are used, this provides further information for assessing the absolute accuracy of the techniques, and supports the suggestion that the balloon and satellite results are reasonably compatible with each other.

They also show that the short term variations are larger during the winter than in May, but in both months are rather small. The seasonal changes shown in the January to May differences are therefore significant, although they are not large in an absolute sense. The satellite derived variations are considerably smaller than the flight to flight variations in the balloon soundings; the reasons for this are not clear at this time.

Similar results for HNO_3 are presented in Figure 10-52c,d. Again, Palestine represents the zonal average well in January and May. For Aire sur l'Adour, the October profile (highest during the LIMS period) is somewhat higher than the zonal average at 24 km, but the agreement in May is very close. The fall and winter variances are considerably larger than those in May. The seasonal differences again are not extremely large, but significant.

C-3

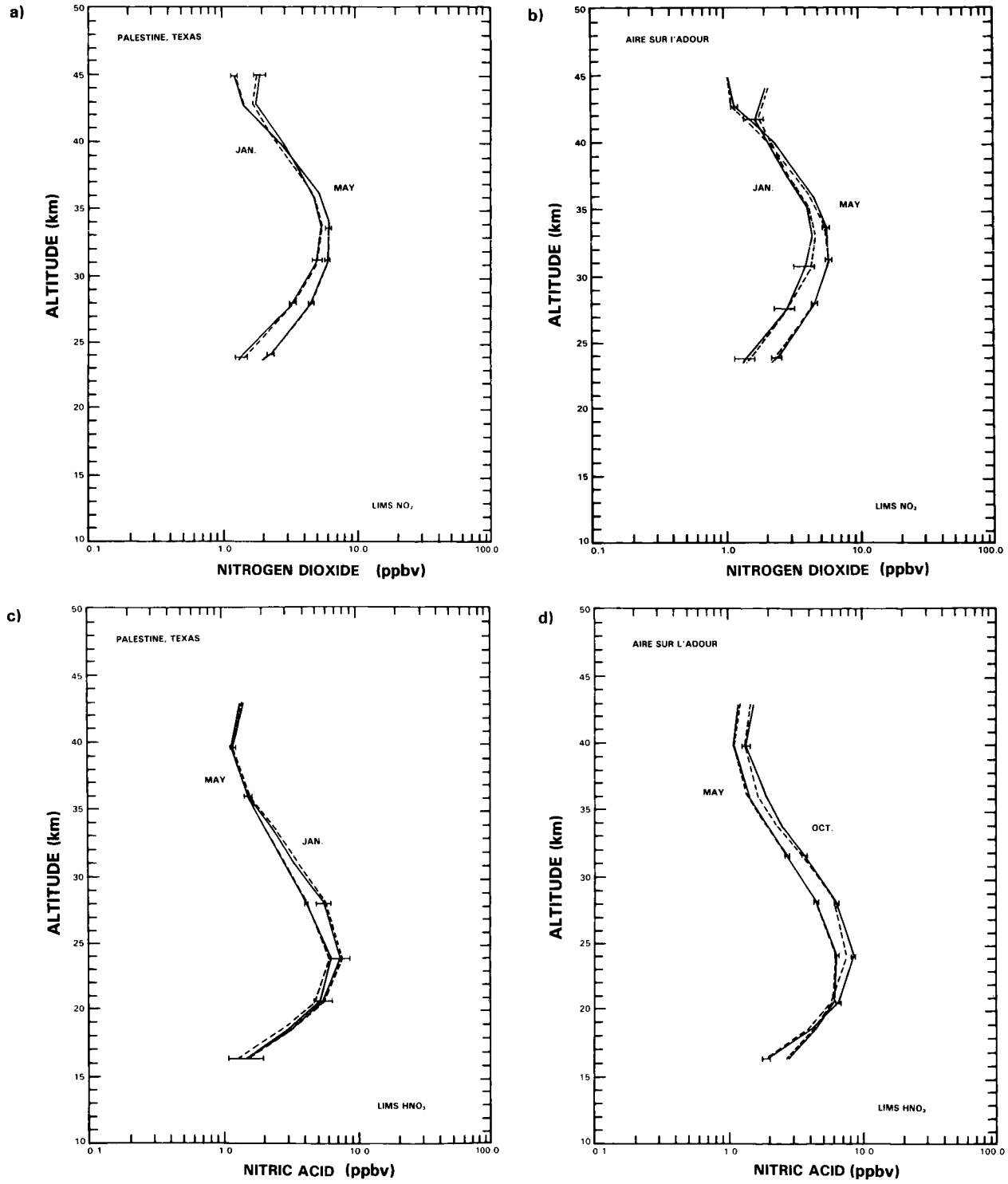

Figure 10-52. Mean profiles of daytime NO_2 and HNO_3 at the balloon launch sites at Palestine, Texas and Aire sur l'Adour, France (solid lines). These are compared to the zonal means (dashed line) at their latitudes, bars show standard deviations of the launch site profiles 32°N and 44°N respectively. a) NO_2 at Palestine, Texas, b) NO_2 at Aire sur l'Adour, France. c) HNO_3 at Palestine, Texas, d. HNO_3 at Aire sur d'Adour.

Below 35 km these results are also in quite good agreement with the balloon data presented in Section 10.1. Above that they appear larger, as noted by Gille *et al.*, 1984b.

10.3 ODD NITROGEN MODELING

Odd nitrogen plays an important role in the photochemistry of ozone at stratospheric heights, and therefore a large number of observational studies have been devoted to characterizing the distributions of nitrogen compounds. Balloon and aircraft measurements have provided crucial information on the local concentrations, altitude profiles and latitudinal behavior of the column abundances of nitrogen species. In addition, simultaneous measurements of several species have been used to assess the completeness of model photochemical schemes. The direct comparison of model results and measured values provides a consistency check between model results and measurements. Attempts to resolve the discrepancies have resulted in better understanding of the mechanisms controlling many trace gas distributions and identification of the types of data needed for subsequent measurements.

Satellite data provides information on the temporal and spatial behavior of the trace constituents. In some cases, simultaneous measurements of several species are available. In addition to providing a large data base for intercomparison of model results and observations, these experimental and associated theoretical studies have revealed that the distributions of odd nitrogen constituents are controlled by close coupling with stratospheric dynamics. For example, study of the observed zonal mean distributions of N_2O and HNO_3 provides information on the balance between advection and eddy mixing in the zonally averaged transport of trace constituents (Guthrie *et al.*, 1984; Ko *et al.*, 1985). As a result, current interest in nitrogen species goes far beyond their photochemical properties and relationship to ozone; rather, it is now clear that a number of more fundamental atmospheric processes can be explored through observations and modeling of odd nitrogen. These will be the subject of this subsection.

10.3.1 Sources of Odd Nitrogen

10.3.1.1 Nitrous Oxide

The primary source of odd nitrogen in the stratosphere is believed to be the reaction

$$N_2O + O(^1D) \rightarrow 2NO \qquad (7)$$

Recently satellite data on the distribution of N_2O have been obtained by the SAMS satellite experiment onboard NIMBUS 7. The global distribution of $O(^1D)$ can also be inferred using satellite data on ozone. Therefore, the distribution of the odd nitrogen source strength resulting from this reaction (assuming presently accepted photochemistry) can be well-characterized using available satellite data, as shown by Crutzen and Schmailzl (1983). Figure 10-53 presents the distribution of the calculated rate of odd nitrogen production through reaction (7) based on that study. The globally integrated rate of NO_y production was found to be about $1.1\text{–}1.9 \times 10^8$ molecule cm^{-2} s^{-1}. It is important to note that the region of primary NO_y production is found in the tropics, where the product of the densities of N_2O and $O(^1D)$ are maximum in the middle stratosphere (see 10.2.3).

The rate of production of NO_y is thus quite sensitive to the meridional distribution of N_2O. The satellite observations of this species exhibit larger abundances in the tropics than at middle and high latitudes,

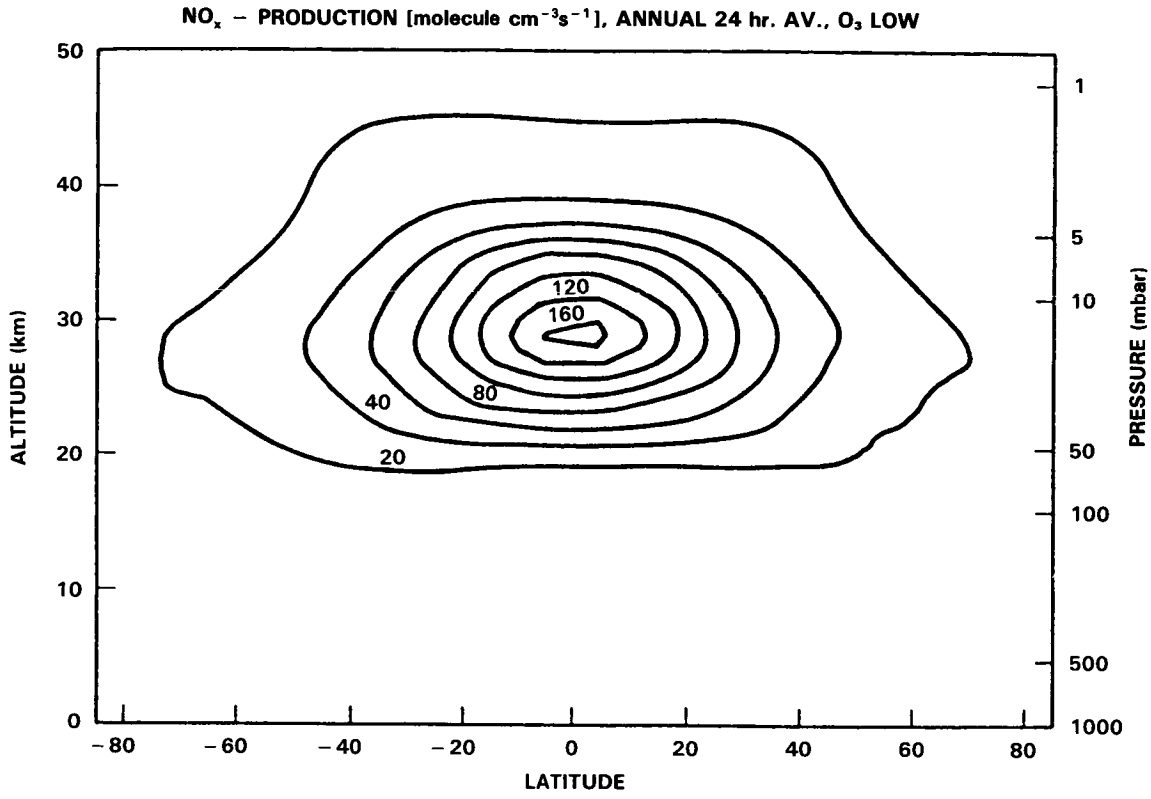

Figure 10-53. Diurnally and annually averaged NO production rate via the reaction O(^{1}D) with N_2O, using the N_2O distributions from SAMS data and the ozone distribution by Duetsch (1978). From Crutzen and Schmailzl, 1983.

roughly consistent with two-dimensional numerical model calculations by Jones and Pyle (1984), Guthrie *et al.* (1984), Ko *et al.* (1985), and Solomon and Garcia (1984b). The SAMS satellite data also exhibit important variations in the details of the N_2O distribution with season (Jones and Pyle, 1984). In particular, the observed distribution of N_2O exhibits a "double-peak" in the spring season, with a local minimum near the equator (Figure 10-48). Gray and Pyle (1985) have conducted detailed studies of the transport processes that are likely to be responsible for this feature, and have shown that momentum deposition associated with the westerly phase of the tropical semiannual oscillation in the zonal winds gives rise to a circulation that yields an N_2O distribution similar to that observed. Thus the distribution of the source of NO_y is very sensitive to transport processes, and the nitrogen species N_2O provides an important test of the completeness of our understanding of stratospheric transport.

Balloon observations of N_2O and other long-lived trace species have revealed important information on local variability of these consitituents, at spatial resolution far beyond the reach of remote sensing instruments. In particular, Ehhalt *et al.* (1983a) have shown that observed vertical variations in N_2O can be characterized by an equivalent displacement height (EDH) relative to a reference profile. This variability is significantly larger than the measurement errors, and changes systematically with altitude for all the species examined. Hess and Holton (1985) have suggested that the observed variance may be related to the dynamical processes associated with stratospheric warmings, i.e., the variance introduced by breaking of large amplitude planetary waves.

While oxidation of N_2O is believed to be the principal source of stratospheric NO_y, other sources must also be considered. Thermospheric odd nitrogen production and its possible transport to the stratosphere will be the subject of the next subsection. Another known source of stratospheric NO_y is provided by galactic cosmic rays (Nicolet, 1975), which have their largest effects at high latitudes. Because of the large rate of NO_y production at low latitudes through reaction (7) and its subsequent transport, this added high latitude source is not very important to the global NO_y distribution. Another possible source of N_2O is associated with mesospheric charged particle precipitation (Zipf and Prasad, 1982) but this process has not yet been quantified insofar as its atmospheric importance is concerned. Finally, odd nitrogen is produced in lightning discharges in the troposphere and perhaps also in the lowest part of the stratosphere in overshooting cumulonimbus clouds (e.g., Tuck, 1976; Noxon, 1976; Logan, 1983). The quantitative importance of this source on a global scale in the stratosphere has also not yet been established.

10.3.1.2 Thermospheric Sources

Odd nitrogen is produced in large amounts at thermospheric heights, via a series of ion-molecule and secondary electron reactions such as

$$e^* + N_2 \rightarrow 2N(^4S,^2D,^2P) + e \tag{8}$$

as discussed, for example, by Strobel *et al.* (1970) and Oran *et al.* (1975).

The dissociation of N_2 proceeds rapidly above about 100 km, resulting in mixing ratios of NO near 100 km of the order of a few ppmv. Since the mixing ratios of NO_y in the stratosphere are only of the order of a few tens of ppbv, even a small flux of thermospheric NO_y to the stratosphere could be of potentially great importance to the stratospheric NO_y budget (see, e.g., Strobel *et al.*, 1970; Brasseur and Nicolet, 1973). On the other hand, NO_y is rapidly destroyed in the sunlit mesosphere via

$$NO + h\nu \rightarrow N(^4S) + O \tag{9}$$

followed by

$$N(^4S) + NO \rightarrow N_2 + O \tag{10}$$

which yields a minimum in the mesospheric NO_y mixing ratio of only a few ppbv near 70-80 km, and essentially destroys the downward flux of thermospheric NO_y. This process clearly requires the presence of sunlight, and, as such, does not occur in the polar night. Therefore, polar night represents a region where effective coupling between thermospheric and stratospheric NO_y may occur, if downward transport processes can act over the time scale of about a season. Theoretical studies by Brasseur (1982), Frederick and Orsini (1982) and Solomon *et al.* (1982) showed that the downward transport of thermospheric NO_y may be significant at high latitudes in winter. Solomon and Garcia (1984b) examined apparent solar cycle variations in BUV and SBUV ozone data, and concluded that transport of thermospheric NO_y to the upper stratosphere (roughly 40-55 km) appeared to be significant for latitudes poleward of about 50-60 °N in the winter season. The study by Russell *et al.* (1984b) employed LIMS data for nighttime NO_2 to show more directly that odd nitrogen transport to the upper stratosphere can clearly be detected in high latitude winter, as shown in detail in Figure 10-54. The large and rapidly increasing mixing ratios observed in the polar winter lower mesosphere are strongly indicative of downward transport from above. Further indications of a high latitude winter enhancement in lower mesospheric NO_y have resulted from observa-

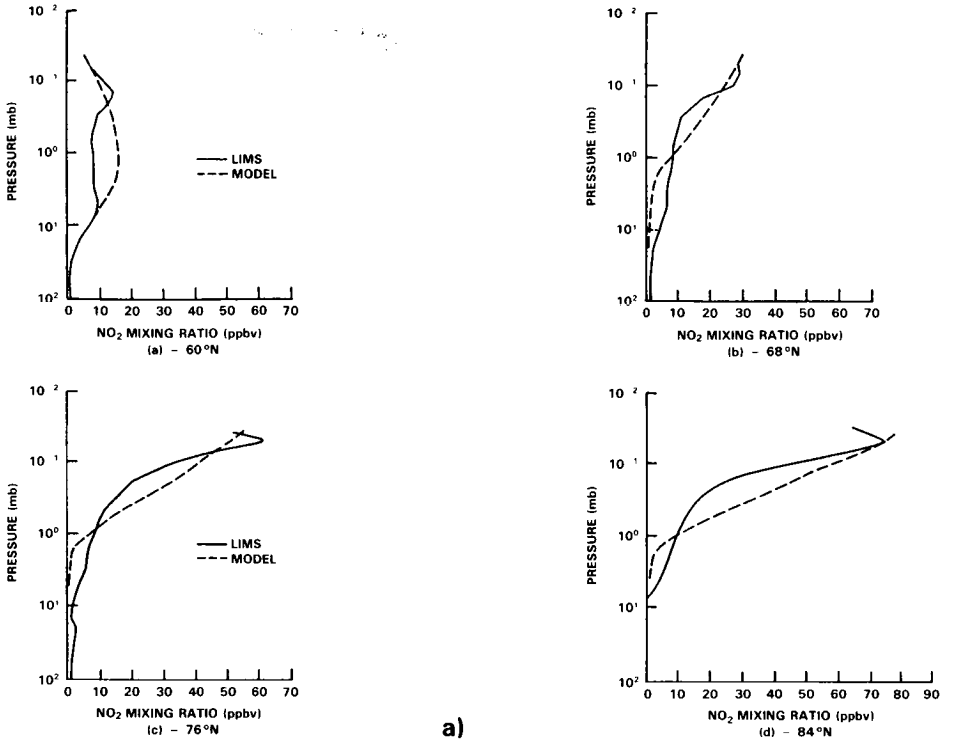

a)

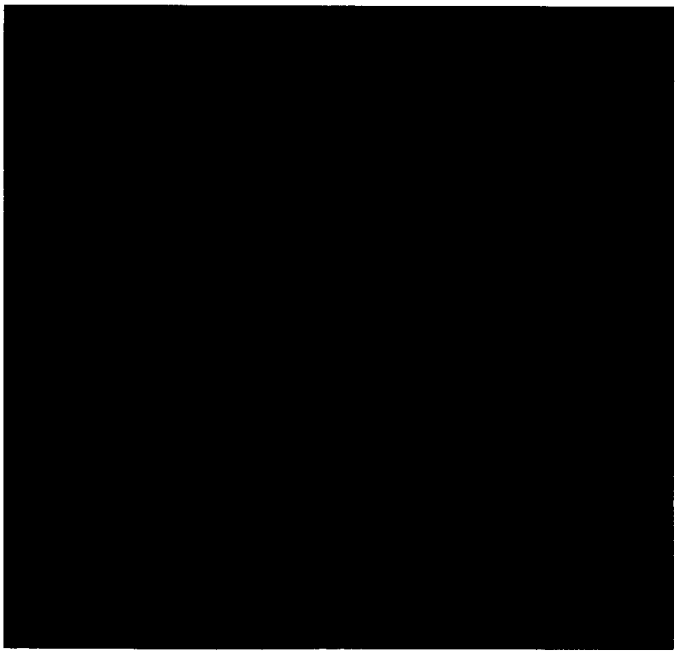

b)

Figure 10-54. (a) Comparison of LIMS zonal mean NO_2 measurements for January 5–9, 1979 with the 2-D model of Solomon and Garcia (1983a), at various latitudes. From Russell *et al.* (1984b); (b) Color plot of LIMS zonal mean NO_2 measurements for January 5–9, 1979.

tions of the NO column abundance above about 50 km as deduced from SBUV observations of NO resonant scattering (Frederick and Serafino, 1985).

A detailed intercomparison of odd nitrogen sources including polar proton events and other high altitude processes was presented by Jackman *et al.* (1980). While thermospheric sources are unlikely to be of importance to the globally averaged NO_y and ozone budgets, observations demonstrate that local ozone and NO_y densities in high latitude winter are substantially influenced by downward transport from the thermospheric source region. More importantly, these data provide excellent tracers for our understanding of mesospheric transport processes.

10.3.1.3 Modelling Studies of the Odd Nitrogen Budget

Although the distribution of N_2O is now relatively well known due to the availability of satellite data, and it is established that the principal stratospheric source of NO_y is likely to be reaction (7) above, the budget of NO_y in model calculations depends upon the transport formulation, and on the uncertainties in the photochemical processes (7), (9) and (10) above. Further, the strongly nonlinear latitudinal gradient in NO_y production via reaction (7) as shown in Figure 10-53 must be considered in the interpretation of one-dimensional globally averaged model profiles of NO_y and their comparison to data. An analysis of the NO_y budget in the one and two-dimensional models by AER (Ko and Sze, 1983; Ko *et al.*, 1985) provides important insight into these questions (see also, model formulation chapter).

Figure 10-55 shows the latitude-altitude cross section of the photochemical production and removal rates for NO_y for equinox conditions calculated from the AER two-dimensional model. Both the production and loss rates show a maximum in the tropics near 30 and 35 km, respectively. Note that the loss rate is about an order of magnitude smaller than the production rate in the tropical mid-stratosphere. Figure 10-56 shows the net photochemical source term (P-L) together with a vector plot of the transport fluxes for the annually averaged budget. Some of the NO_y produced in the tropical stratosphere is removed by photochemical reactions as it is transported to mid- and high latitudes. The rest is removed by transport into the troposphere, particularly in the extratropical regions. Figure 10-57 shows a more detailed accounting of the budget by dividing the atmosphere into boxes. Within each box, the burden, the chemical production and loss rates are given, along with the fluxes across the boundaries due to transport. Note that the transport fluxes are, with the exception of the equatorial stratosphere, significantly larger than the local photochemical terms, indicating the importance of transport in determining the NO_y distribution.

Considering the differences in formulation between one and two-dimensional models, there is no *a priori* reason to expect the calculated globally averaged concentrations of NO_y in a two-dimensional model to agree with the result from a one-dimensional model. However, it is important to discuss how one-dimensional models of NO_y can be interpreted in the context of two-dimensional models, since one-dimensional models are often used in assessment studies, and since NO_y plays an important role in modulating the effect of chlorine perturbations on ozone, especially at high chlorine levels. Figure 10-58 shows calculated NO_y profiles from the AER two-dimensional model compared with that of the AER one-dimensional model, using an identical treatment of radiation and photochemistry. The qualitative similarity between the two models may be explained in terms of the budget on a global basis. The budget from a one-dimensional model indicates a production and loss rate of 0.3mt/year (4.5×10^{26} molecules/sec) and 0.1 mt/year (1.2×10^{26} molecules/sec), respectively, with an export of 0.2 mt/year (3.3×10^{26} molecules/sec) into the troposphere. The ratio of these terms is similar to that in the two-dimensional model although the absolute magnitudes obtained in the one-dimensional model are somewhat smaller. This is to be ex-

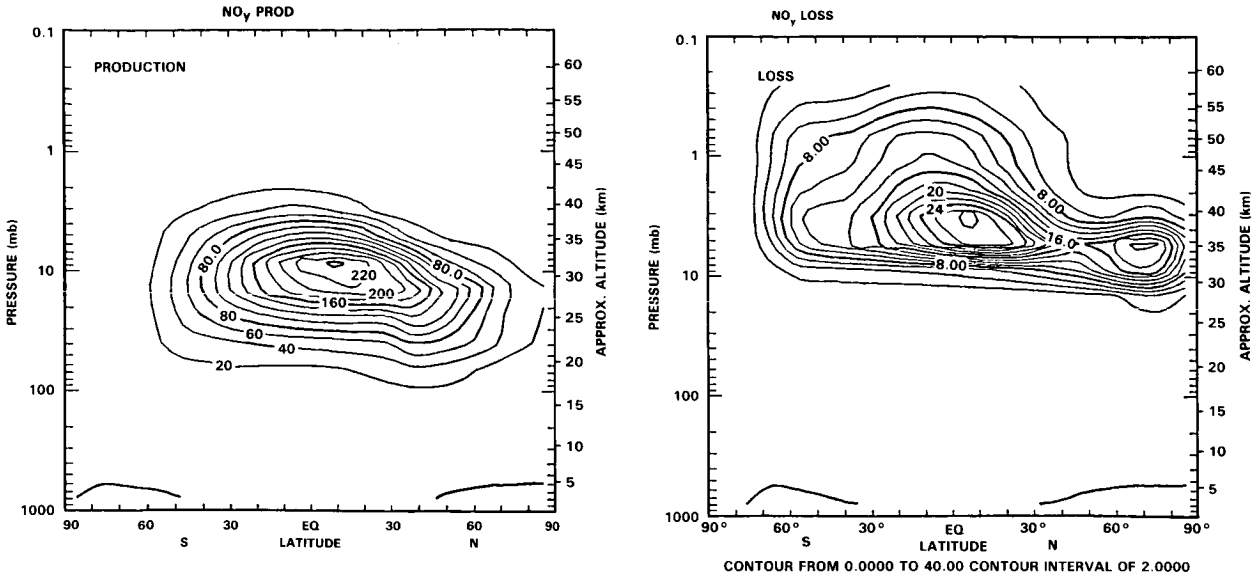

Figure 10-55. Calculated NO_y production and loss rates (molecule cm^{-3} s^{-1}) from the AER two dimensional model (Ko *et al.*, 1985).

pected since the one-dimensional model is adjusted to simulate the N_2O distribution at mid-latitudes (where the N_2O abundances are smaller than in the tropics) and the production rate is calculated using an equinox 30° degree sun angle. In spite of the similarities, one must also recognize the intrinsic differences between one and two dimensional models. The one-dimensional model cannot account for the covariance in the product of $O(^1D)$ and N_2O in calculating the global production rate (Tuck, 1979; Ko and Sze, 1982; Owens *et al.*, 1982a). The analysis in the AER two-dimensional model showed that this accounts for about 10-15% of the differences in the production rate. The one-dimensional model also cannot simulate the effect of horizontal transport, which is important in determining the latitudinal variations of the profiles in the two-dimensional model and will also modify the response of the two-dimensional model results to changes in production rates.

Comparison of the model results shows that the 1-D model result tends to underestimate the peak concentrations around 40 km. In the lower stratosphere, the 1-D simulated NO_y is higher than 2-D models using small eddy diffusion — and comparable to that simulated by 2-D models using large eddy coefficients (See e.g. Ko *et al.*, 1984).

In this section we will examine how uncertainty in rate data would affect the calculated NO_y profiles. A large part of the discrepancies among 1-D NO_y profiles can be explained in term of the treatment of the photodissociation rates for N_2O and NO. Since the balance of NO_y is, to a large extent, maintained by photochemical production and transport, in this section we will concentrate on the effect of the uncertainties in the rate data concerning the production rate.

A sensitivity study is performed using the DuPont 1-D model which analyses the response of the calculated NO_y concentrations to changes in the production rate from uncertainties in the rate data.

The study includes modification of the $O(^1D)$ concentrations by modifying the photolysis rate of O_3 and the quenching of $O(^1D)$. Specifically, the photolysis rate for O_3 and the $O(^1D)$ quenching rate are

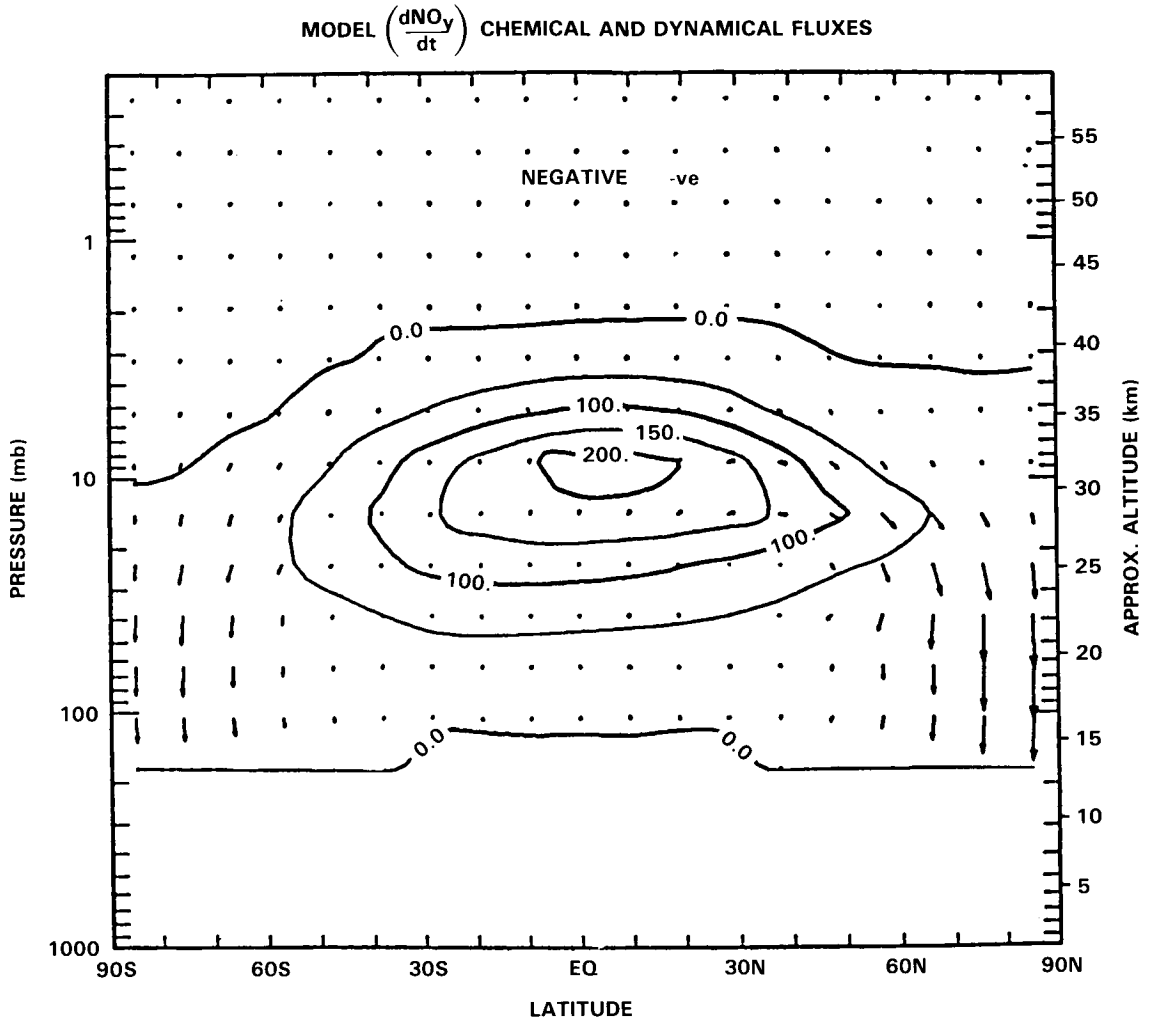

Figure 10-56. Net photochemical production/loss rate (P-L, including washout, (molecule cm^{-3} s^{-1}) for NO_y on an annually averaged basis. Also plotted indicating the transport fluxes. Note that transport is away from the net production region in the tropics and downward into the troposphere at extra-tropical latitudes (from the model of Ko *et al.*, 1985).

varied by 40% and 30% respectively corresponding to the maximum uncertainties cited in the JPL publication. The effects of varying the rate constant of $O(^1D)$ and N_2O (by $\pm$ 50%) and N+NO (by $\pm$ 30%) are also evaluated. The result is summarised in Figure 10-59 which shows the ratio of the perturbed NO_y concentration to the standard 1-D profile. The response of the model is found to have a square root dependence around 40 km where the vertical transport is negligible. In the lower stratosphere, where photochemical production is balanced by vertical transport the response is linear in the production perturbation. In the upper stratosphere, the response to the production changes is small since the balance is between transport into the region and local photochemical losses.

The DuPont analysis shows there could be a factor of two uncertainties in the calculated production and loss rate if the maximum uncertainties in each rate are adopted to obtain the largest possible deviations. This should be reflected in a corresponding uncertainty in the calculated NO_y of about 40% at 40

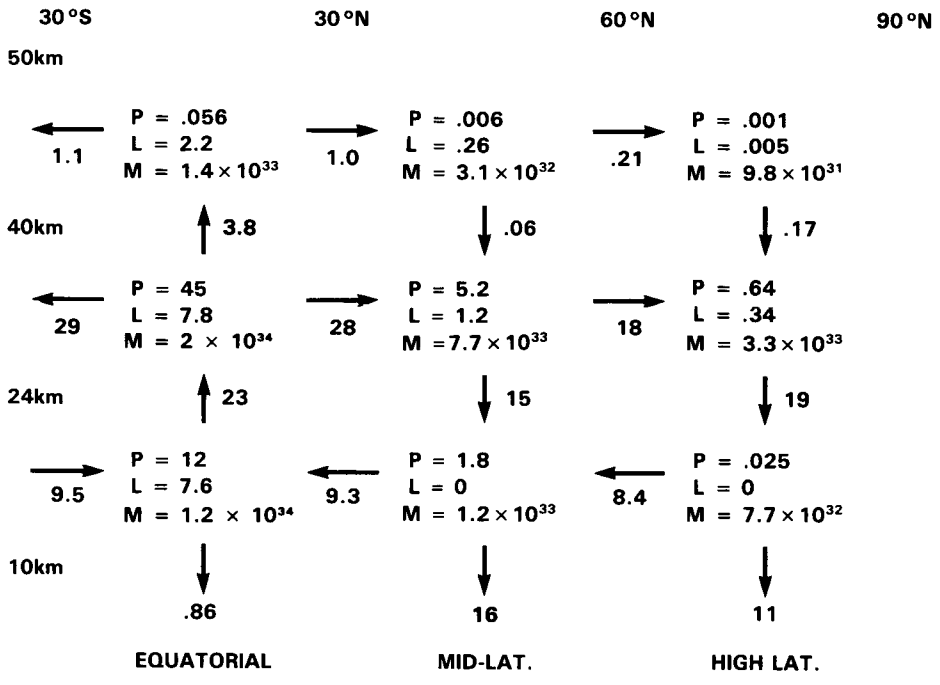

Figure 10-57. Box budget of NO_y from the model of Ko *et al.*, 1985. The atmosphere is divided into boxes covering the tropics, the mid-latitudes and the polar regions from 10-24 km, 24-40 km, and 40-50 km. Within each box, the NO_y burden, in 10^{25} molecules, is indicated. Photochemical loss and production rates, and transport across each boundary of each box, are also indicated in units of 10^{25} molecule s^{-1}

km and close to factor of two in the lower stratosphere. However, a more realistic estimate of the combined uncertainties should be of the order of about 30%.

The response of a 2-D model is expected to be somewhat different since horizontal transport plays an important role. We expect the response to be closer to linear in the stratosphere since transport is important everywhere. In particular, the calculated NO_y in the lower stratosphere should respond linearly to the production term since the concentration has to go up proportionally to maintain the transport out of the stratosphere to balance the excess.

Thus, in the lower stratosphere, where the concentration of NO_y plays a crucial role in modulating the effect of Cl_x on O_3, uncertainties in rate data could have a large impact.

10.3.2 Distributions and Comparisons to Data

Stratospheric odd nitrogen distributions can be examined in detail due to the availability of satellite data for NO_2 (from LIMS, SAGE, and SME), and HNO_3 (from LIMS), as well as ground based and aircraft data on the latitudinal variations of the distributions of these species, as presented in Sections 10.1 and 10.2. Indeed, a number of theoretical studies have been devoted to obtaining a fuller understanding of the observed variations in these constituents, and have led to significant progress in the conceptual basis for dynamical-chemical coupling.

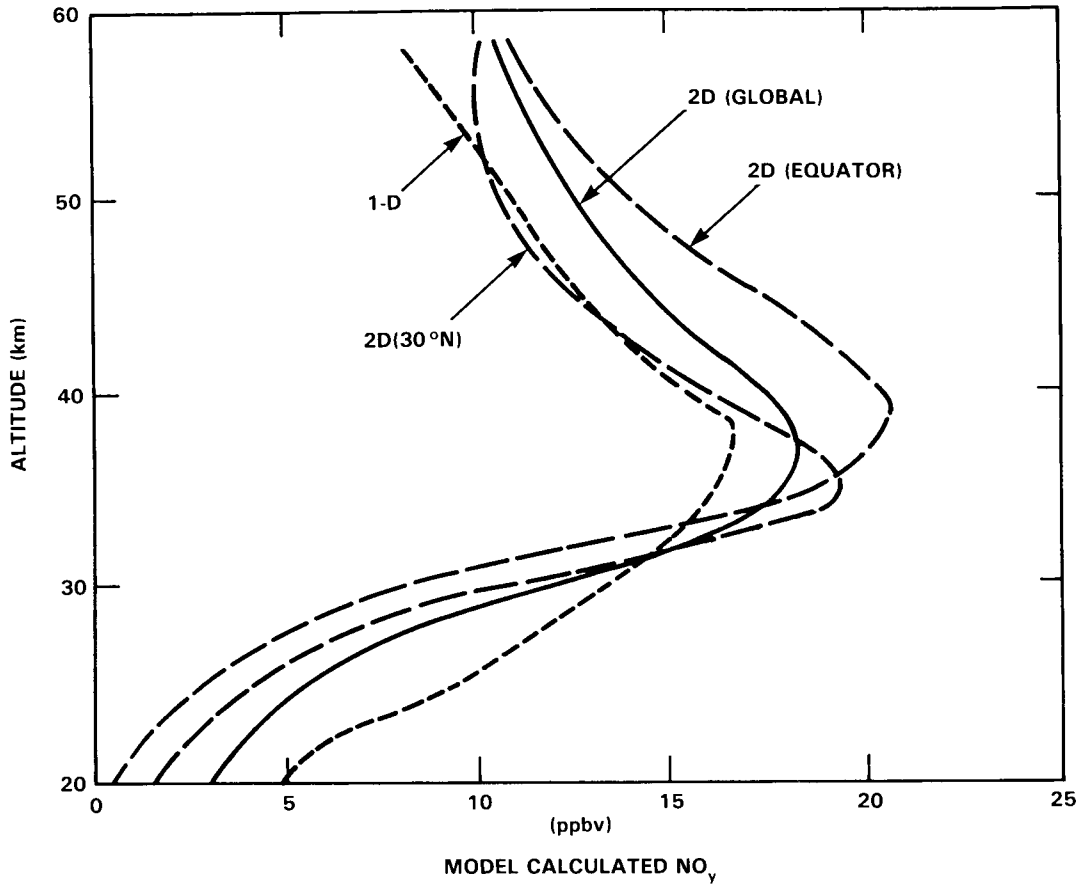

Figure 10-58. Comparison of model calculated NO_y profiles from the AER 1-D and 2-D models.

10.3.2.1 Local Variability in NO_2

Perhaps the most dramatic illustration of dynamical-chemical coupling is provided by observations of stratospheric NO_2. Ground-based studies, particularly those of Noxon (1978a, b, 1979), first presented evidence for this phenomenon. Noxon (1979) observed extremely large gradients in the total NO_2 column during February, 1977, and showed that the distribution of the total NO_2 column depends sensitively on dynamical processes. The unusually large gradient with latitude (see Figure 10-60) led to the observed phenomenon being called a Noxon "cliff" in NO_2. Knight *et al.* (1982) and Evans *et al.* (1982a) suggested that formation of N_2O_5 should be quite important in determining the distribution of NO_2 in high latitude winter. The details of the nature of the dynamical-chemical coupling remained a mystery, however, until laboratory measurements of the temperature dependence of the N_2O_5 absorption cross section were made by Yao *et al.* (1982). Solomon and Garcia (1983a, b) applied these laboratory data in photochemical/trajectory model calculations of the February, 1977 "cliff" observed by Noxon, and showed that the distribution of NO_2 in the cold, high-latitude region depends strongly on the photochemical history of air parcels. In particular NO_x can be largely converted to N_2O_5 at high latitudes in winter, where the number of sunlit hours in the day is small, and the temperatures are cold, leading to a depletion in the abundance of NO_2 in favor of N_2O_5. Rapid transport of these air parcels in the meridional direction (North-South) can occur in the presence of large scale planetary waves on a time scale faster than the photolysis time of N_2O_5, yielding very low NO_2 column abundances at mid-latitude. Such conditions occurred during the February, 1977 "cliff" observed by Noxon.

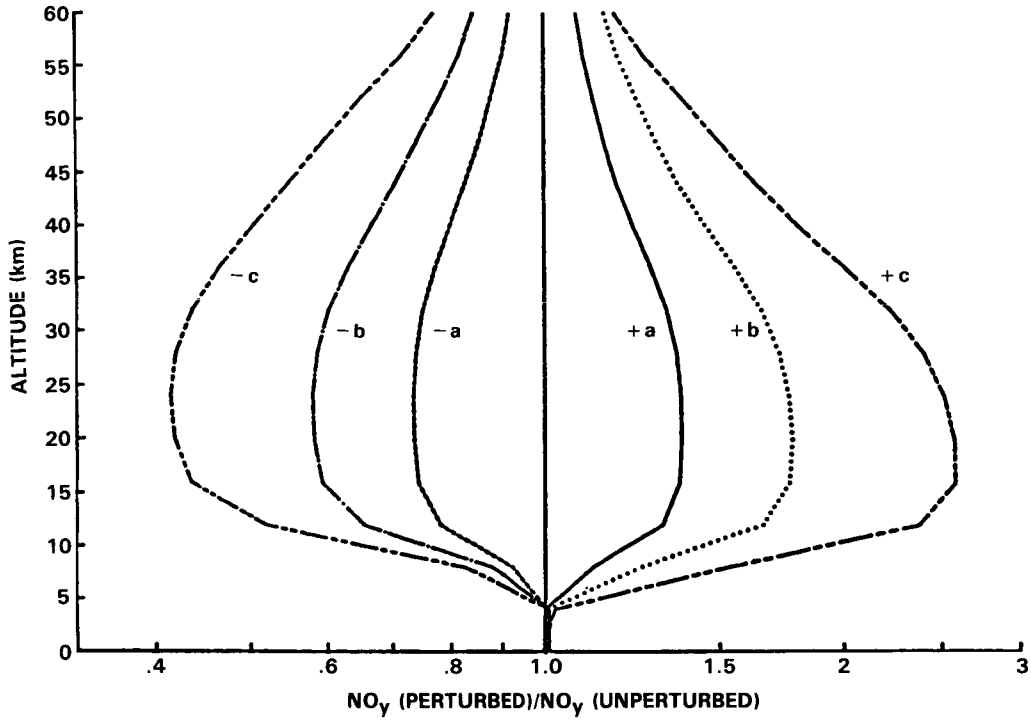

Figure 10-59. Sensitivity study of the response of the DuPont 1-D model profile of NO_y to uncertainties in the rate data. For each case, the reaction of photolysis rates are adjusted to the maximum and minimum values allowed by the uncertainties cited in the rate recommendation. Case a corresponds to adjustment of the photolysis of ozone by ±40%. Case b corresponds to case a plus adjustment of the $O(^1D)$ quenching rate by ±30%. Case c, corresponds to case b plus the uncertainties in the rates of $O(^1D) + N_2O$ (± 50%), and N + NO (± 30%) are considered.

Additional insight into the behavior of odd nitrogen species under "cliff" conditions is available from the balloon chemiluminescent NO observations of Ridley *et al.* (1984). Figure 10-61 shows the NO profile observed by Ridley *et al.* on February 19, 1977 (i.e., for the same "cliff" observed by Noxon in that period), compared to a vertical profile observed at the same location under zonally symmetric (undisturbed) conditions. The profile obtained on February 19 is close to the normal profile near 30 km, but is dramatically different below about 28 km, where much lower NO densities were observed. Thus it is clear that NO_x is indeed reduced during "cliff" conditions, but this reduction is not uniform with altitude: rather, it is confined to the lower part of the stratosphere. Because of the altitude dependence of the N_2O_5 lifetime, this vertical variation in the perturbed profile supports the identification of N_2O_5 as the primary reservoir involved in the Noxon "cliff" phenomenon (Ridley *et al.*, 1984).

Section 10.2 presented satellite observations of Noxon "cliffs" from all three of the available NO_2 satellite data bases. A detailed study of the "cliff" observed by the LIMS satellite experiment during February 1979 was presented by Callis *et al.* (1983b). It was shown that a steep latitudinal gradient observed near 10 mbar was consistent with trajectory calculations during this period, as indicated in Figure 10-62.

An observational and theoretical study of the behavior of NO_2 and its reservoir in high latitude winter was conducted using the SME NO_2 data for the entire winter of 1982 (Zawodny, 1985a, b). The SME data show that large variations in NO_2 are observed not only as a function of latitude as shown in Figure

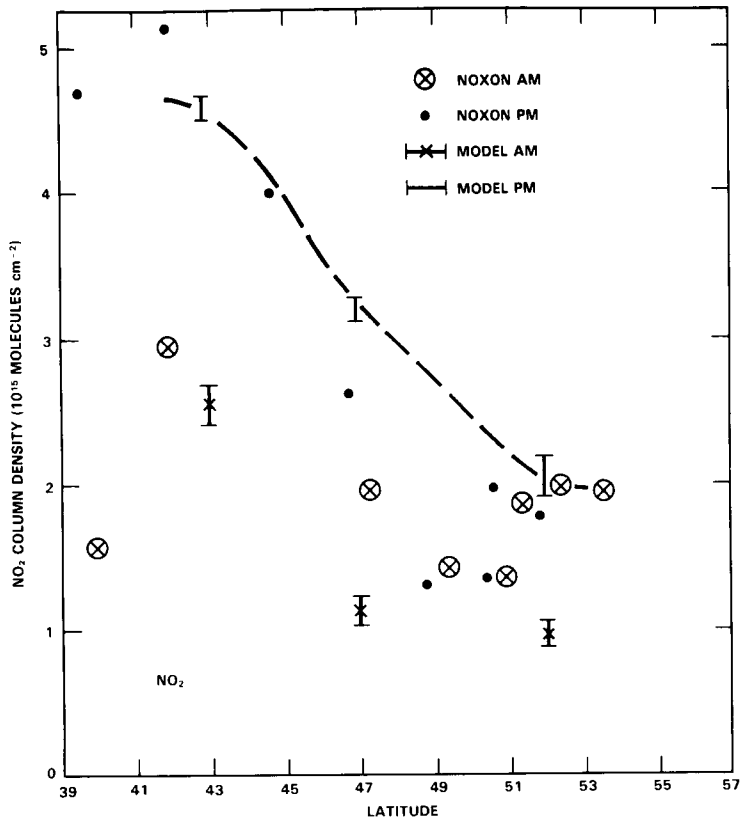

Figure 10-60. Total column abundances as a function of latitude observed by Noxon (1979) in February, 1977, compared to the model calculations of Solomon and Garcia (1983b).

10-60, but also as a function of longitude (i.e., on adjacent orbits). Unlike ground-based or aircraft studies, then, the strength of satellite data for this problem lies in the ability to examine the spatial behavior of NO_2 in several directions. Parcel trajectory calculations can be used to accurately estimate the time required for a moving air parcel in a stationary wave to pass from one orbit to the next. Typically, this time scale is on the order of a day or less for SME orbits over North America during wave displacements. Observed variations from one orbit to the next therefore provide very detailed information on the characteristics of the reservoir species presumably involved in the observed variability; i.e., the photochemical formation and destruction time scales for the reservoir are revealed by the changes in NO_2 between adjacent orbits. Figure 10-63a (see also Figure 10-41) displays a typical pattern of NO_2 variation at the 10 mbar level observed on day 40. The region of very low NO_2 on the westernmost side of the observations corresponds roughly to the location of the displaced polar vortex on this date. Figure 10-63b shows trajectory/chemistry model calculations for the same day, displaying a similar gradient with respect to latitude and longitude (see Zawodny, 1985a, b for details). The increase in NO_2 calculated by the model near 60 °N from west to east is due to the photolysis of N_2O_5 formed principally in the polar night region in the days previous to the observations, and, most importantly, this increase occurs on a time scale of only a day or so. The similarities between model and measured NO_2 therefore suggest that the reservoir species must have a time scale for photochemical loss which is close to that for N_2O_5. This strongly suggests that the principal reservoir is likely to be N_2O_5, as it is in the model. Direct observations of N_2O_5, particularly in high latitude winter, are badly needed to confirm or refute the apparent role of N_2O_5 in determining the local variability of NO_2.

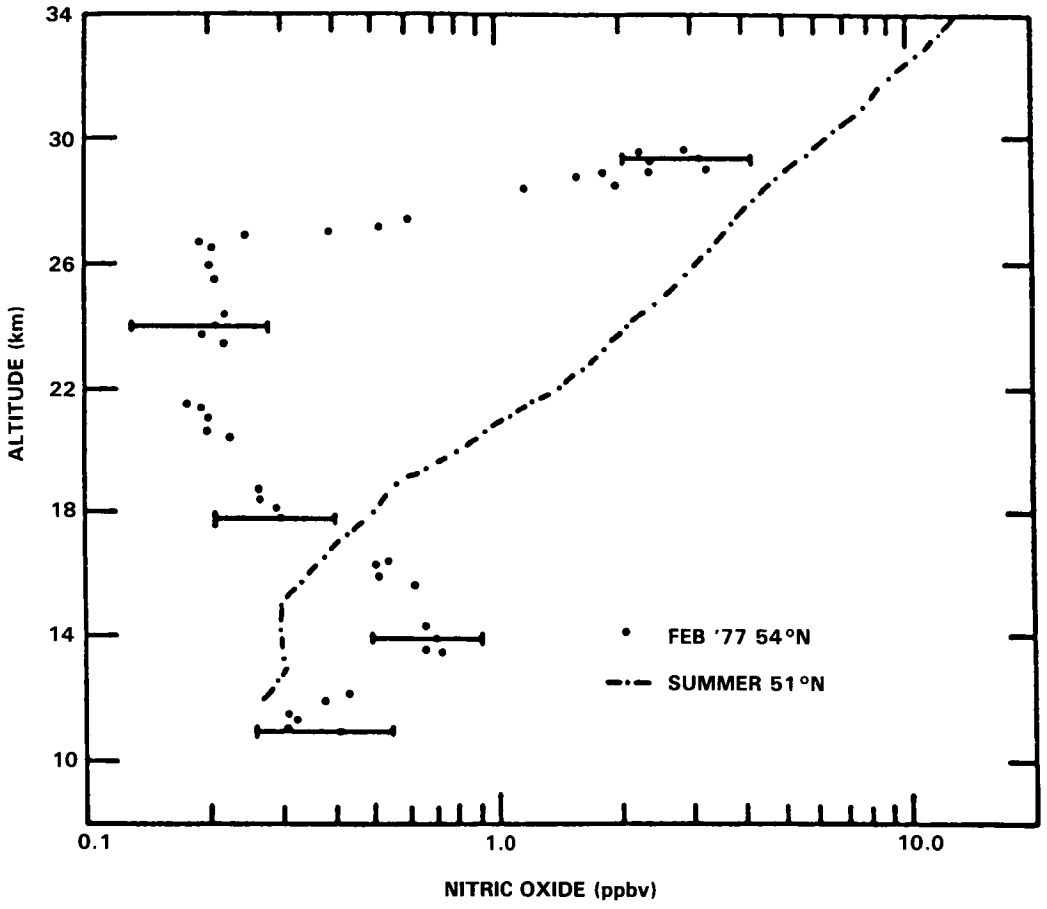

Figure 10-61. The NO distribution for February 19, 1977, compared with an average summer profile for 51°N. From Ridley *et al.* (1984).

10.3.2.2 Global Distributions of NO_y Species

In addition to its importance in determining the dramatic local variations in NO_2 under zonally asymmetric conditions, N_2O_5 plays a major role in the annual cycle of NO_2 under averaged conditions (see Ko *et al.*, 1984). Figure 10-64 presents calculated distributions of NO_2 at midnight and noon from the model of Garcia and Solomon (1983), Solomon and Garcia (1983a, 1984a) for comparison with the distributions shown in Section 10.2 (satellite data). Note that the calculated distribution of NO_2 exhibits a minimum in high latitude winter (even in the zonal and monthly mean distribution shown here) due to the formation of N_2O_5, as discussed above. This feature is also reflected in the satellite and aircraft total column data. *In situ* observations at high latitudes also reveal a similar depletion in NO at altitudes below about 30 km in winter as compared to summer. Ridley *et al.* (1984) showed that NO vertical profiles obtained in summer at 54°N contained systematically larger abundances than those measured in winter, and they attributed the differences between seasons to the enhanced abundance of N_2O_5 in the winter lower stratosphere.

Figure 10-64 also shows that the calculated nighttime NO_2 maximizes near 40 km in the tropics, similar to the observations by LIMS. This local maximum is related to the maximum in odd nitrogen production shown in Figure 10-53 above, and is closely tied to the N_2O distribution, as discussed above.

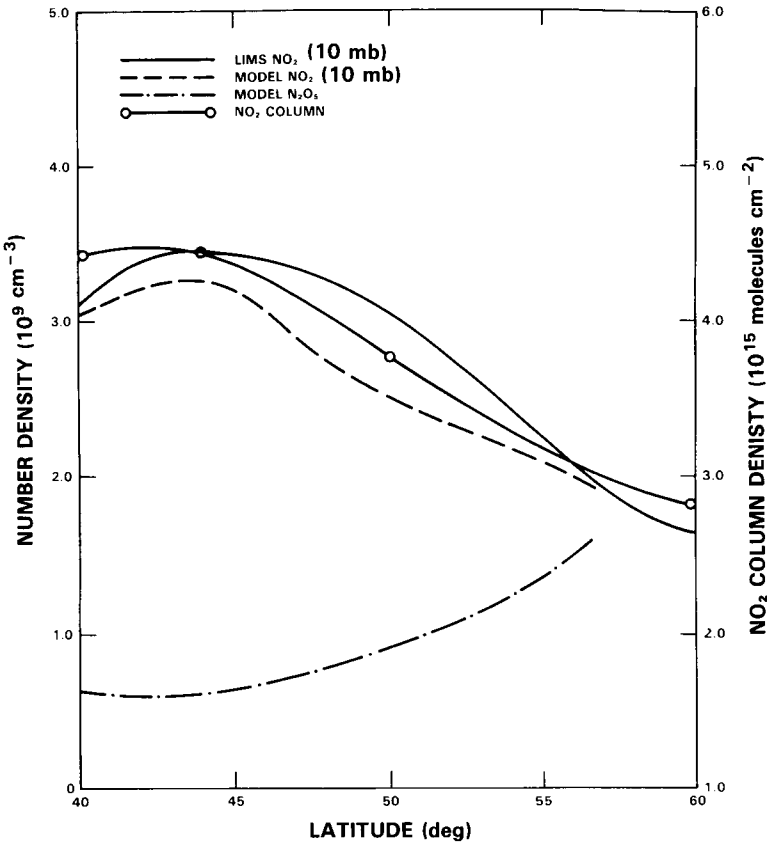

Figure 10-62. Latitudinal gradients in NO_2 observed by LIMS in January, 1979, compared to model calculations. From Callis *et al.* (1983b).

It should be emphasized that stratospheric NO_2 abundance decays during the night to form N_2O_5, which then photolyzes during the following day to yield a temporal increase in NO_2. This phenomenon is clearly reflected by the observed diurnal variation in total column and *in situ* observations of NO_2 and NO (see, e.g., Noxon *et al.*, 1979a; Ridley *et al.*, 1977; Kerr *et al.*, 1982). Therefore, since the available satellite data on NO_2 were obtained at different local times, their intercomparison can only be performed through photochemical modeling of the diurnal variability. Using the LIMS observations of O_3 and temperature, Solomon *et al.* (1985a) have studied the diurnal variations to be expected in NO_2. These calculations use the daytime LIMS measurement of NO_2 (near 1 pm) to constrain the amount of NO_y. Thus the daytime measurements by LIMS are assumed to be exact, but the calculated diurnal variations around this value depend strongly on photochemistry, and provide a means of comparing daytime LIMS data to SME (near 3 pm local time), to SAGE (sunrise and sunset), to the nighttime LIMS data, and to photochemical theory. Figure 10-65 presents a typical comparison of this type using the monthly and zonally averaged data from each satellite experiment. In general, the various satellite instruments were found to be in rather good agreement with one another, and with presently accepted theory controlling diurnal variations.

Available balloon data provide important, and somewhat more direct, information on NO_2 diurnal variations. During BIC 1 the Oxford University BPMR obtained measurements of NO_2 over both dawn and dusk, the flight covering nearly a 24 hour period (Roscoe *et al.* 1985a). Data from the upper levels

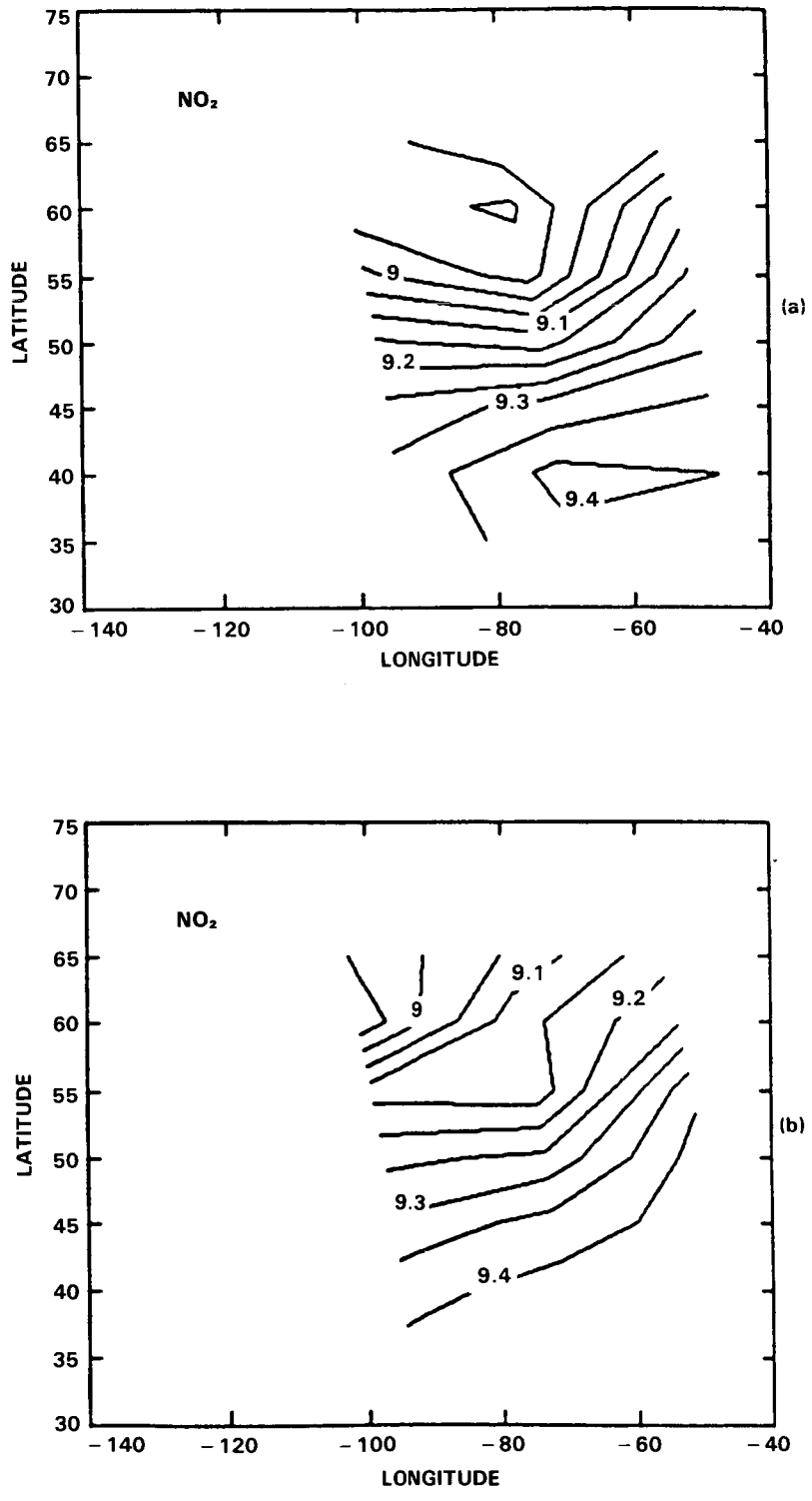

Figure 10-63. Latitudinal-longitude contours of the logarithm of NO_2 densities on day 40, 1982, (a) observed by SME and (b) calculated using the parcel trajectory method. See Zawodny, 1985a, b.

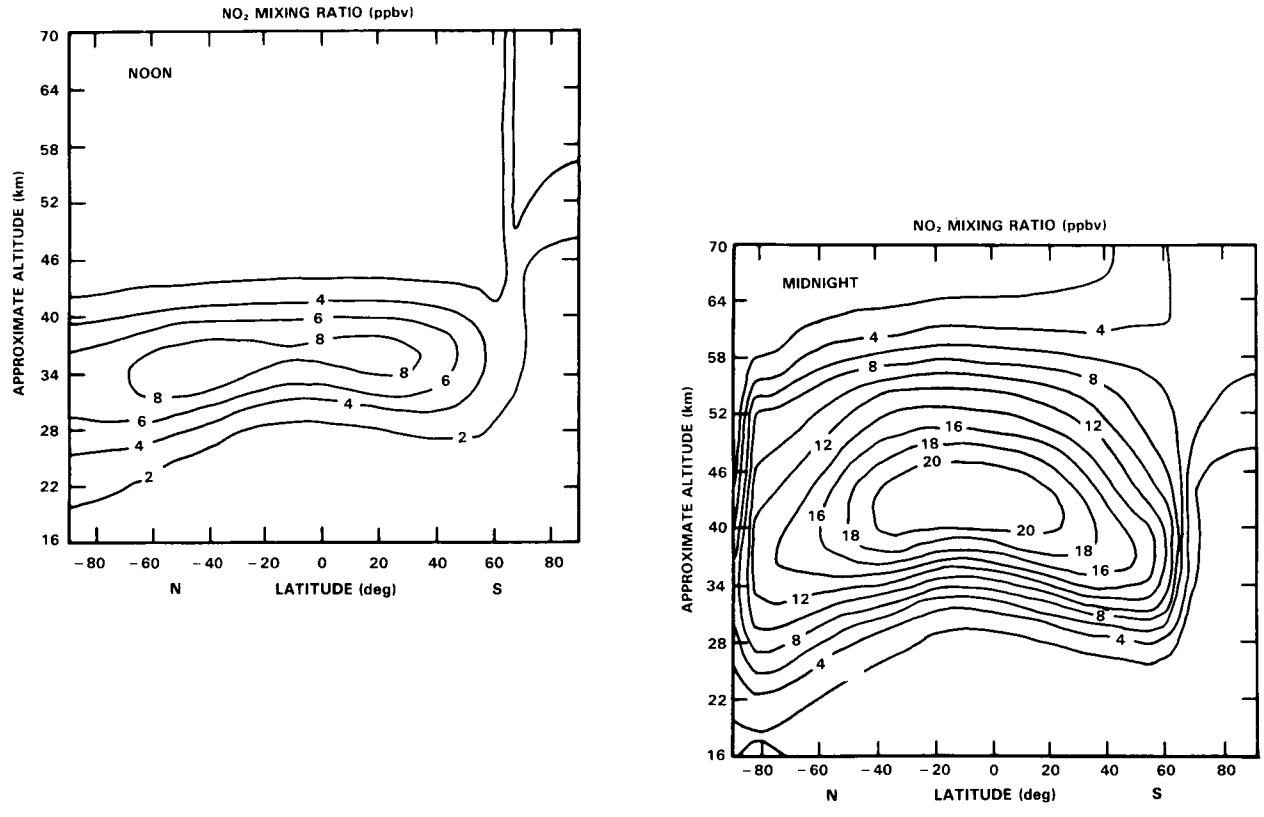

Figure 10-64. NO_2 mixing ratios at noon and midnight, from the model of Solomon and Garcia (1983a, 1984a).

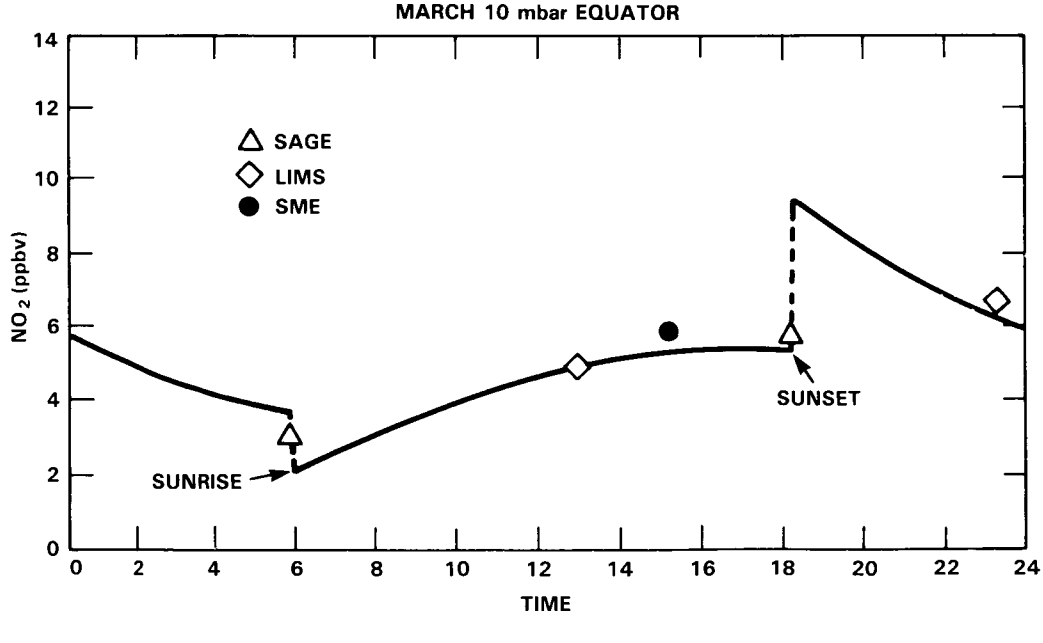

Figure 10-65. Comparison of monthly mean satellite NO_2 data 10 mbar at the Equator, and a model calculation.

at ~38 and 42 km are compared with a diurnal photochemical model in Figures 10-66 and 10-67 (data at lower levels were affected by the El Chichon volcano). The changes at dawn and dusk and the night-time decay of NO_2 are consistent with theory. Notice, for example, the slower night-time decay of NO_2 at ~42 km compared with ~38 km, consistent with a greater role of N_2O_5 formation at the lower altitude. Thus qualitatively the measurements confirm the theory.

Roscoe *et al.* (1985a) considered whether the data might provide a more quantitative test. The night-time decay of NO_2 can be written:

$$\frac{d[NO_2]}{dt} = -2k_1 [NO_2] [O_3] \quad (11)$$

where $NO_2+O_3 \xrightarrow{k_1} NO_3+O_2$ is followed rapidly by $NO_3+NO_2+M \xrightarrow{k_2} N_2O_5+M$. The equation can be rewritten:

$$\frac{d\ln[NO_2]}{dt} = -2k_1 [O_3] \quad (12)$$

to show the simple dependence of the night time decay on O_3. During BIC 1 there were a number of measurements of O_3 in the upper stratosphere, including measurements in the microwave (Robins *et al.* 1985) and the UV photometric measurements of Robbins (1985). Preliminary analyses show significant differences between these data. A good measurement of the night time variation of NO_2 could possibly distinguish the ozone value, using Equation (12).

Diurnal calculations were performed in which the model ozone values were replaced by, first, the microwave measurements and, second, the preliminary UV data. Figures 10-66 and 10-67 show the calculated diurnal variations at 38 and 42 km. However the standard error of the observed NO_2 decay (with only five points characterizing the period of darkness) is so large at both heights that the ozone data cannot be distinguished. Two conclusions may be reached. The NO_2 data, which represent probably the first measurements of a complete diurnal cycle, are of insufficient accuracy to be used to make a critical test of the photochemistry. (Nevertheless, physical insight suggests, for example that the role of N_2O_5 is confirmed by the measurements). A critical test requires measurements with higher precision. Second, a critical test will also require measurements of ozone to higher absolute accuracy. It must be regretted that the El Chichon aerosol cloud affected the results around 30 km since the signal-to-noise of the BPMR maximises at this height and it is here that the role of N_2O_5 is most important.

Since the distributions of nighttime NO_2 and HNO_3 are available from satellite data the distribution of NO_y can be obtained from data, at least in part (Callis *et al.*, 1985a, b; Solomon *et al.*, 1985a). A measurement of NO_2 and HNO_3 near 11 pm (as obtained by LIMS) does not, however, represent a direct measurement of total NO_y since production of N_2O_5 during the period from sunset to the measurement time must be an important process. This can be readily taken into account using diurnal photochemistry as shown in Figure 10-65, and a value for NO_y can therefore be inferred from the satellite data. Figure 10-68 presents a contour plot of the NO_y distribution derived from zonally and monthly averaged conditions in January (Solomon *et al.*, 1985a). The inferred maximum abundance of NO_y is about 21 ppbv near 40 km, in good agreement with the two-dimensional photochemical models discussed in Chapters 12 and 13. At lower altitudes, however, the two-dimensional models exhibited large variations in calculated NO_y, depending on the transport processes and treatment of HNO_3 rainout imposed in the models.

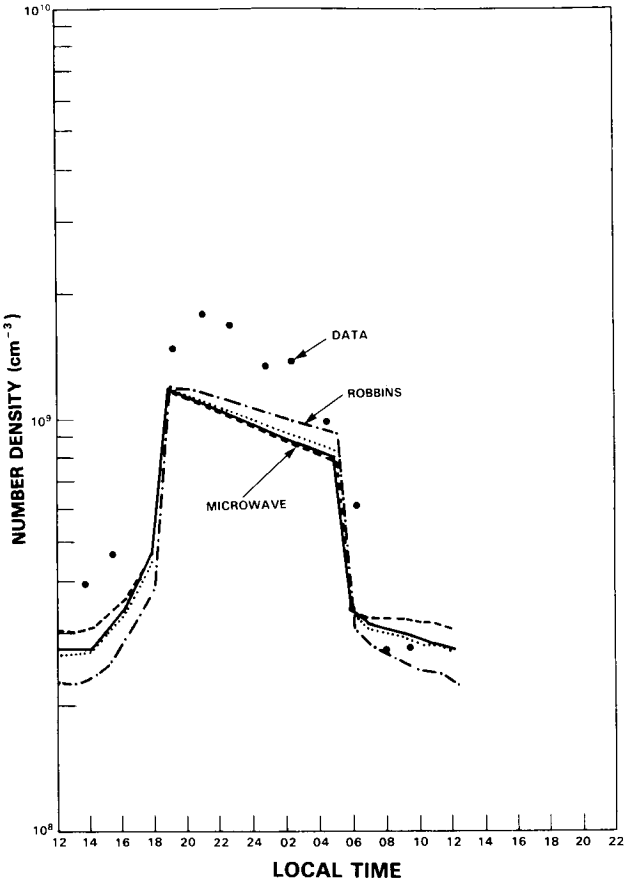

Figure 10-66. Observed diurnal variations in NO_2 at 38 km observed by Roscoe *et al.* (1985b), and model calculations including various ozone profiles (see text).

Figure 10-69 presents the latitude variation of NO_y inferred from the LIMS data at 3, 16 and 30 mbar compared to several two-dimensional models. Particularly in the tropical lower stratosphere most models tend to underestimate the inferred abundance of NO_y by a considerable margin. The magnitude of the gradient predicted by the residual Eulerian AER model is in good agreement with the observations, but the model is systematically low compared to the inferences drawn from LIMS. On the other hand, the classical Eulerian model of Pyle is much closer to the observations in the tropics, but exhibits a gradient that is somewhat shallower than the observed (see Chapter 12 on model formulation). Further observations of NO_y are badly needed to elucidate the causes of these discrepancies and to improve our understanding of odd nitrogen in the lower stratosphere.

A best estimate lower limit for a mid-latitude equinox NO_y profile can also be deduced directly from *in situ* data by summing the individual best estimate profiles for NO, NO_2, and HNO_3. This should be considered a lower limit, particularly at altitudes below 32 km, since no contribution from N_2O_5 or other reservoir species has been included. Figure 10-70 presents the lower limit profile derived from the *in situ* data compared to the total NO_y inferred from LIMS for April, 1979 at 32 °N. The two estimates are in good agreement.

An interesting problem in the chemistry of odd nitrogen in the stratosphere is the distribution of HNO_3 in winter. As shown above in the satellite subsection, the observed gradient of HNO_3 increases sharply

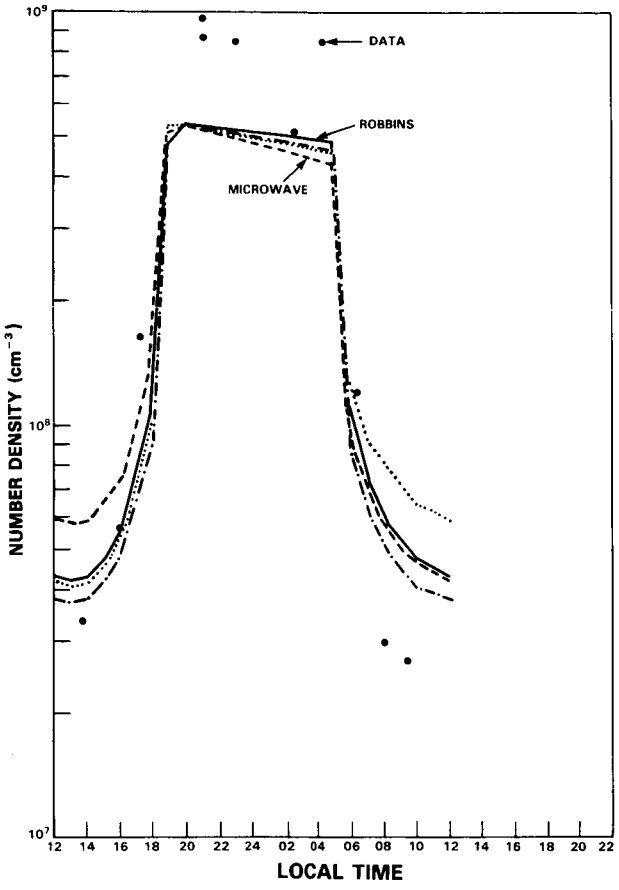

Figure 10-67. Same as Figure 10-66, but for 42 km.

with latitude inside the polar night region. Satellite observations of ozone and methane suggest that the circulation in high latitude winter must be directed downward and poleward in the zonal and seasonal mean. Such a circulation must then lead to downward transport of HNO_3 poor air from above, and a depletion of HNO_3 in high latitude winter, in contrast to trends in the data. Figure 10-71 presents a calculated contour distribution showing this feature. Comparison (for example) of Figures 10-42 and 10-71 suggest that our present understanding of HNO_3 chemistry may be incomplete during winter at high latitude. An additional source of HNO_3 during high latitude winter could resolve these discrepancies. More detailed studies by Austin *et al.* (1985b) using parcel trajectory methods along with LIMS data in the polar night strongly suggest that an additional source of HNO_3 must be present in high latitude winter.

10.3.2.3 Latitudinal Survey of HNO_3

The column abundance of HNO_3 has previously been reported by several investigators using aircraft platforms (Murcray *et al.*, 1975, Coffey *et al.*, 1981a and Girard *et al.*, 1982). The satellite observations (Gille *et al.*, 1984b) have been shown to be consistent with the data from the aircraft survey.

Since no significant diurnal variation is expected of HNO_3, the data are relatively easy to interpret as the exact local time at which the measurement is made is not crucial. The major contribution to the column abundance originates from the lower stratosphere below 25 km (about 90%) where the photochemical

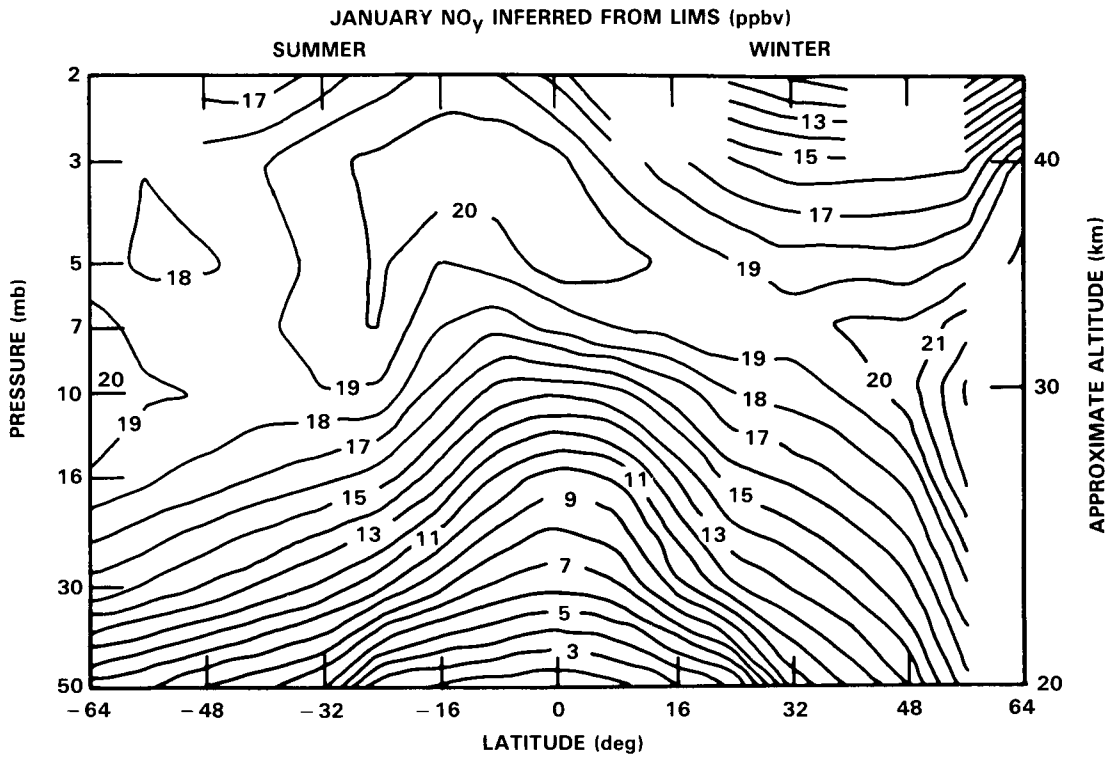

Figure 10-68. NO_y inferred from LIMS for January, 1979. See text.

lifetime of HNO_3 is comparable to or longer than transport time constants. The species HNO_3, which is one of the few downward diffusing species for which extensive observational data are available, is a useful tracer for diagnosing the transport of trace gases in the lower stratosphere.

The data show a factor of three increase in the column abundance from the equator to 45 degree latitude, and up to an order of magnitude increase from equator to pole. In addition, the abundance in the winter hemisphere is also higher in the high latitude regions. Since HNO_3 is produced in the stratosphere and removed rapidly in the troposphere by heterogenous processes, regions dominated by upwelling motion should have a lower concentration of HNO_3 than regions with subsiding motion. This observed latitudinal behaviour is consistent with what could be expected from models with diabatic circulation where upwelling in the tropics results in lower HNO_3 abundance. The seasonal variability is also related to possible photochemical exchanges with reserviour species such as N_2O_5 (Solomon and Garcia 1983a; Ko *et al.*, 1984). The role of N_2O_5 is particularly important near the polar night region in the winter hemisphere where intrusion of air from the polar night may cause significant fluctuations of the observed HNO_3 at particular longitudes (Solomon and Garcia 1983b, Noxon *et al.*, 1983).

Figure 10-72 shows calcuated column abundances of HNO_3 from different model groups. The results separate rather nicely into two groups with models using large eddy difficusion coefficients ($K_{yy} \sim 1\times10^{10}$ $cm^2\ s^{-1}$, $K_{zz} \sim 1\times10^4-1\times10^5$ and those using small diffusion coefficients ($K_{yy} \sim 3\times10^9$ $cm^2\ s^{-1}$). Models using large eddy coefficients (Ko *et al.* 1984) obtain results with smaller latitudinal contrast. In spite of the use of large diffusion coefficients, the DuPont model (Miller *et al.*, 1981) produced a large contrast. This could be due to the choice of K_{zz} to stimulate the higher tropopause at the equatorial region.

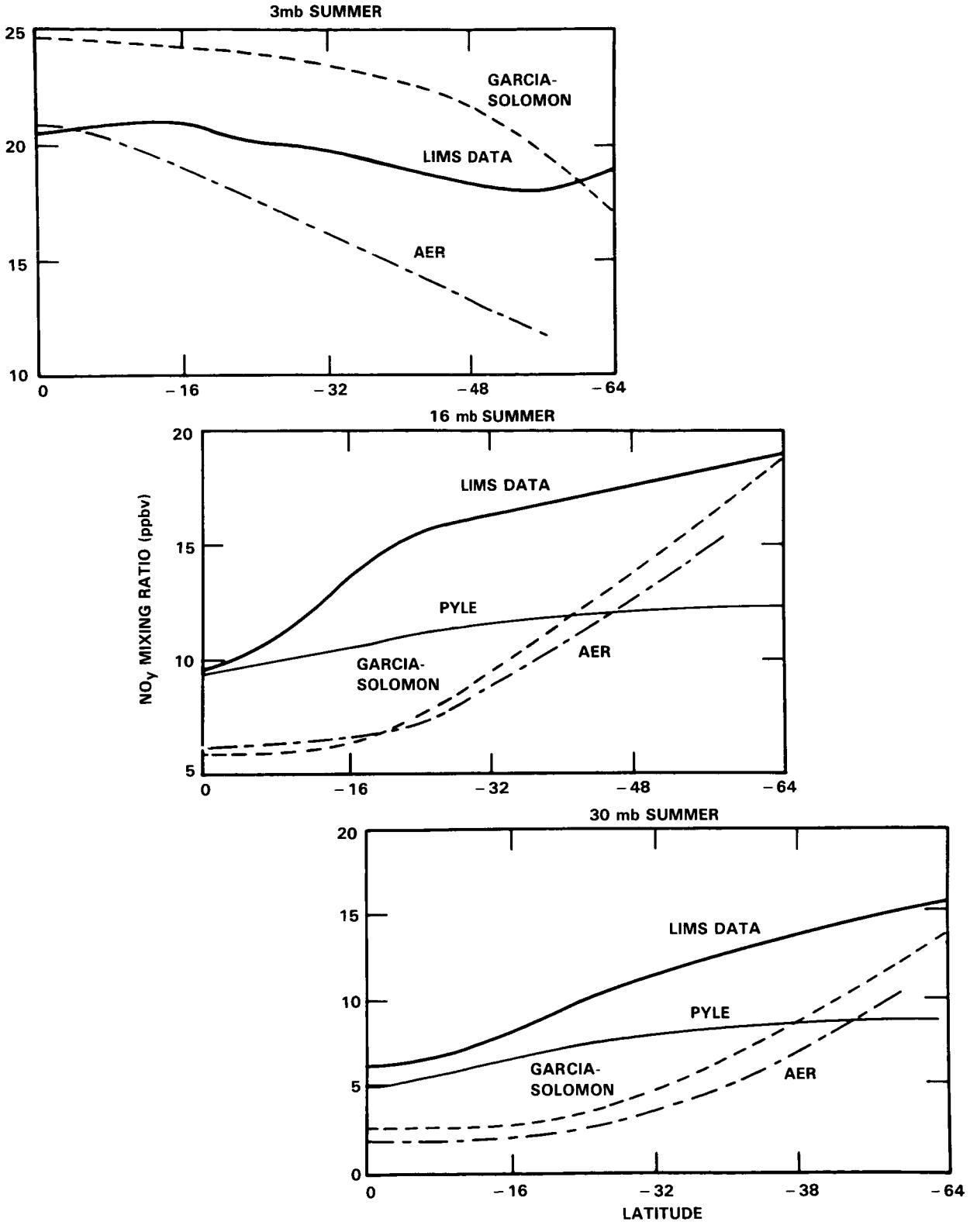

Figure 10-69. Latitudinal gradients in NO_y observed by LIMS, and calculated in various 2-D models, at the 3 mb, 16 mb, and 30 mb levels.

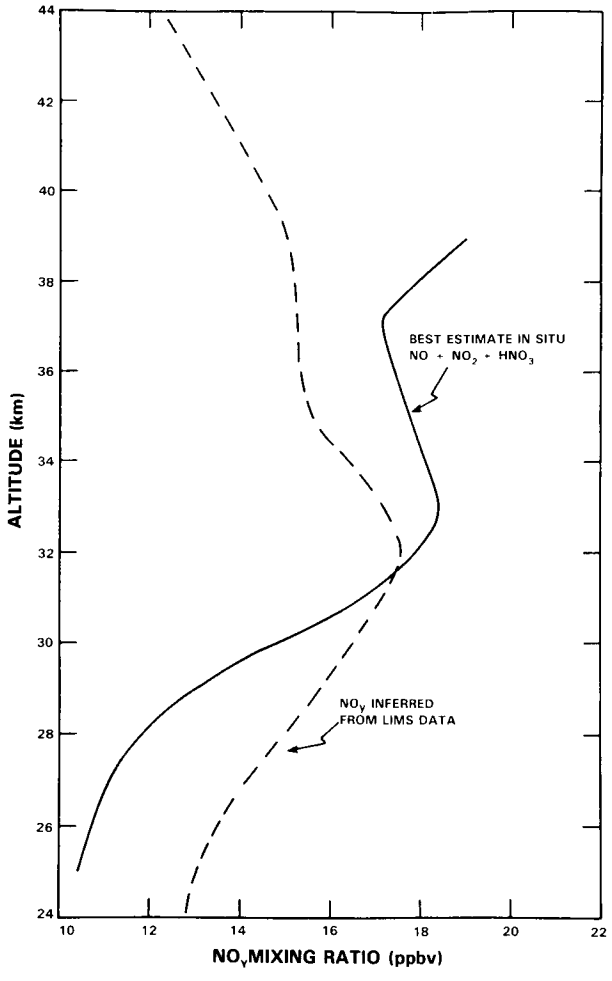

Figure 10-70. Best estimate of the sum of NO, NO_2, and HNO_3 at mid-latitudes in spring from in situ data, and the corresponding values from LIMS.

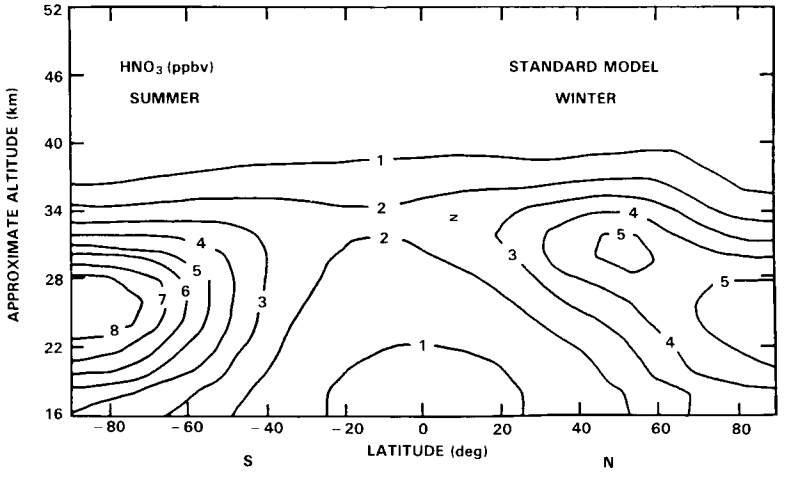

Figure 10-71. Model calculated HNO_3 distributions near winter solstice. From Austin *et al.* 1985a).

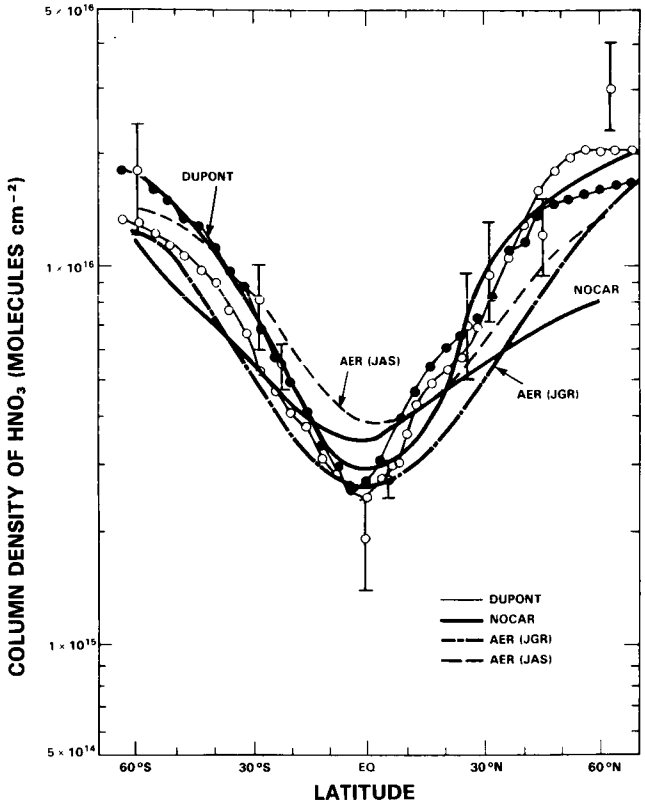

Figure 10-72. Column abundances of HNO_3 from a number of two-dimensional models, and from observations. See Ko *et al.* (1985).

The simulated abundances from models using small eddy coefficients (Solomon and Garcia 1983a; Ko *et al.*, 1985) show larger latitudinal gradients.

The model calculated column abundance of HNO_3 is sensitive to the dynamical treatment both in the mean circulation and eddy mixing in the lower stratosphere (Ko *et al.*, 1985). Further observations of the latitudinal variation of the column abundance of HNO_3 from satellite and aircraft platforms may help elucidate the appropriate parameterization for mixing processes in the lower stratosphere.

10.3.3 Photochemical Considerations

In this subsection, some of the photochemical processes influencing the distributions of the NO_x species will be discussed.

10.3.3.1 The NO/NO_2 Ratio in the Stratosphere.

Nitric oxide which is produced in the stratosphere by the oxidation of N_2O is rapidly converted to nitrogen dioxide mainly by ozone

$$NO + O_3 \rightarrow NO_2 + O_2 \qquad (13)$$

but also by HO_2, CH_3O_2 and ClO through

$$NO + HO_2 \rightarrow NO_2 + OH \tag{14}$$

$$NO + CH_3O_2 \rightarrow NO_2 + CH_3O \tag{15}$$

$$NO + ClO \rightarrow NO_2 + Cl \tag{16}$$

During the day, it is destroyed either by photodissociation

$$NO_2 + h\nu \rightarrow NO + O \tag{17}$$

or by reaction with atomic oxygen

$$NO_2 + O \rightarrow NO + O_2 \tag{18}$$

Since the atmospheric attenuation near 400 nm (where NO_2 absorbs) is weak through the entire middle atmosphere, the photodissociation frequency of NO_2 keeps its optically thin value (about $1 \times 10^{-2} s^{-1}$ for an overhead Sun) to as low an altitude as 15 km, so that the lifetime of nitrogen dioxide is never larger than a few minutes during the day. Consequently NO_2 is in immediate photochemical equilibrium with NO during sunlight hours and the NO/NO_2 ratio is given by

$$\frac{[NO]}{[NO_2]} = \frac{J(NO_2) + k_{18}\,[O]}{k_{13}\,[O_3] + k_{14}\,[HO_2] + k_{15}\,[CH_3O_2] + k_{16}\,[ClO]} \tag{19}$$

A comparison of the various terms appearing in the above expression shows that the most effective transfer from NO to NO_2 is due to ozone (reaction 13) and that the other processes contribute for less than 25% in the whole stratosphere and for less than 10% below 30 km. Both photodissociation and reaction with atomic oxygen have to be considered in the conversion from NO_2 to NO, the first process being dominant below 42 km and the second one above this level. During the night, both of these reactions are inefficient and therefore nitric oxide is converted to NO_2 throughout the whole stratosphere.

The comparison between the NO/NO_2 ratio inferred from *in situ* observations and obtained by a full model calculation is an important test to validate our present knowledge of the odd nitrogen photochemistry. The accurate calculation of this ratio however is not straightforward since the parameters involved vary with geophysical conditions and may thus change for example during the period of a ballon flight. The value of the J_{NO_2} coefficient is very sensitive to the local albedo, i.e. to cloud coverage, and may also vary with atmospheric temperature (Madronich *et al.*, 1983). Model calculations show that the NO/NO_2 ratio can change by a factor of 2 with cloud coverage or surface conditions.

Further, extreme accuracy in temperature and ozone measurements is needed to test the ratio in a meaningful manner (Harries, 1982).

A recent comparison between the NO/NO_2 ratio derived from the measurements of McFarland *et al.*, (1985) at Gimli, Manitoba (50 °N) and Palestine, Texas (32 °N) and the calculated NO/NO_2 ratio between 20 and 30 km agrees within ±40% and suggest that the observations are, within the error bars, consistent with theory. However additional simultaneous measurements of NO and NO_2 together with the temperature and the J_{NO_2} coefficient are required to test this photochemistry more accurately.

10.3.3.2. HNO_3/NO_2

The photochemical time constant for HNO_3 is some hours in the sunlit upper stratosphere and equilibrium between HNO_3 and NO_2 can be assumed to a good approximation. Comparison of the measured and calculated HNO_3 to NO_2 has been used to test photochemical theory. In equilibrium:

$$\frac{[HNO_3]}{[NO_2]} = \frac{k_4[OH]\ [M]}{J(HNO_3) + k_6[OH]} \tag{20}$$

so that the ratio depends just on rate constants, a photolysis rate and the OH concentration.

Early investigation based on ballon data suggested that the observed ratio was low compared with models (Evans *et al.*, 1976, Harries 1978), and the measurements themselves, taken at different latitudes and local times, were also significantly different. The problem of modelling HNO_3 in the middle and upper stratosphere has been apparent for some time. Whether the problems with the ratio comparisons were simply due to this or, for example to a poor model description of OH was not clear.

Testing chemistry using such ratio measurements is particularly subject to systematic errors in the observation. Nevertheless the LIMS measurements of HNO_3 and NO_2 provide the opportunity for extensive study with nearly global coverage at a range of zenith angles. Pyle and Zavody (1985a) have used the LIMS data to test aspects of the photochemistry. Rather than comparing the modelled and observed HNO_3 to NO_2 ratios, they have derived OH using Equation 20 and compared this with the limited stratospheric measurements of OH to OH derived, again using the satellite data, by calculation of its sources and sinks. In this latter case H_2O, from LIMS data, and $O(^1D)$, assumed to be in photochemical steady state with LIMS O_3, define the source. Similarly, the sink terms are defined by using LIMS data and making certain photochemical steady state assumptions. The reader is referred to the HO_x chapter (9) for a detailed discussion of the use of satellite data in deriving OH. A detailed estimate was made of the likely error in the two derivations of OH. The derived values in low and middle latitudes agree within these estimated errors and are consistent with the few atmospheric measurements of OH.

Figure 10-73 shows a comparison of the derived OH at 32 °N including the estimated errors of the determinations due to errors in the rate constants and errors in the LIMS observations. The agreement between the two methods constitutes a modest positive test of this subset of NO_x -HO_x photochemistry and does not support the earlier suggestions of limitations in theory based on ballon measurements. Nevertheless, an anticipated bias in LIMS HNO_3 could change this conclusion. Note that the LIMS HNO_3 is systematically higher than ballon measurements, but less than models, above about 30 km (see below). Correspondingly in Figure 10-73 the OH derived using equation (20) is less than OH derived from its sources and sinks. The possibility remains of an unidentified sink for HNO_3, although note again that the error in derived OH and errors in the kinetic data are significant. For a satisfactory test, simultaneous measurements of OH, HNO_3 and NO_2 are urgently required.

10.3.3.3 Absolute Abundance of HNO_3 at Mid-Latitude in the Upper Stratosphere

The nitric acid concentration predicted by model calculations above 25-30 km is about a factor 1.5 to 2 larger than the values measured by ballon-borne instruments, but closer to the LIMS measurements. This discrepancy with *in situ* data cannot presently be explained by current uncertainties in the chemical parameters involved in the calculation. Predicted HNO_3 abundance depends on the total NO_y concentra-

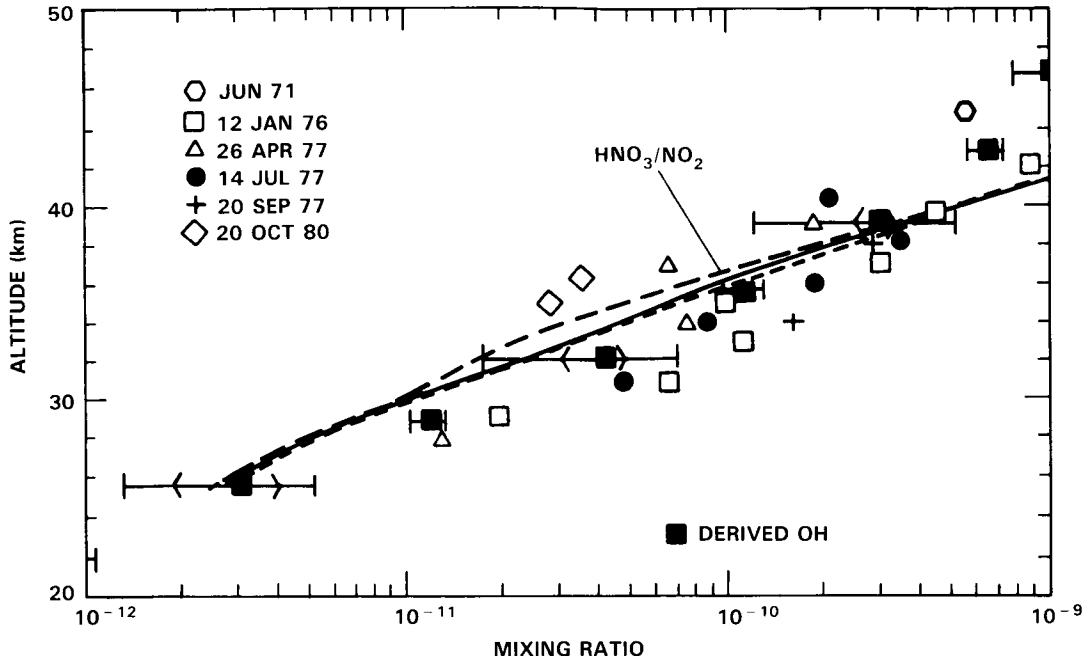

Figure 10-73. OH derived from LIMS data using the equilibrium between HNO_3 and NO_2 (dashed line) and by calculation of sources and sinks (solid line). Errors in the derivation due to estimated LIMS errors (↔) and due to estimated errors in kinetic and photochemical data (↔) are also shown. Based on Pyle and Zavody (1985a).

tion by which is calculated in the model. Most models however predict a NO_y mixing ratio close to 18-22 ppbv at 35 km in acceptable agreement with the values inferred from LIMS data. In any case, the 30% difference in NO_y among most models cannot explain a factor of 1.5 to 2 difference between observed and calculated HNO_3 amount.

Differences in the treatment of the diurnal averaging of the HNO_3 formation rate also lead to significant changes in the calculated concentration above 25 km. The use of a 24 hour average of the rate instead of the calculation of the rate with averaged OH and NO_2 concentrations reduces the resulting nitric acid abundance but does not entirely resolve the discrepancy.

Unless an important mechanism is omitted in the theoretical approach, it is more likely that the overestimation of the predicted HNO_3 concentration may be related to an improper calculation of the solar transmission in the Schumann-Runge bands and consequently of the HNO_3 photodissociation frequency. The use of smaller O_2 cross section in the Herzberg continuum has already brought the calculated HNO_3 concentration into closer agreement with observations (Froidevaux and Yung, 1982: Basseur *et al.*, 1983).

10.3.3.4 NO_3 at Night

Perhaps the area of largest current discrepancy between odd nitrogen observations and photochemical theory lies in the observed behavior of NO_3 at night. NO_3 is formed by the reaction.

$$NO_2 + O_3 \rightarrow NO_3 + O_2 \quad (1)$$

and it is destroyed by reaction with NO_2 to form N_2O_5 in a three-body process. During the day, it also photolyses rapidly at visible wavelengths, so that the daytime abundance is expected to be extremely small. At night, however NO_3 is expected to build up to large abundances near 40 km or so. The rate of formation of NO_3 is particularly dependent on temperature through the strong negative temperature sensitivity of reaction (1) and the expected total column abundance should therefore be several times greater in summer at middle and high-latitudes than it is in the winter. NO_3 total column observations by Norton and Noxon (1985), however, show clearly that the observed abundances at 40°N in summer are no larger than they are in winter, and are many times smaller than model predictions. Therefore, Norton and Noxon (1985) conclude that a scavenger must exist for stratospheric NO_3. Nighttime NO_3 profiles are also available from the balloon measurements of Naudet *et al.* (1984). These data show greater abundances in spring than in fall near 40 km, whereas the opposite is predicted by photochemical theory using climatological mean observations of ozone and temperature for the latitude where the observations were obtained (Norton and Noxon, 1985). More extensive observations of NO_3 as a function of latitude and season are badly needed to characterize this discrepancy in greater detail, but the consistency of these observations suggests the existence of a gap in our understanding of odd nitrogen photochemistry.

10.4 SUMMARY AND CONCLUSIONS

This chapter has demonstrated that substantial progress in our understanding of stratospheric odd nitrogen has been achieved in the past few years. Indeed, a number of questions that might have been termed "outstanding problems" in 1980 have been largely resolved. Others remain subject for ongoing research, and with our improved understanding additional challenges have also emerged.

The availability of satellite data on NO_2 and HNO_3 has been a major achievement in stratospheric research, allowing us to quantify our knowledge of the temporal and spatial variations in NO_y to a remarkable extent. No less that five new techniques are also now used to detect NO_2 from balloons, enabling a much fuller understanding of NO_2 to be achieved. Intercomparison of balloonborne techniques for measuring NO_2 and NO has greatly added to the value of the existing dataset, and has led to firm knowledge of the detailed profiles of these species at mid-latitude. NO_3 has been observed both by ground-based and balloon methods, revealing an important inconsistency with photochemistical theory over much of the annual cycle. N_2O_5 and $ClONO_2$ have also been tentatively measured. Diurnal variations in NO_2 have been directly measured from a balloon, and are also revealed by the combination of available satellite data obtained at various local times. Both are in broad agreement with photochemical theory regarding the interchange between members of the NO_y family. Direct measurements of the important ratio between NO and NO_2 and are also available from balloons, and are consistent with theoretical predictions. Observations of NO_2 and HNO_3, and their ratio, are now available from satellites as well as balloons, yielding new information on HNO_3 chemistry and inferences about the OH content of the stratosphere. NO_2 observations following the eruption of the El Chichon volcano suggest that important changes in stratospheric photochemistry are associated with major eruptions.

The combination of available data on NO_2, HNO_3, and NO has greatly improved our knowledge of total NO_y. This information is particularly important both because it enables us to better understand the budget of the family as a whole, and because NO_y plays a major role in model predictions of ozone perturbations. It is important to emphasise that the NO_y derived from the data is in marked disagreement with two-dimensional model predictions below about 30 km. This suggests that boundary conditions or low-altitude NO_y sources are not properly treated in the models.

On the other hand, the derived NO_y above 30 km is in good agreement with model predictions. Here again, this good agreement is partly due to the availability of new data (principally from satellites), which has guided theoretical study. In particular, available satellite observations of N_2O have enabled a much more quantitative understanding of the sources of NO_y via N_2O oxidation to be achieved.

Satellite observations of NO_2 in the polar night region have also quantified our knowledge of thermospheric sources, providing the first observational evidence that thermospheric NO_y can be transported to the upper stratosphere. This possibility was first raised in about 1970, and has only now been addressed directly with observations.

The availability of improved data on N_2O has greatly enhanced our understanding of stratospheric transport processes. Satellite observations on N_2O have shown that tropical circulation patterns are likely to be strongly linked to the semi-annual oscillation. Further, balloon data for N_2O at higher vertical resolution than that resolved by the satellites has shown that vertical variability exists systematically, and on very fine spatial scales. These are yet to be completely understood theoretically, but the variance associated with stratospheric sudden warmings seems to play a significant role in this phenomenon.

Ground based, balloon, aircraft, and satellite data have all been used to address the variability of NO_2 at high latitude in winter in much more detail than previously possible. These data have greatly quantified our understanding of the distribution of N_2O_5 and its role in the Noxon ''cliff'' phenomena. Balloon data have shown that the ''missing'' NO_2 in the ''cliff'' region occurs at altitudes from about 15-30 km. Theoretical studies have revealed that the Noxon ''cliff'' is primarily due to meridional transport processes and combined photochemical effects in the presence of large-scale waves.

Studies of the latitudinal variations in HNO_3, both from aircraft and from satellites, have also to led to important insights into transport processes, showing in some detail how advection and dispersion compete in tropical latitudes.

In spite of these numerous advances, several outstanding problems must be considered unresolved. The ratio between HNO_3 and NO_2 remains imperfectly simulated by current models, although it should be emphasised that possible errors in kinetic data regarding OH reactions might resolve the apparent discrepancy. Another possibility is that the HNO_3 photolysis rate may be under estimated, particularly in the Schuman-Runge bands. Further laboratory kinetic studies, and *in situ* simultaneous observations of OH, NO_2 and HNO_3 could be used to address this question. Satellite data also suggests that an unknown chemical source of HNO_3 may be present in the high latitude winter stratosphere. Further observations are badly needed, and should include both Northern and Southern Hemisphere data.

Observations of the Noxon ''cliff'' also suggest that the temperature sensitivity of the N_2O_5 photolysis rate at the very cold temperatures of the Antarctic winter may not be completely well understood. Further observation of the ''cliff'' phenomenon in the arctic is needed, as well as laboratory studies. Direct measurements of N_2O_5 are also of the most critical importance to a fuller understanding of NO_2 variability. Other temporary reservoirs such as $ClONO_2$ and HNO_4 also require quantitative study as detailed functions of latitude and season.

Data on diurnal variations in NO_2 from balloons and satellites, while of considerable qualitative use, are not yet sufficiently accurate nor temporally detailed to definitively test photochemical theory. Highly accurate simultaneous observations of several species (i.e. NO, NO_2, and N_2O_5 as a minimum) are needed to address these issues.

Finally, the nighttime behaviour of total column NO_3 observed by Norton and Noxon shows that important mysteries remain present in the behaviour of stratospheric odd nitrogen species, and a dependence on only a few relatively well known parameters such as O_3 and temperature. Yet, the observations reveal seasonal variability that defies current interpretation.

In closing, we remark that continual research into the problems of stratospheric odd nitrogen must involve a variety of methods and tools. Theoretical studies should include multi-dimensional and simple box models. Laboratory kinetics remain of critical importance, and several areas have been mentioned as uncertain here. Satellite and aircraft data on temporal and spatial variations are needed, as well as high vertical and short time resolution data from balloons.

10.5 FUTURE RESEARCH

The review presented in this chapter has revealed that the study of NO_x is an active field of atmospheric research. A number of indications of future research requirements have emerged, and are summarised here.

The power of the new satellite data sets has been clearly demonstrated. Researchers (and funding agencies) should recognise the importance of continuing to exploit these sources of information to the maximum.

A problem remains with the explanation of the distribution of high altitude (>30 km) HNO_3. Current models show considerable excesses over both satellite (LIMS) and balloon measurements. Similarly, we do not currently understand the balance of HNO_3 at high latitudes: the suggestion that there is an unidentified source of high latitude HNO_3 needs to be tested.

There are several independent suggestions on the importance of N_2O_5 as a temporary reservoir under dark conditions. N_2O_5 has recently been reported as detected by the ATMOS experiment at night in mid-latitudes. Future work needs to identify and measure N_2O_5 at higher latitudes, and under polar night conditions. Furthermore, until N_2O_5 photolysis rates are better determined, we will not be able to adequately understand the time variation of exchange between NO, NO_2, HNO_3 and N_2O_5. Other temporary reservoirs such $ClONO_2$ may be of lesser importance, but should be similarly studied.

Some of the most stringent tests of theory have come from measurements of diurnal variations. However, measurement accuracy and time resolution need to be increased substantially to allow a very "tight" comparison.

Considerably more work is needed to understand NO_3. The past 5 years have given us a valuable new set of observations of this species, but these have revealed that our understanding of the seasonal variation of NO_3 is not properly understood. Is there a summer-time "scavenger" of NO_3?

It is now a truism that we need more observations, particularly simultaneous observations of groups of species which might provide a "closed" test of some aspect of the chemistry or physics. Even so, it must be stressed that experimentalists must continue to generate ideas, and hardware, to permit such experiments, and to seek to achieve the highest accuracies possible. In connection with the present chapter, an example would be the simultaneous measurement of NO, NO_2, N_2O_5, HNO_3, and NO_3 at an absolute accuracy in the 5%-10% range, with a time resolution of ~ 5 minutes; height resolution is not so demanding: as much as 5 km would not be critical.

Finally, we recognise that, in the same way that Nimbus 7 (SAM, LIMS), SAGE, and SME have caused a minor revolution in the quantity and nature of the data available to us, the simultaneous measurements to be made by the instruments complement on the Upper Atmosphere Research Satellite (UARS) can be expected to have a major impact on our understanding on NO_x, and many other areas of atmospheric science. It is important that researchers prepare properly to exploit these data: it is also important that agencies ensure that facilities are in hand to ensure efficient distribution of the UARS results to the community.